TECHNISCHE
UNIVERSITÄT
WIEN
Vienna | Austria

ICEBE
IMAGINEERING
NATURE

Master Thesis

LaserEye: Design and Construction of a Combined Laser Doppler Velocimeter and Raman Spectrometer Prototype

carried out for the purpose of obtaining the degree of Dipl.-Ing. or DI, submitted at TU Wien, Faculty of Mechanical and Industrial Engineering, by

Günter Wedl

Mat.Nr.: 09926574

under the supervision of

a.o.Univ.Prof. Dipl.-Ing. Dr. Michael Harasek

Dr. Christian Jordan

Dr. Bahram Haddadi

Institute of Chemical, Environmental and Bioscience Engineering, E166-02-2

Vienna, June 2022

Affidavit

I declare in lieu of oath, that I wrote this thesis and performed the associated research myself, using only literature cited in this volume. If text passages from sources are used literally, they are marked as such.

I confirm that this work is original and has not been submitted elsewhere for any examination, nor is it currently under consideration for a thesis elsewhere.

I acknowledge that the submitted work will be checked electronically-technically using suitable and state-of-the-art means (plagiarism detection software). On the one hand, this ensures that the submitted work was prepared according to the high-quality standards within the applicable rules to ensure good scientific practice "Code of Conduct" at the TU Wien. On the other hand, a comparison with other student theses avoids violations of my personal copyright.

City and Date	*Signature*

Acknowledgements

This work was supported by AWS within the framework of the project P1905372 - 2-in-1-Lasereye.

I would like to thank my thesis adviser Michael Harasek, Bahram Haddadi and Christian Jordan for their guidance, help and constant support during the whole research work.

Appreciation is also extended to the members of the Institute of Chemical, Environmental and Bioscience Engineering, who gave me the support all the time.

I also want to say thank you Krisztina Wedl and Sophie Wedl, who always remind me what is important in life and thank all my friends and study colleagues for the great time.

"If you want to find the secrets of the universe, think in terms of energy, frequency, and vibration." – Nikola Tesla

Table of Contents

Abstract

The LaserEye concept, presented by Haddadi et al., 2018 (DOI 10.1016/j.cej.2017.10.027) combines a laser Doppler velocimeter and a Raman spectrometer, using only one light source for both measurements. It was shown in the Proof of Concept (PoC), that a simultaneous measurement of the velocity and Raman spectrum of a liquid process stream is possible. The PoC used a single laser source, but two sensor heads which had been arranged in 90° to each other.

In this thesis a new prototype based on the LaserEye concept is designed, which needs only one measuring opening to measure velocity, direction, composition, and concentration of a process stream simultaneously. The further developed LaserEye consists of a laser source, a telescope optic to adjust the measurement volume and a beam splitter unit which divides the incoming excitation beam in three beams with equal optical power. Further, an off axis parabolic mirror not only focuses the three excitation beams on the target but also collects the scattered light and an edge filter divides the scattered light in a short-wave partial beam used for LDV measuring and elastic scattered, long wave light, which contains the spectroscopic information, used for Raman spectroscopy. A LDV unit then delivers the velocity and the direction of the tracer particle in the process stream which scattered the light, and a Raman spectrometer returns the composition and the concentration of the substances in the measurement volume.

Furthermore, a new measurement method was found to obtain the velocity and the direction information of the 3-dimensional target movement with only one laser source, one sensor and without frequency shift. Therefore, a 3-dimensional measurement volume is created with the three irradiating beams from which the velocity and direction of the tracer particles in the process stream can be calculated.

Due to its compact and robust built, the new measurement method, which is in registration as Patent (A 50019/2021), is perfectly fitted as LDV unit in the Laser Eye.

Kurzfassung

Das LaserEye-Konzept, welches 2018 von Haddadi et al. (DOI 10.1016/j.cej.2017.10.027) vorgestellt wurde, kombiniert ein Laser-Doppler-Anemometer (LDA) und ein Raman-Spektrometer, wobei für beide Messgeräte dieselbe Lichtquelle für simultane Messungen verwendet wird. In einer ersten Ausführung wurde gezeigt, dass eine Messung der Geschwindigkeit und des Raman-Spektrums in einem Strömungskanal simultan möglich ist. Der konzeptionelle Beweis verwendete eine Laserquelle, aber zwei Sensorköpfe, die im 90°-Winkel zueinander angeordnet waren.

In dieser Arbeit wird ein neuer Prototyp basierend auf dem Konzept des LaserEye vorgestellt, der mit nur einer Messöffnung Geschwindigkeit, Richtung, Zusammensetzung und Konzentration eines Prozessstroms simultan messen kann. Das weiterentwickelte LaserEye besteht aus einer Laserquelle, einer Teleskopoptik zur Einstellung des Messvolumens und einer Strahlteilereinheit, die den einfallenden Erregerstrahl in drei Strahlen gleicher optischer Leistung aufteilt. Ein außeraxialer Parabolspiegel fokussiert die drei Anregungsstrahlen auf das Ziel und sammelt das gestreute Licht. Ein optischer Filter teilt das gestreute Licht in einen kurzwelligen Teilstrahl, der für die LDA-Messung verwendet wird und in einen elastisch gestreuten, langwelligen Teilstrahl, welcher die spektroskopische Information enthält und für die Raman-Spektroskopie verwendet wird. Eine LDA Einheit liefert dann die Geschwindigkeit und die Richtung der Tracer-Partikel im Prozessstrom an denen das Licht gestreut wurde und ein Raman-Spektrometer liefert die Zusammensetzung und die Konzentration der Substanzen im Messvolumen.

Zusätzlich wird ein neues Messverfahren vorgestellt, um die 3-dimensionalen Geschwindigkeits- und Richtungsinformationen der Tracing-Partikel im Prozessstrom mit nur einer Laserquelle, einem Sensor und ohne Frequenzverschiebung zu ermitteln. Dafür wird mit drei einfallenden Laserstrahlen ein 3-dimensionales Messvolumen aufgespannt, aus dem die Geschwindigkeit und Richtung der Tracer-Partikel im Prozessstrom berechnet werden kann.

Aufgrund der robusten und kompakten Bauweise eignet sich dieses neue Messverfahren, welches zum Patent angemeldet (A 50019/2021) wurde, besonders gut für den Einbau als LDA Einheit im LaserEye.

List of Abbreviations and Symbols

LDV ..... Laser Doppler Velocimeter
SHRS ..... Spatial Heterodyne Raman Spectrometer
SHS ..... Spatial Heterodyne Spectrometer
OAP ..... Off Axis Parabolic
BS ..... Beam Splitter
rpm ..... Rotation Per Minute
PWM ..... Pulse Width Modulation
SIP ..... SIlicon Photomultiplier
FWHM ..... Full Width Half Maximum
µC ..... micro controller
DOTP ..... DiOctyl TerePhthalate
PVC ..... PolyVinyl Chloride
SNR ..... Signal to Noise Ratio
GBW ..... Gain BandWith product
CCD ..... Charged-Coupled Device
VCC ..... supply voltage
C ..... Capacitor
R ..... Resistor
U ..... voltage
I ..... current
FFT ..... Fast Fourier Transformation
P ..... Power
S_{PD} ..... Sensitivity
I_R ..... Raman Intensity
LCD ..... Liquid Crystal Display
DC ..... Direct Current
A ..... Area/cross section
V ..... overall velocity
v_i ..... component velocity
f, f_i ..... frequency
λ ..... wavelength
θ ..... angle
Δθ ..... angle between two beams
$\bar{\nu}$ ..... absolute wavenumber

c ..... speed of light
p_0 ..... amplitude of the induced oscillating dipole moment
ε_0 ..... permittivity of vacuum
σ ..... wavenumber
ħω ..... vibration quants
m ..... mode
E ..... Energy
G ..... Grating
L ..... Lens
d ..... Distance between grooves
W ..... Wavefront
D ..... Detector
S ..... Sample
M ..... Mirror
MA ..... Measurement Area
CW ..... Continuous Wave
LP ..... laser source
MO ..... Microscope Objective
GF ..... fiber

1 Introduction and Motivation

A key role in adjustment and optimization of industrial processes and process streams in chemical plants is played by the measurement of physical and chemical properties like velocity, turbulence, chemical composition, or concentration. To evaluate transient processes with steep changes in the concentration and velocity, like in plug flow reactors, stirring vessels or batch reactors correctly it is important to monitor process parameters at the same time and position. To characterize those flows of process streams in industrial plants, a system for simultaneous measurement of velocity and Raman spectra was presented in (Haddadi et al., 2018).

In this work the method for simultaneous measurement of velocity, composition, and concentration relying on well-known laser Doppler velocimetry (LDV) and Raman spectroscopy will be optimized and build in one measurement device using standard components. As presented in (Haddadi et al., 2018), both techniques were combined using the same laser as light source, making sure sampling from exactly the same position at the same time. In addition, a novel method allows to characterise the process flow 3-dimensional and gain directional information of the flow.

While in (Haddadi et al., 2018), the proof of concept was done using a commercial LDV and Raman spectrometer, in this work the LaserEye is a discrete built with standard components. Therefore, research on existing LDV and Raman spectrometer was done and the best option for combing them to a functional prototype were chosen.

To develop new ideas and optimized designs, limits and goals for the LaserEye have to be set. In industrial environment high loads of e.g., dust or vibrations may occur. The LaserEye device should be small, robust for industrial application and easy to build. To minimise maintenance, the design should be kept as simple as possible. This could be achieved by using as less parts as possible, renounce of moving parts and building the LaserEye in a sealed housing.

The LaserEye should have only one measurement opening from where it should be able to measure simultaneous the velocity and composition/concentration of a process stream, since in industry multiple openings in e.g., a pipe can be problematic due pressure, temperature or corrosive media.

The package size of the LaserEye should be small and compact within reasonable size, not only to handle it safely and easily mount it external on e.g., a pipe, but also to have a good trade of

between its size and performance, since the optical performance is lower with smaller optical components, especially mirrors.

For industrial use, the LaserEye has to be as cheap as possible. Therefore, different approaches are possible:

- Building the Lasereye with commercially available components which could result in lower performance due to possible incompatibilities of the used components to each other.
- Building the LaserEye custom made with selected matched components for high accuracy and different performances, depending on the used laser, which is one of the most expensive parts of the LaserEye.

For a custom made LaserEye, the lasers source will be selected to best fit for the process stream which should be measured, since the optical properties of industrial used substances strongly differ. Therefore, wavelength of the LaserEye is limited on one hand by the process stream which should be measured, e.g., for most hot gaseous streams infrared light (~1050nm) cannot be used. On the other hand, the measurement opening where the LaserEye should measure will mostly be quartz glass, since it withstands the typical chemicals and pressure occurring in process streams, which limits the wavelength to above UV light (~450nm). This limitation can be lowered by using the e.g., very expensive sapphire glass.

In industrial processes, solid, fluidic and gaseous process streams are common. The LaserEye should be able to handle all these process streams. To be able to measure the velocity in fluidic and gaseous process streams seeding particles might be necessary. These particles may exist in the process stream or must be added. For existing particles, the particle concentration is crucial, since if the concentration is too low, no light might be scattered and if the concentration is too high, the excitation beams might be blocked before reaching the focus point.

For surveillance of a process stream, it is important to know with which velocity the substances stream, in some cases in which direction the process stream goes and if the stream might has stopped (zero-point detection). One goal of the LaserEye will be to measure high velocities and the direction of the flow, so that turbulences can be detected and may be measured.

Since the LaserEye is an optical device, it needs an optical opening which could be either a sight glass or in an advanced version a fiber. Using a sight glass, the LaserEye would be independent of pressure, temperature or corrosivity of the process stream since it would be a non-invasive measurement. The focus point of the LaserEye can be freely adjusted when

measuring through a sight glass, so that not only scanning measurement is possible but also the measurement of different phases of a flow.

With the Raman spectrometer, all Raman active substances can be detected but it is most likely that due to the short measuring time only the main substances will be measured. One way to identify the Raman spectra, the measured spectra can be compared to the expected Raman spectra which allows fast measuring. Another way to identify the Raman spectra would be a classification where only unique peaks would be searched in a database while the slowest measuring of the Raman spectroscopy would be substance identification where the whole spectra must be compared with a database.

In this thesis, the LaserEye will be built for solid process streams and prepared for fluidic process streams, including building a flow channel as test environment and making first experiments with the flow channel.

2 Literature Research

In this thesis a measurement device consisting of a laser Doppler velocimeter, and a Raman spectrometer is presented. To select the appropriate measurement variant from the different existing laser Doppler velocimeters and Raman spectrometers, the state of the art methods in current literature and new ideas on Laser Doppler Velocimetry and Raman Spectroscopy will be discussed.

2.1 Laser Doppler Velocimeter

The Laser Doppler Velocimeter (LDV) is used for measuring velocity based on the Doppler effect. The Doppler effect describes the phenomena that a reflected wave (e.g., sound wave or light wave) changes its frequency based on the velocity of the object (target) it is reflected from when the observer remains on a fixed position, e.g., the changing sound of a passing-by train. Similarly, if a laser is focused on a moving target the irradiating beam is scattered. Due to an optical interference between the scattered light and the excitation beam, a beat wave develops, of which the Doppler frequency f_d could be measured. The frequency of the doppler shifted scattered light corresponds linear to the velocity of the target (Morita et al., 2016). Figure 1 (a) shows the measurement principle of a LDV and Figure 1 (b) the measured frequency.

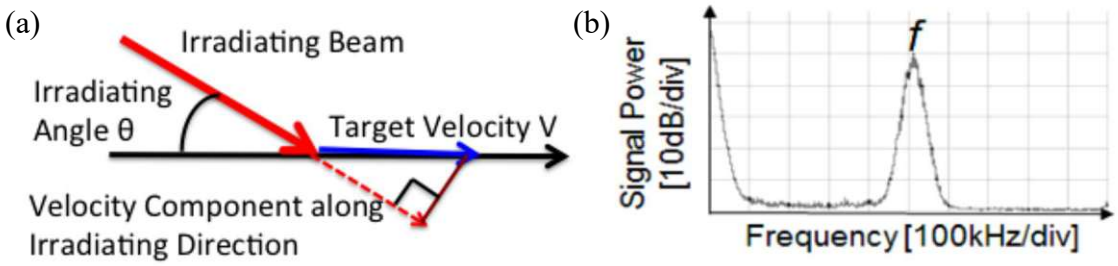

Figure 1: Principle of measurement (a) and observed Doppler-shifted frequency f_d (b) (Ibrahim et al., 2018)

In (Mikami & Fujikawa, 2016), the target velocity V for the case shown in Figure 1 is calculated by

$$V = \frac{f \cdot \lambda}{2 \cdot \cos\theta} \qquad (1)$$

where f (or f_d) is the measured Doppler frequency, λ is the irradiating beam wavelengths and θ is the irradiating angle.

In literature, several different measurement principles for Laser Doppler Velocimetry are known. The most important principles for this thesis will be discussed here.

Chan et al. (2019) published a LDV using one irradiating laser beam and measuring the Doppler shifted light thrown back the excitation beam path.

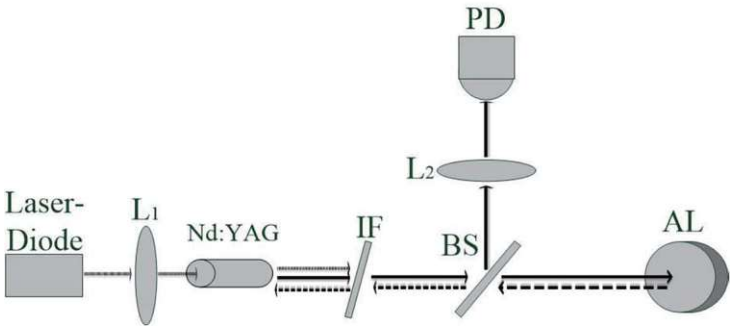

Figure 2: Setup of a LDV using one irradiating laser beam and measuring the Doppler shifted light thrown back the excitation beam path using the self-mixing effect (Chan et al., 2019)

In Figure 2 the laser diode is used to pump photons through lens L1 into the mirror coated neodymium doped yttrium-aluminium-garnet (Nd:YAG) crystal (Geusic et al., 1964) which produces the laser beam for the measurement. After passing the interference filter IF and the beam splitter BS, the excitation beam hits the turning aluminium target AL, where the Doppler shift occurs. The scattered Doppler shifted light then travels back into the Nd:YAG crystal where the self-mixing[1] effect in form of amplification of the frequency shifts take place, which will be focused through lens L2 and can be measured with the photo diode PD. Based on this principle but in a more compact design, (Ibrahim et al., 2018) placed the photo diode on the

[1] Self-mixing interference effect occurs when a portion of light emitted from a laser is backscattered from a movable target and re-enters into the laser cavity. The feedback optical field interacts with the gain medium and mixes with the light field inside the cavity, generating a modulation of both the amplitude and the frequency of the lasing field. (Ang, 2017)

back side of the laser crystal. Figure 3 shows the block diagram of this self-mixing laser Doppler velocimeter, where f_0 is the laser frequency and f_d is the Doppler frequency.

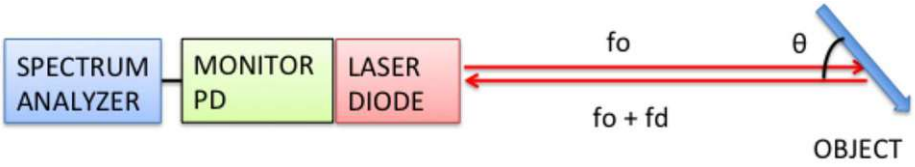

Figure 3: Block diagram of a self-mixing Laser Doppler Velocimeter (Ibrahim et al., 2018)

The velocity is calculated in (Ibrahim et al., 2018) through

$$V = \frac{f_d \cdot \lambda}{2 \cdot \cos\theta} \qquad (2)$$

where f_d is the measured Doppler frequency, λ is the irradiating beam wavelength and θ is the irradiating angle.

The measuring result of this LDV type is strongly dependent on the angle between target particle and laser beam, depending on the application this LDV is used for, the angle-dependency of the irradiation beam could be a major downside.

To get rid of the angle dependency of the "1-beam LDV", (Bin Muhamad et al., 2011) had shown a LDV design using two laser beams with the same frequency, forming a measurement volume in the cross section of their focus point, as irradiation beams and measure the Doppler shifted light thrown back the excitation beam path.

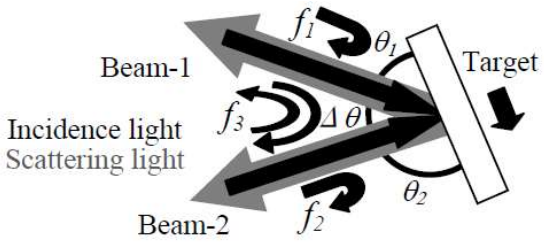

Figure 4: Principle of 2-beam LDV (Bin Muhamad et al., 2011)

Measuring the scattered Doppler shifted light of a cross section LDV, where the beat wave travels back the optical excitation path, the angle between beam 1 and beam 2 Δθ is used to calculate the velocity (Bin Muhamad et al., 2011):

$$V = \frac{\lambda}{2 \cdot sin\, \Delta\theta} \sqrt{f_1^2 + f_2^2 - 2 f_1 \cdot f_2 \cdot cos\, \Delta\theta} \qquad (3)$$

The third frequency f_3 appears because the moving object is placed on the cross-section of beam 1 (f_1) and beam 2 (f_2). This allows the scattering light from the moving object to return not only through the same original optical path but also through another optical path. It is defined in (Bin Muhamad et al., 2011) with

$$f_3 = \frac{f_1 + f_2}{2} \qquad (4)$$

Due to the use of the known angle Δθ between the two irradiation beams 1 and 2 the problem of the angle dependency is solved. On the other hand, the measurement of the Doppler shifted light is not easy since special laser sources are needed.

This issue can be solved by measuring the scattered Doppler shifted light directly from the cross section and not the scattered Doppler shifted light along the excitation paths (Morita et al., 2016).

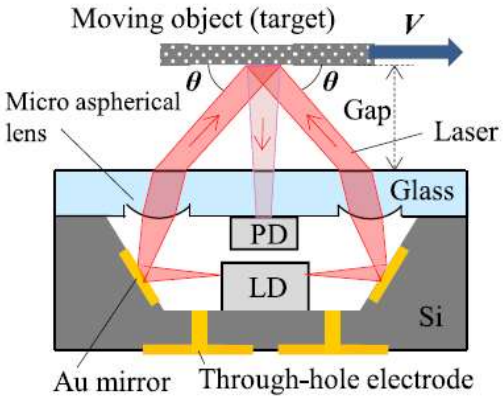

Figure 5: Measurement of Doppler shifted scattered light from cross section from 2 beam LDV (Morita et al., 2016)

In Figure 5 a laser diode LD produces two excitation beams which form a cross section on the target and the scattered light from the measurement volume is then analysed by a photo diode PD.

In (Morita et al., 2016) the velocity is obtained by calculating the beat frequency f_d with

$$\Delta f_L = -\frac{V}{\lambda} \cdot cos\Delta\theta,\ \Delta f_R = \frac{V}{\lambda} \cdot cos\Delta\theta \ and \ f_d = (f + \Delta f_R) - (f + \Delta f_L) = 2\frac{V}{\lambda} \cdot cos\Delta\theta \quad (5)$$

Where f_L and f_R are the measured Doppler shifted frequencies of the left and the right beams respectively and $\Delta\theta$ is the angle between the two laser beams. The velocity can be obtained through converting to

$$V = \frac{\lambda \cdot f_d}{2 \cdot cos\,\Delta\theta} \quad (6)$$

With the cross section 2-beam LDV, directional information can be obtained using different frequencies of the used excitation beams (Chen et al., 2018). This could be achieved by e.g., using a Bragg cell, a double frequency laser or a tuneable laser source.

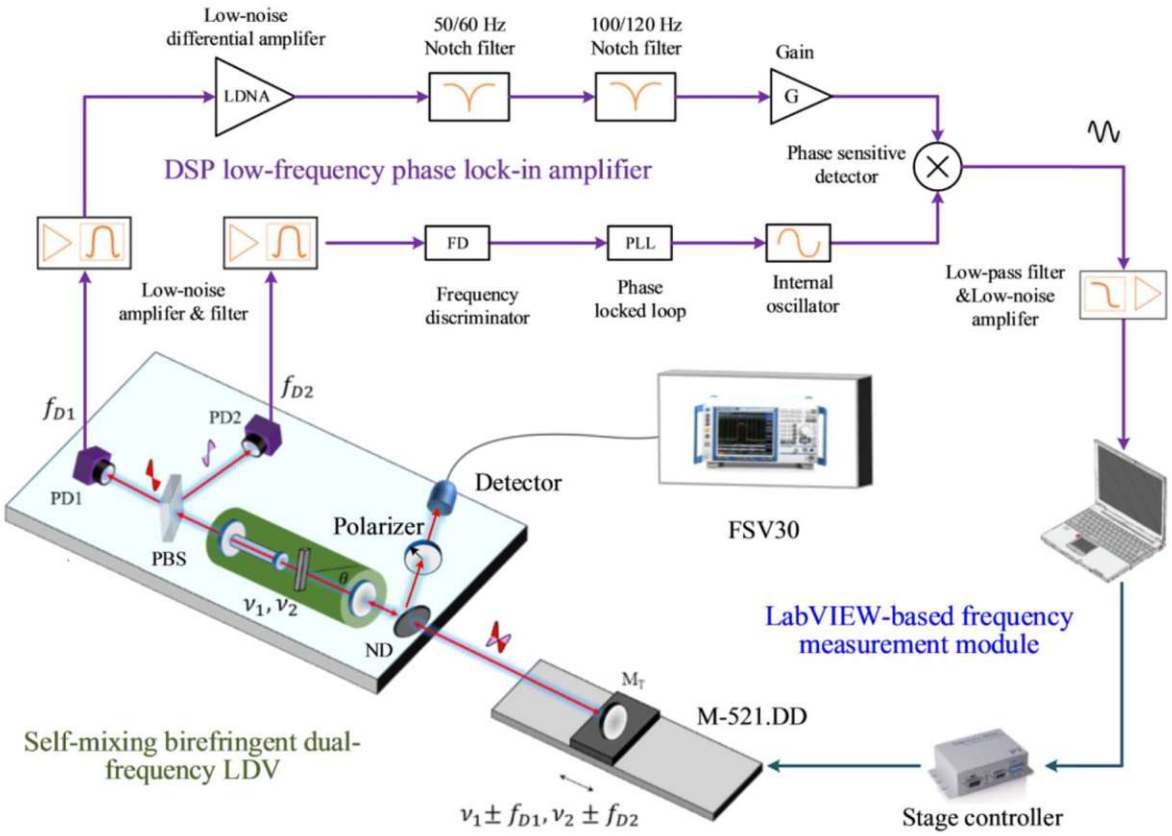

Figure 6: 2-beam cross section LDV with directional information (Chen et al., 2018)

In Figure 6, the laser beam emitted by a He-Ne laser with two orthogonally polarized dual frequency components ν_1, ν_2, is attenuated by a neutral density filter ND and then focused onto a linear in beam direction moving object MT. A portion of light, which is reflected by the object, propagated back into the lasing cavity, and interacts with the gain medium and the light field there. The interactions generate modulations of both the amplitude and the frequency of the two modes of the laser, thus introducing in the Doppler frequency shifts which can be detected by the photo diodes PD1and PD2. To separate the signal for PD1 and PD2, a polarized beam splitter PBS is used. The directional information is then derived from the inclination of the signal form, from a sinusoidal to a saw tooth distorted signal form.

To gain direction information more easily (Mikami & Fujikawa, 2016) suggest to use a 3-beam LDV.

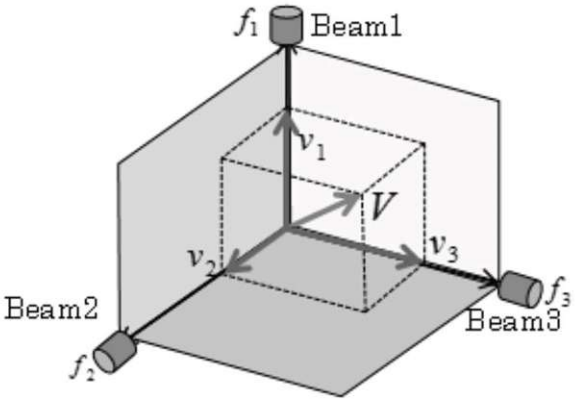

Figure 7: Measurement of Doppler shifted scattered light from cross section 3-beam LDV (Mikami & Fujikawa, 2016)

In Figure 7 (Mikami & Fujikawa, 2016) divided a laser beam into three beams by using conventional fiber couplers. These irradiation beams are set to be intersected perpendicularly to each other and therefore, each laser beam direction can be considered as one axis of one orthogonal coordinate system. The three beams of the laser are irradiated on a single spot on the moving target. The scattered light goes back through the same optical path as the conventional LDV and are interfered with the reference light beam. As a result, three Doppler shift frequencies f_1, f_2 and f_3 are simultaneously observed which can be used to calculate the component velocity

$$v_i = \frac{f_i \cdot \lambda}{2} \ (i = 1,2,3) \qquad (7)$$

And with the component velocity v_i the absolute value of the overall velocity V can be obtained with

$$V = \sqrt{v_1^2 + v_2^2 + v_3^2} \qquad (8)$$

This 3-beam LDV can measure the magnitude of the velocity and the direction of the velocity vector relative to the sensor head. The velocity on each beam axis is given as following, where θ_1, θ_2 and θ_3 are angles between the velocity vector and each axis.

$$v_i = V \cdot \cos \theta_i \qquad (9)$$

And therefore,

$$\theta_i = cos^{-1}\frac{v_i}{V} \qquad (10)$$

The scope of the LaserEye is to characterize a flow and determine its chemical composition. Therefore, it would be best to not only determine the velocity of the flow but also gather direction information. This could be archived by either using a 3-beam LDV as described by (Mikami & Fujikawa, 2016) or a 2-beam LDV with different frequencies of the excitation beams e.g., using a Bragg cell, tuneable laser or two laser sources as described in (Chan et al., 2019) or (Maru, 2011). Depending on the used LDV, multiple sensor heads could be required, so that the measurement from one position would not be possible.

2.2 Raman Spectroscopy

Raman spectroscopy is a molecular spectroscopic technique, used to identify molecules or substances. It was successfully demonstrated in 1928 by Sir C.V. Raman and K.S. Krishnan (Raman, 1928) by showing the inelastic scattering of light by a fluid. Since the effect of Raman scattering is very weak, the Raman scattered radiation is returned at a factor between 10^{-6} -10^{-8} of the energy input to the sample, Raman spectroscopy is mainly used in combination with a strong laser source.

When light is incident on matter, Photons can be absorbed or scattered. Absorption of light most likely occurs with infrared (IR) or ultraviolet (UV) radiation (Petry et al., 2003). While IR absorption results in the excitation of vibrational modes of the molecules, UV absorption results in the excitation of an electronic transition which is often followed by fluorescence phenomena.

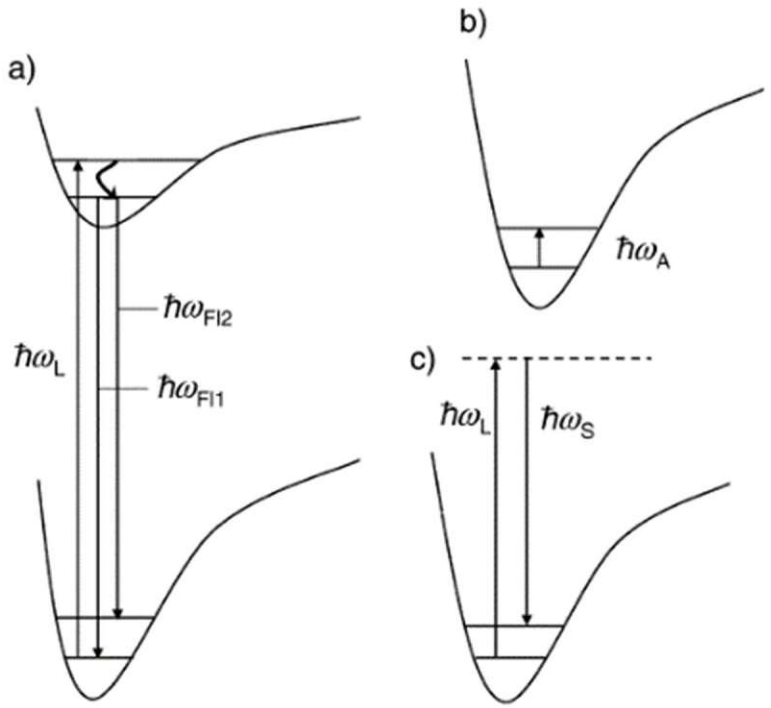

Figure 8: Simplified quantomechanical model illustrating the energy states of a) fluorescence, b) IR absorption, and c) Raman scattering (Petry et al., 2003)

Figure 8 shows the energy states of (a) fluorescence, (b) infrared absorption and (c) Raman scattering. While in fluorescence, an electron of the molecule, stimulated by the laser energy $\hbar\omega_L$, jumps to a higher energy state, and emits light $\hbar\omega_{FL1}$ and $\hbar\omega_{FL2}$ while falling back to its origin energy state, in infrared absorption the electron rises the energy level of the molecule by $\hbar\omega_A$ which leads to (characteristic) vibration of the molecule. In Raman scattering, an energy transfer occurs because of the coupling between the laser energy $\hbar\omega_L$ and the quantized states of the scattering system. Most of the scattered photons have the same wavelength as the incident photons which is called Rayleigh scattering, but a small fraction of light, approximately 1 out of 10^8 photons, is scattered at a different optical frequencies $\hbar\omega_S$ leading to inelastic scattering, which is called (spontaneous) Raman effect. Depending on the coupling, the incident photons either lose (Stokes) or gain (anti-Stokes) energy, which separates the Raman scattering in Stokes (lose) and anti-Stokes (gain) scattering, shown in Figure 9.

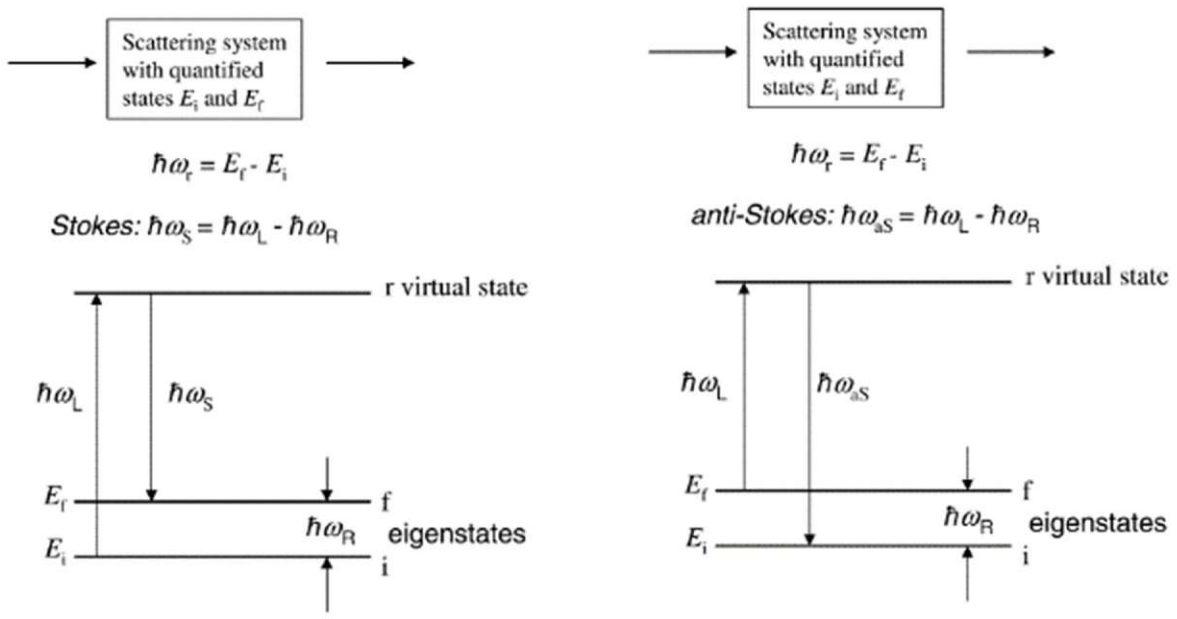

Figure 9: Model of Stokes Raman and anti-Stokes Raman scattering (Petry et al., 2003)

The Stokes Raman effect results from a transition from the lower energy state E_i to the higher energy state E_f, while the anti-Stokes effect results from a transition from the higher energy state E_f to the lower energy state E_i. The anti-Stokes intensity is less than the Stokes intensity because the anti-Stokes scattering occurs from an excited state E_f, which is, according to the Boltzmann distribution, less populated than the ground state E_i (Petry et al., 2003). Hence, in most cases the Stokes Raman spectrum is detected. The difference between Rayleigh Scatter, Stokes Raman Scatter and anti-Stokes Raman Scatter is shown in Figure 10.

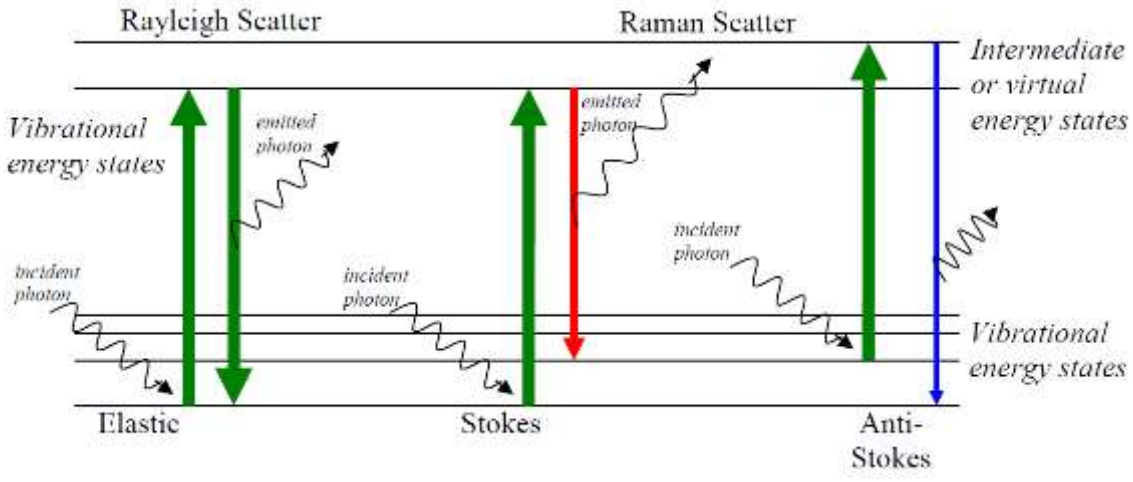

Figure 10: Rayleigh Scatter, Stokes and anti-Stokes Raman scatter (Nathaniel et al., 2011)

Monochromatic light (e.g. laser light) interacts with molecular vibrations or phonons, resulting in the energy of the source photons being shifted up (resulting in a lower frequency, Stokes shift) or down (resulting in a higher frequency, anti-Stokes shift) (Nathaniel et al., 2011). Since the total energy of the system remains constant after the molecule shift to a new state, the scattered photon will have a different energy, and therefore a different frequency which is characteristic for the molecule.

In (Barnett & Angel, 2017) a spatial heterodyne Raman spectrometer[2] is described which is a variant of a Michelson interferometer shown in Figure 11.

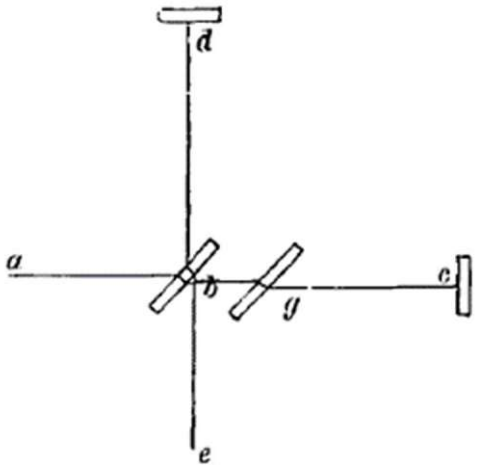

Figure 11: Michelson Interferometer (Michelson, 1910)

The Michelson Interferometer is using a beam splitter *b* to split the light from source *a* into two arms. Each of those light beams is reflected on mirrors *c* and *e* toward the beam splitter which then combines their amplitudes using the superposition principle, resulting in interference pattern which are directed to a detector *d*. To obtain interference fringes with a white-light source, the two optical paths must be equal for all wavelengths (Hariharan & Hariharan, 2007). Therefore, a compensating plate *g* is introduced in the second beam, which is not needed if a cube beam splitter is used.

The spatial heterodyne Raman spectrometer described in (Barnett & Angel, 2017) uses two stationary diffraction gratings, G_1 and G_2 (Figure 12) replacing the mirrors of the Michelson Interferometer. In Figure 12 the laser hits the sample S where light is scattered. The scattered

[2] A spatial heterodyne Raman spectrometer samples the entire interferogram simultaneously in the spatial domain. Since each spectral element at the input is modulated by a unique spatial frequency at the output, the fringe image is a constant plus the Fourier transform of the input spectrum about the heterodyne wavelength (the wavelength producing parallel output wave fronts) (Englert et al., 2010).

light is collected with lens L_1, and the laser light is filtered with an optical filter F so that only the light waves containing the Raman spectrum W_1 remains. The beam splitter BS splits the light waves W_1 equal to the diffraction gratings G_1 and G_2.

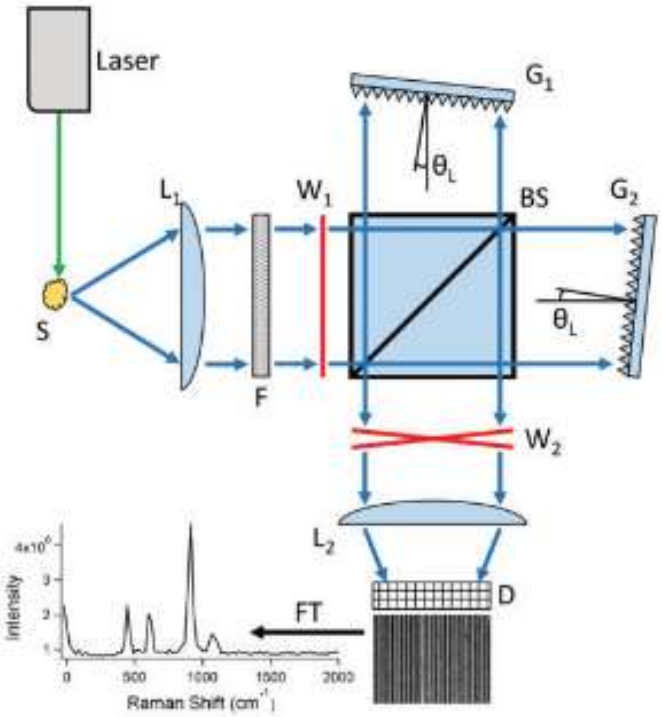

Figure 12: Spatial heterodyne spectrometer based on (Barnett & Angel, 2017)

The face normal of the diffraction gratings is tilted by the Littrow angle θ_L, such that one wavelength, the Littrow wavelength, satisfies the Littrow condition and diffracts along the same optical path as the input light. The Littrow condition is given by (Nevie et al., 1999)

$$sin\,\theta_L = \frac{\lambda}{2d} \qquad (11)$$

where θ_L is the Littrow angle, d is the distance between the grooves of the grating and λ is the wavelength of the laser. All other wavelengths of light diffract at wavelength-specific angles, inducing a wavelength-specific wavefront tilt. When the tilted wavefronts recombine through the beam splitter, the crossed wavefronts W_2 from each diffraction grating induce a spatial phase shift along the dispersion plane of the gratings, causing interference to occur, thus producing a set of Fizeau fringes[3]. The plane of the diffraction gratings is imaged with a lens L_2, onto an array detector D. The Fourier transform of these fringes recovers the spectrum.

[3] Spatial fringes named after Armand Hippolyte Louis Fizeau (1819-1896), a French physicist (Kajava et al., 1993)

The resolving power of the spatial heterodyne Raman spectrometer is determined by the number of grooves of the diffraction grating illuminated and is not a strong function of the entrance aperture size. Thus, very small diffraction gratings can be used while maintaining high resolution and high light throughput.

A simplified version of this spatial heterodyne spectrometer is presented in (Egan et al., 2020), where one grating is substituted with a mirror M1.

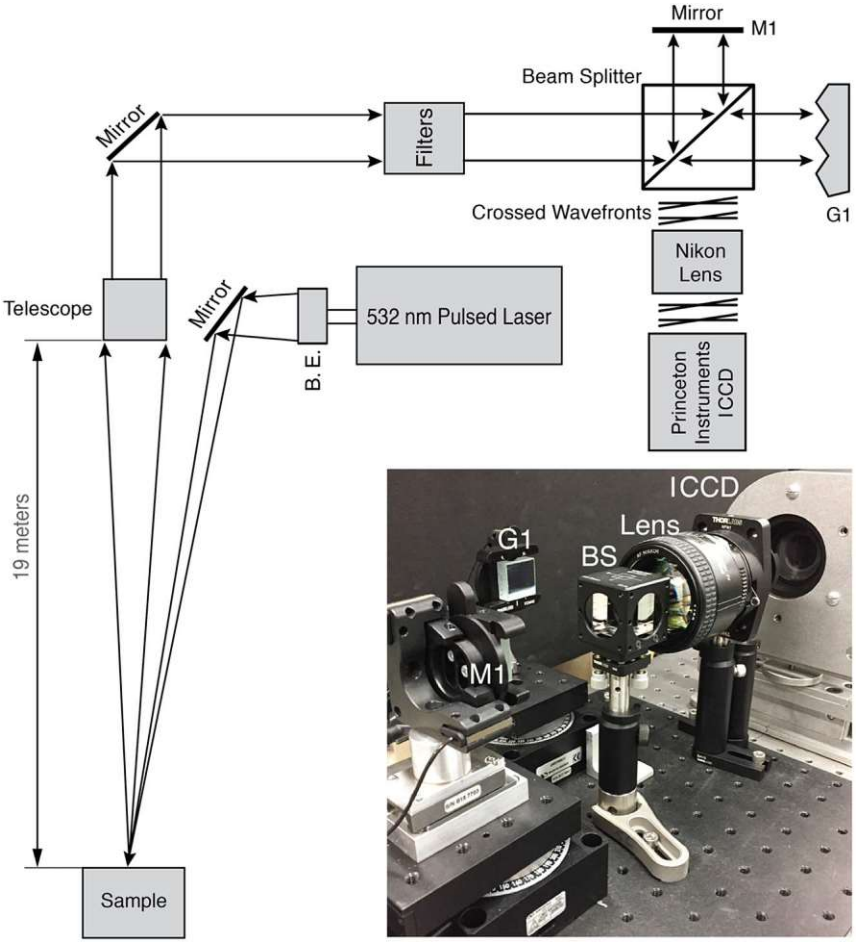

Figure 13: Spatial heterodyne spectrometer based on (Egan et al., 2020)

The working principles of the spatial heterodyne spectrometer shown in Figure 13 are the same as from (Barnett & Angel, 2017). When light enters the spatial heterodyne spectrometer, it is reflected off diffraction gratings at wavenumber-dependent angles. The gratings produce crossed wavefronts which can be detected as spatial interference fringes and can be converted to a spectrum using Fourier transformation. Using one grating instead of two in an Spatial Heterodyne Spectrometer (SHS) leads the detector to record a larger number of photons, since light in the mirror arm is not diffracted into orders outside the field of view of the detector (Egan

et al., 2020). Also, the bandpass of this spatial heterodyne spectrometer is doubled, whereas the spectral resolution is cut in half.

Another type of Raman spectrometer is presented in (Harris et al., 2010), shown in Figure 14.

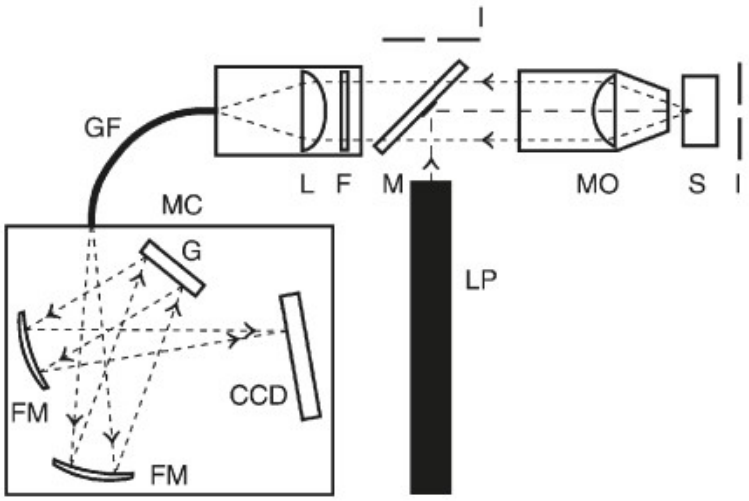

Figure 14: Raman spectrometer (Harris et al., 2010)

The light of the laser source *LP* is turned by 90° by a small mirror *M* and coupled into a microscope objective *MO*. The achromatic objective focuses the laser light onto the sample *S*. Raman backscattered light is collimated by the same objective. To block unwanted Rayleigh scattered light from the detector, backscattered light passes through a filter *F* and is then focused with a lens *L* into a fiber *GF*. The fiber transmits Raman scattered light to a monochromator *MC* with an entrance slit, holographic grating G, and a CCD detector. The focusing mirrors FM adjust the light path on the grating. For better resolution, more complex monochromators can be used as presented in (Li et al., 2014).

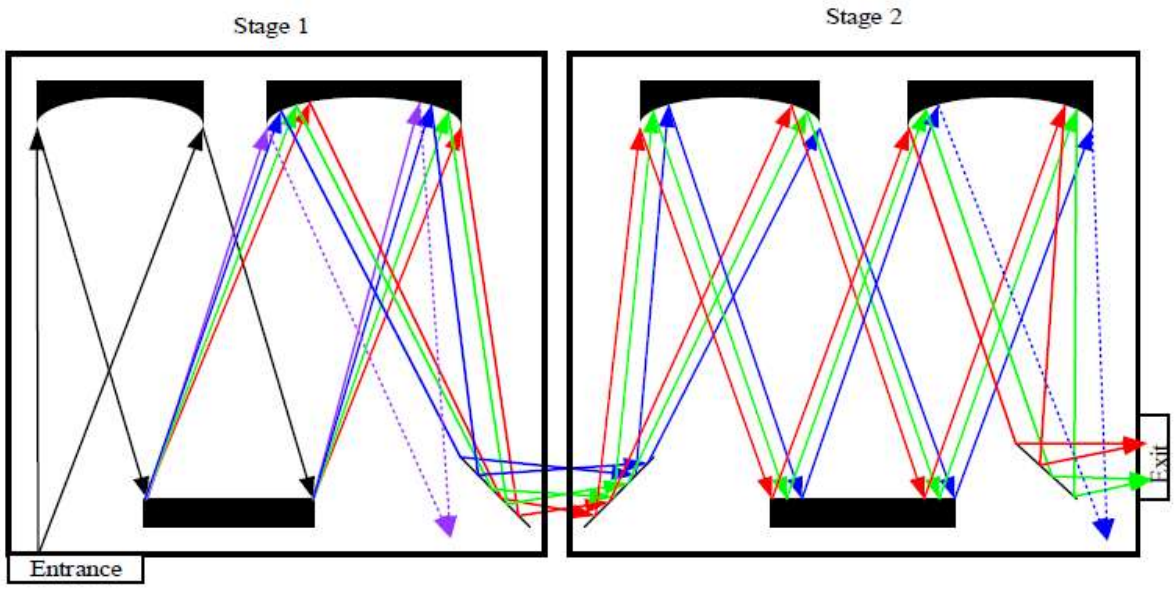

Figure 15: Additive double monochromator (Li et al., 2014)

Rayleigh light rejection and spectral decomposition can be achieved by using a multistage monochromator. In case of double monochromators as shown in Figure 15, the dispersion caused by the second monochromator can be added or subtracted from the dispersion of the first monochromator (Li et al., 2014). The rejection of Rayleigh light in a multistage monochromator is realized by using intermediate slits to block some of the unwanted wavelength band. This principle can be continued by using e.g., a triple monochromator, which has higher Rayleigh rejection than a double monochromator. Although the multistage monochromator achieves high stray-light rejection and permits the measurement of Raman signals very close to the laser wavelength, this is compromised by the large size, complex configuration, high cost and loss of throughput (Li et al., 2014).

3 Design of the Prototype

Since Raman light and LDV light are complementary filtered parts of the total scattered light, the development of the prototype should be done in different stages, where the first stage would concentrate on the LDV measurement and the second stage on the Raman Spectrometer. In a first approach, the measurement was done using some controlled spinning discs and later a fluid moving in a channel. Since a first draft of design of the new LaserEye existed, it was obvious to improve this draft.

In the beginning of the work on this thesis, a Proof of Concept (PoC) was done in (Haddadi et al., 2018). Also, a non-functional demonstration unit for a compact combined LDV and Raman spectrometer, titled as LaserEye (single probe, one-directional) existed which was the starting point of this work. The schematic of this probe can be seen in Figure 16, where Figure 16 (a) show the beam deployment and Figure 16 (b) the detection unit. The beam deployment optic was implemented using a laser source (532 nm), a fiber coupler K1, a fiber beam splitter and two collimators K2, K3, while the detection optic consists of a telescope K4, a splitting unit K5, S1 to separate the LDV-light from the Raman light, a photodiode to receive the LDV signals and a focus lens K6 to bundle the Raman light on the spectrometer input.

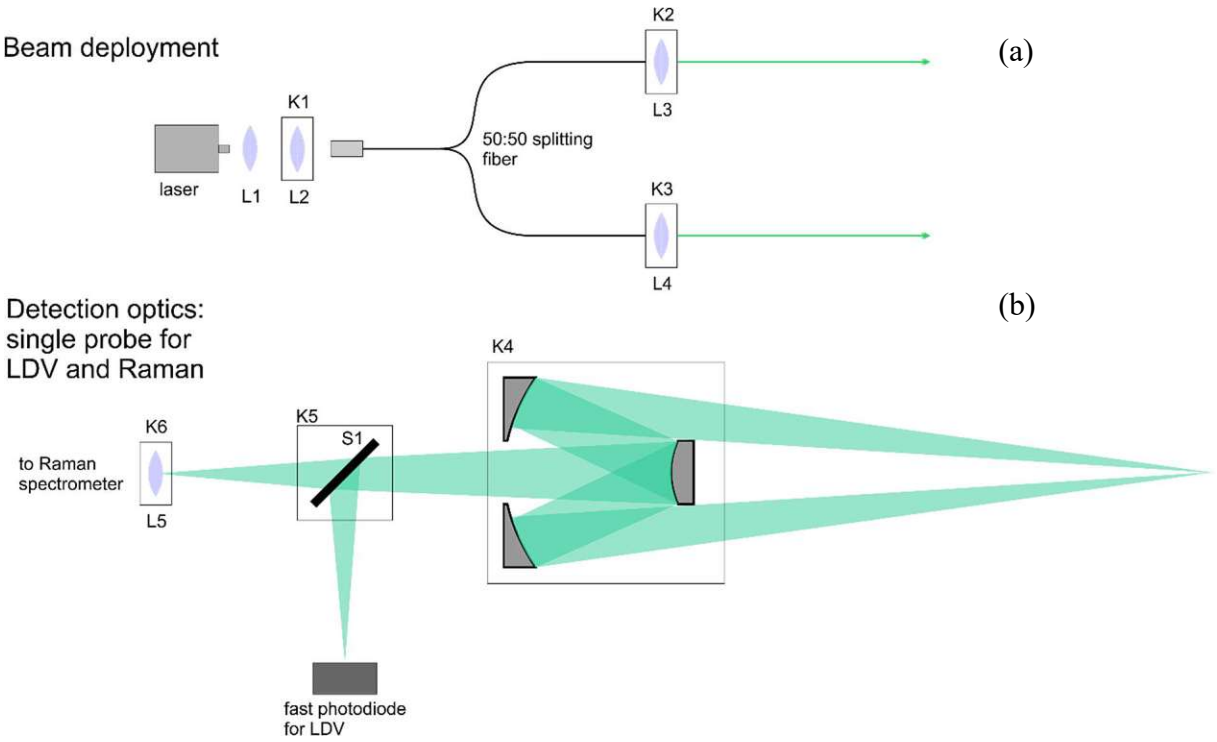

Figure 16: Schematic of the beam deployment (a) and detection optic (b) of the first Laser Eye showcase unit

One of the main problems of that first test setup had been, that the collimators from the fibre outlet where off focus, so that no measurement was possible. Also, the design is not favourable due to the loss of the scattered light, caused by the shadow of the intern mirror in telescope (see Figure 16 b). The probe can be seen in Figure 17.

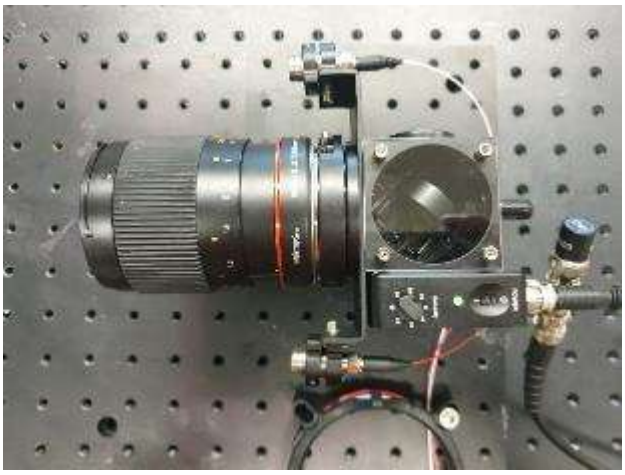

Figure 17: Existing probe at the start of the project

As Raman Spectroscopy is one of the key features of the LaserEye setup, lenses in the path of the scattered light should be avoided since the scattered laser light might produce new Raman spectra while passing through the glass of the lenses. Therefore a “lens-less” draft existed, where “lens-less” refers only to the path of the scattered light, which is crucial for the Raman Spectroscopy, not containing lenses. The starting draft can be seen in Figure 18.

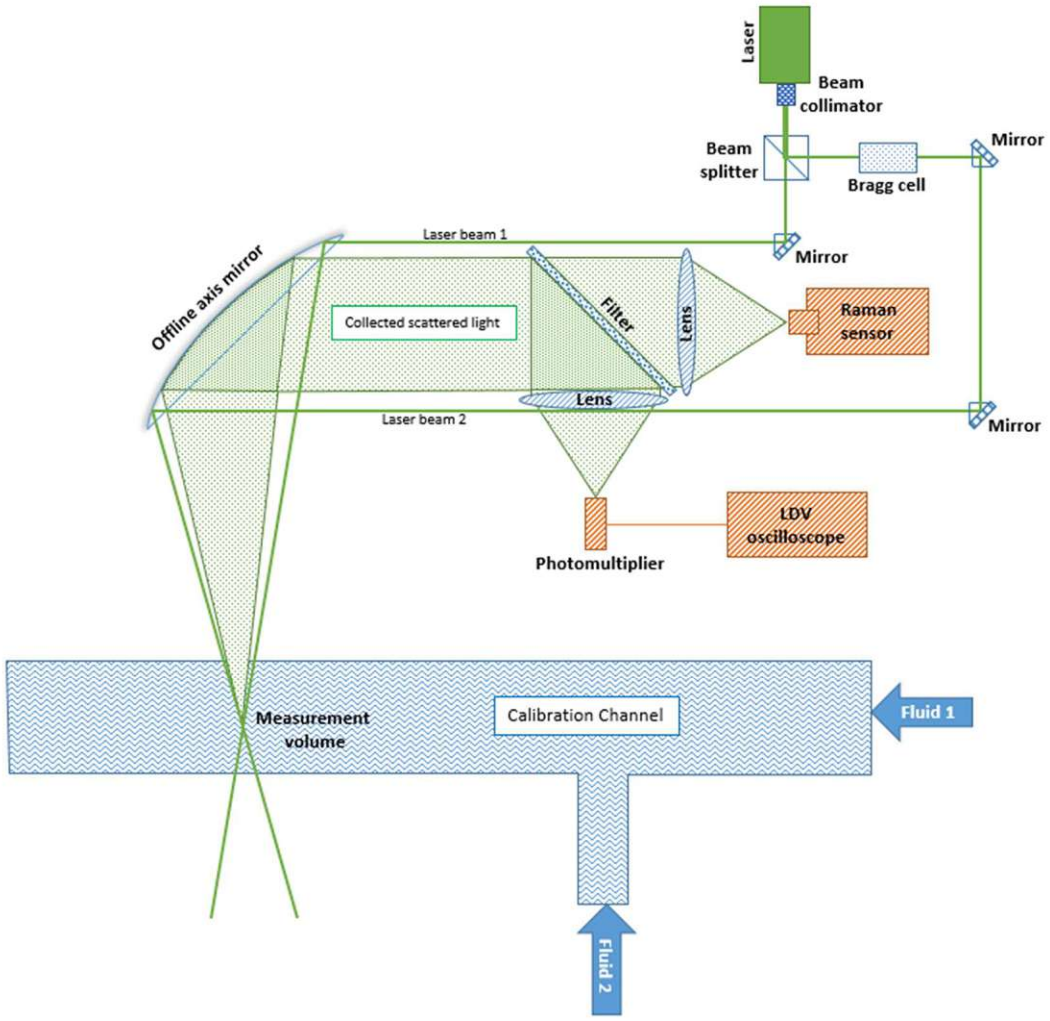

Figure 18: Existing design of the “lens-less” LaserEye

One of the major issues of this draft was, that it used a Bragg cell for frequency modification of the laser light which is not only rather expensive but also inflict a lot of optical losses in one optical path. Also, with a slightly reorganization of the design, two mirrors (each in one arm after the beam splitter) could be saved. Another issue would be the usage of a lens in front of the Raman spectrometer, which is a side effect of using an external commercial Raman spectrometer.

3.1 Layout/Design – laser Doppler velocimeter

In the previous chapter different approaches for a LDV have been introduced, including a 3-beam LDV as presented by (Mikami & Fujikawa, 2016) or a 2 beam LDV with different frequencies of the excitation beams as described in (Chan et al., 2019) or (Maru, 2011). Therefore, multiple possibilities for the design of the LDV, suitable for the LaserEye exist and will be discussed below.

(i) 2-beam LDV with two sensors

Instead of using a fiber system with a telescope, a mirror system will be used with the advantage, that this lens free[4] design will provide collimated and cleaned light for further analysis. Inspired from (Mikami & Fujikawa, 2016) and (Morita et al., 2016), a system using two sensors was developed to gain direction and velocity information.

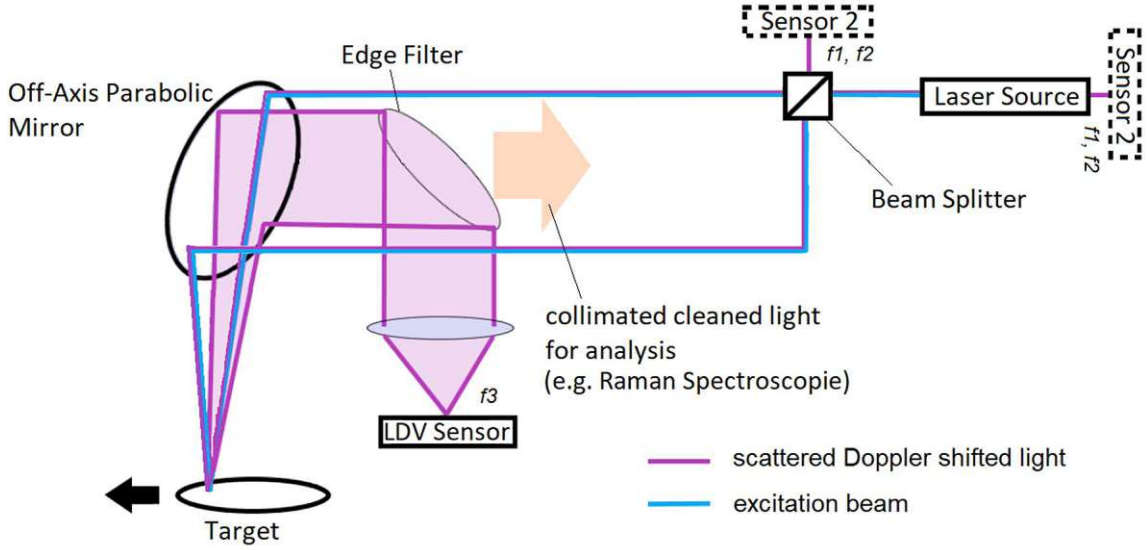

Figure 19: Measurement principle of 2-beam LDV with two sensors, where sensor 2 can either use the self-mixing effect of the laser or by the beam splitter

[4] Lens free means, before the scattered light is split in Rayleigh and Raman light, the scattered light don´t cross a lens

An excitation laser beam is split in two beams which hit an off axis parabolic (OAP) mirror. The OAP mirror focuses the laser beams on one point creating a cross section. Doppler shifted scattered light will occur as:

- scattered light traveling back the optical path of the excitation beams (f_1, f_2)
- light of the cross section (f_3) scattered in all directions

The frequency of the scattered light of the optical paths and directly from the cross section will differ. The frequency of the Doppler shifted scattered light from the cross section depends on the velocity of the test object and the angle between the test object and the laser beams hitting it, while the frequency of the Doppler shifted scattered light from the optical excitation beam path is depended on the velocity V of the test object and the angle between these two beams.

If the velocity is known from the second sensor, the angles can be calculated from the frequencies obtained from the first sensor, which will give direction information. Therefore, if all frequencies are measured, the direction and the velocity of the test object can be determined.

The velocity V of the test object is known by sensor 2 (Morita et al., 2016),

$$V = \frac{f_d \cdot \lambda}{2 \cdot cos\,\theta} \qquad (12)$$

Where θ is the angle between beam axis and target (velocity vector). From sensor 1 the velocity information for each beam can be obtained (Mikami & Fujikawa, 2016):

$$v_1 = \frac{f_1 \cdot \lambda}{2} = V \cdot cos\,\theta_1\,,\ v_2 = \frac{f_2 \cdot \lambda}{2} = V \cdot cos\,\theta_2 \qquad (13)$$

And further

$$\theta_1 = cos^{-1}\frac{f_1 \cdot \lambda}{2 \cdot V},\ \theta_2 = cos^{-1}\frac{f_2 \cdot \lambda}{2 \cdot V} \qquad (14)$$

Where θ_1 and θ_2 are the angles between velocity vector and each beam-axis. Therefore, the two angles of the velocity vector are known.

This method would have the advantage, that direction information could be gathered with a 2-beam LDV without Bragg cell or other frequency manipulation and that the scattered light directly from cross section don´t need amplification since a big amount of light is collected with the mirror. Therefore, velocity measurement is also possible with only few scattered photons. This method only gives information of two directions, which could or could not be sufficient,

depending on the application used, e.g., for surveillance of paper rolls in paper production, this method would be sufficient.

This concept would provide the following advantages:

- Combination of measurement of scattered light directly from cross section and from the excitation path with two different sensors
- Usage of two different spectra, which occur due the combination of two different measurement methods using the dependency of the velocity from different angels
- The information in these spectra, contains not only the velocity but also the direction of the particle movement

This concept only provides information in one direction.

(ii) 3-beam LDV

Inspired by the 3-beam LDV described in (Mikami & Fujikawa, 2016), where a 3-dimensional LDV with only one laser source and without frequency shift of the partial beams was presented, the following layout was developed.

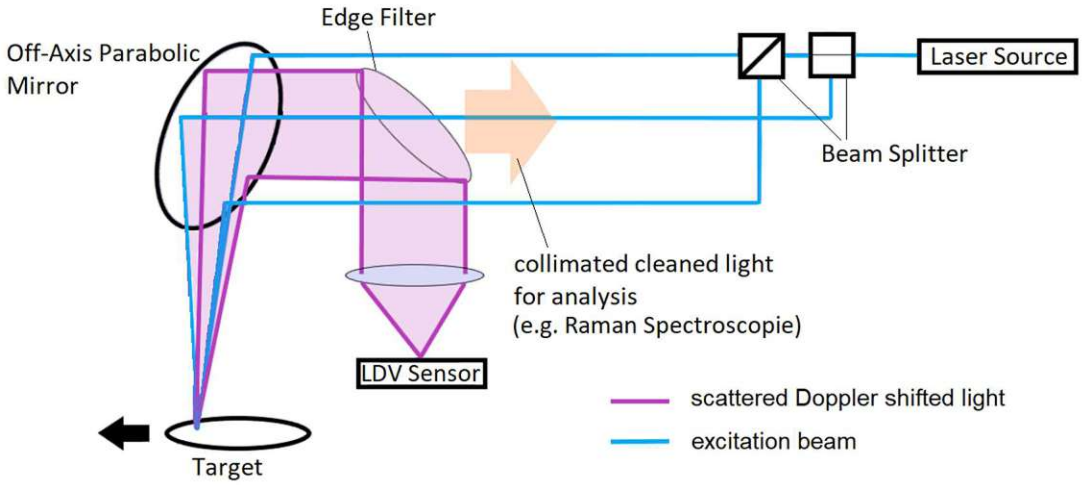

Figure 20: Measurement principle of 3-beam LDV with one Sensor

The scattered light occurring can be seen as three 2-beam LDV. With this, the angles used to calculate the velocity would be $\Delta\theta_i$ in Figure 21.

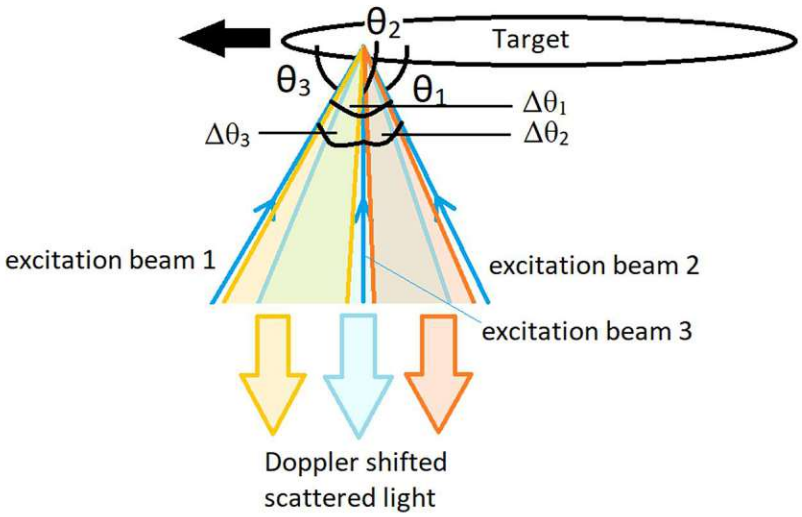

Figure 21: Scattered Doppler shifted light from 3-beam cross section LDV

When collecting the scattered light from the cross section, three different frequencies occur if the three excitation beams have different angels to each other ($\Delta\theta_1$, $\Delta\theta_2$, $\Delta\theta_3$), which could be interpreted as three 2-beam LDVs with shared excitation beams. Therefore, the calculation of the velocity is like the calculation from Sensor 2 of the 2-beam LDV

$$v_i = \frac{f_i \cdot \lambda}{2 \cdot \cos \Delta\theta_i} \quad (15)$$

The problem here is, that the corresponding frequency f_i to the angle $\Delta\theta_i$ is unknown. Therefore, a shutter-system will be introduced in the next layout.

Since v_i (i=1,2,3) is the particle (test object or target) velocity in the axis of the two beams which enclose $\Delta\theta_i$, the overall velocity can be calculated with

$$V = \sqrt{v_1^2 + v_2^2 + v_3^2} \quad (16)$$

(iii) 3-beam LDV with shutter and one sensor

The frequency of the measured scattered light from the 3-beam LDV belonging to the corresponding beam pair is unknown. Therefore, fast shutters to measure particles (test objects

or targets) with short dwell time could be used to determine which peak accords to which beam pair. If one beam is covered by a shutter, the remaining peak belongs to the remaining beam pair. Therefore, at least two shutters would be sufficient to find all corresponding peaks and beam-pairs.

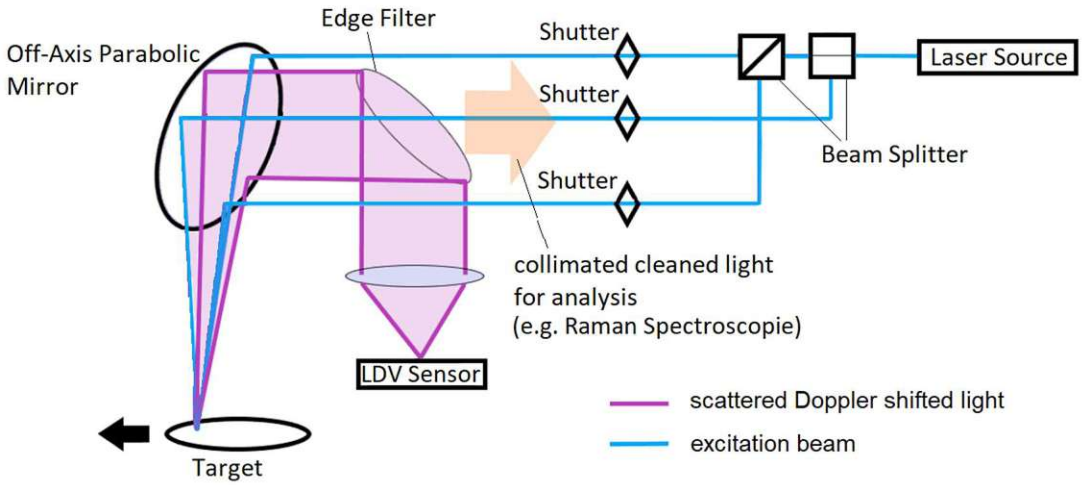

Figure 22: Measurement principle of 3-beam LDV with shutter

(iv) 3 beam LDV with shutter and two sensors

Going back to the first concept (i) presented above, a combination of the introduced 3-beam LDV with shutters and two sensors could have some advantages. The information of direction and velocity from the 3-beam LDV where calculated from the scattered Doppler shifted light traveling back the excitation beam path in (Mikami & Fujikawa, 2016). But also, the scattered light collected directly from the cross section ("LDV-sensor" or "sensor 1" in Figure 24) described here delivers three different frequency peaks (if the excitation beam angles are different). In Figure 23 the occurring scattered light is shown.

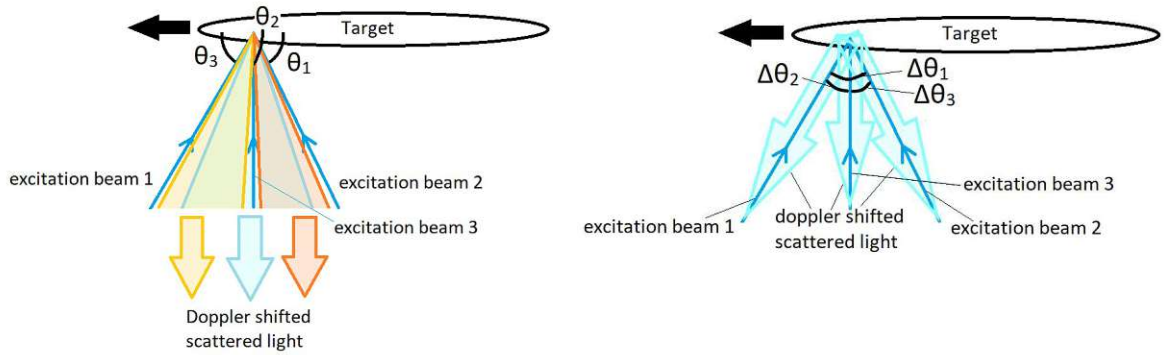

Figure 23: Scattered Doppler shifted light from 3-beam cross section LDV

When collecting the scattered light from the cross section on sensor 1, three different frequencies occur due to the three different excitation beam angles, which could be interpreted as three 2-beam LDVs with shared excitation beams. These frequencies are depending on the angle between the excitation beams, while the frequencies of the scattered light traveling back the excitation beam path depend on the offset angle between target (particle) and beam.

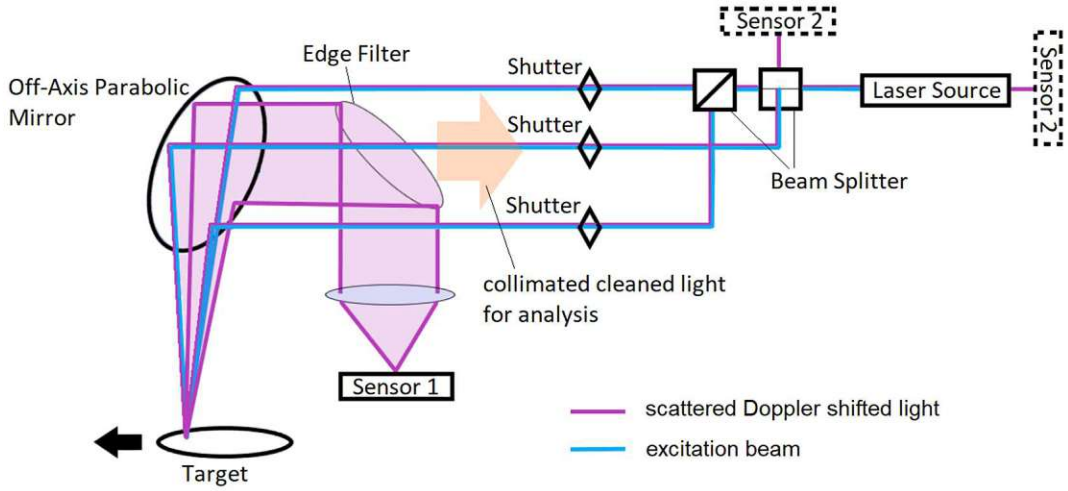

Figure 24: Measurement principle of 3-beam LDV with shutter and two sensors

One way the velocity information of the target can be obtained is by using sensor 2. When one beam is covered, the two frequencies occurring at sensor 2 are like from a 2-beam LDV with

the scattered light travelling back the excitation path and therefore, the velocity is given by (Bin Muhamad et al., 2011)

$$V = \frac{\lambda}{2 \cdot \sin \Delta\theta} \sqrt{f_1^2 + f_2^2 - 2 \cdot f_1 \cdot f_2 \cdot \cos \Delta\theta} \quad (17)$$

Another way to gain the velocity information could be using the formula given in (Mikami & Fujikawa, 2016):

$$v_1 = \frac{f_1 \cdot \lambda}{2} = V \cdot \cos \theta_1 \, , v_2 = \frac{f_2 \cdot \lambda}{2} = V \cdot \cos \theta_2 \, , v_3 = \frac{f_3 \cdot \lambda}{2} = V \cdot \cos \theta_3 \qquad (18)$$

And converted, the angle of the velocity vector by:

$$\theta_1 = \cos^{-1} \frac{f_1 \cdot \lambda}{2 \cdot V}, \theta_2 = \cos^{-1} \frac{f_2 \cdot \lambda}{2 \cdot V}, \theta_3 = \cos^{-1} \frac{f_3 \cdot \lambda}{2 \cdot V} \quad (19)$$

The velocity V can be obtained using sensor 1

$$v_i = \frac{f_i \cdot \lambda}{2} \; (i = 1,2,3) \qquad (20)$$

$$V = \sqrt{v_1^2 + v_2^2 + v_3^2} \qquad (21)$$

3.2 Layout/Design – Raman Spectrometer

Because of its easy, simple and low-cost implementation, the chosen Raman spectrometer layout is based on (Egan et al., 2020) 1-grating 1-mirror spatial heterodyne Raman spectrometer (SHRS). It can be built with flat standard components and does not need concave mirrors. Also, it can be effortlessly changed to the 2-grating SHRS as presented in (Barnett & Angel, 2017) for better (double) spatial resolution.

The spatial heterodyne Raman spectrometer described in (Egan et al., 2020) guides the Raman scattered light to the spatial heterodyne interferometer where the amplitude is divided 50/50 by a cube beam-splitter into two equidistant arms of the interferometer (Figure 13). In one arm of the interferometer, a λ/10 plane mirror reflects the incident light, in the other arm, a diffraction grating of minimum 150 grooves/mm diffracts the light at wavenumber-dependent angles, thus creating path length differences that can be sampled at the output of the interferometer. In the Littrow condition, the wavenumber of light which angle of incidence and reflectance upon the diffraction grating are equal, is retro-reflected from the grating, producing a planar wavefront of constant intensity across the intensified charge-coupled device (ICCD). Wavenumbers not equal to the wavenumber of light whose angle of incidence and reflectance upon the diffraction

grating are equal are diffracted at angles relative to the optical axis, which recombine as crossed wavefronts in space at the beam-splitter, producing cosinusoidal spatial fringes. The crossed wavefronts at the grating surface were imaged by a camera lens and recorded by an ICCD. The Raman spectrum is recovered after applying the FT upon the interferogram and windowing the regions of the FT that contain Raman peaks.

3.3 Layout/Design – Selection of the layout

From the above presented LDV layouts, (ii) 3-beam LDV layout was chosen to be built. Because of the advantage of 3-dimensional and directional information and the possibility to extend it to the concept of (iii) and/or (iv), it seemed the best choice for the scope of this thesis.

For the Raman spectrometer, the simple grating simple mirror SHRS was chosen due its easy and low cost built (compared to classic monochromator).

The complete layout is shown in Figure 25.

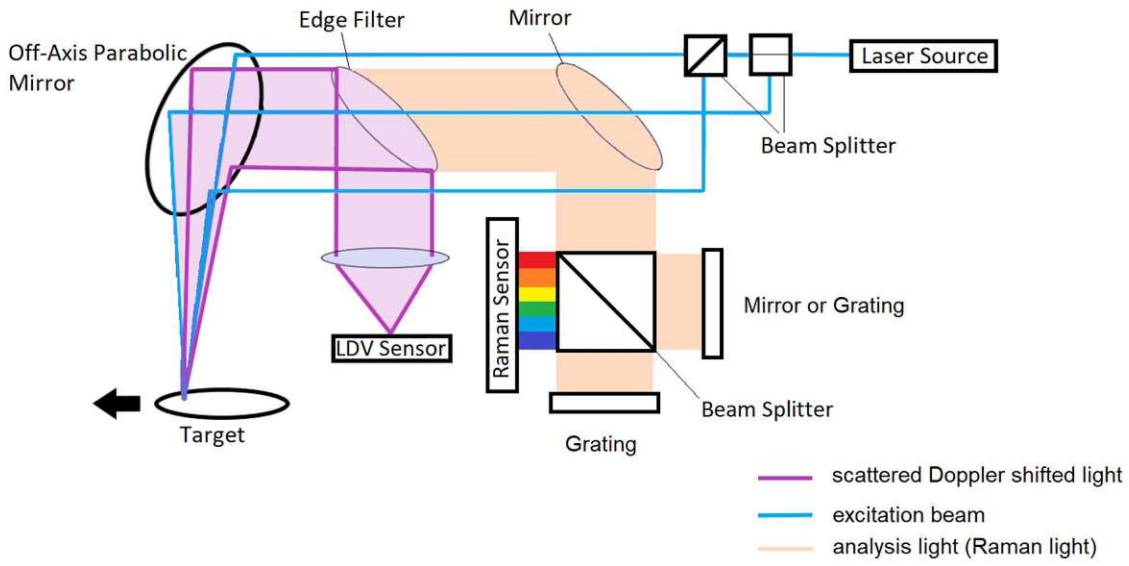

Figure 25: Schematic of the LaserEye

3.4 Simulation

The goal of the simulation was to prove if the design is basically working and determine the necessary components and their specifications.

The simulation of the new designs was done with the computer program FRED (Photon Engineering, n.d.). This optical simulation software was chosen after evaluating multiple optical simulation software because it fitted all needs for this thesis, e.g., a database of optical components from most of the big vendors or the import possibility of new optical components, which are often provided by the vendors, and finally, it offers free temporary licences for students.

After the data of the components, provided by the vendor, had been imported into FRED, the chosen LDV design was built. Therefore, the spaces between the components had been calculated from the drawings resulting in a path length of approximately 400 mm, where the three optical paths of the excitation beams are nearly equidistant. For the laser source, various laser diodes had been simulated. In Figure 26 the green and red beams are the excitation beams while the purple beams are the scattered light. Figure 26 shows the LDV in a two-beam configuration (a), a three-beam configuration (b) and the scattered light of the three-beam configuration (c). For the surface where the light scatters, the data of an aluminium surface was used.

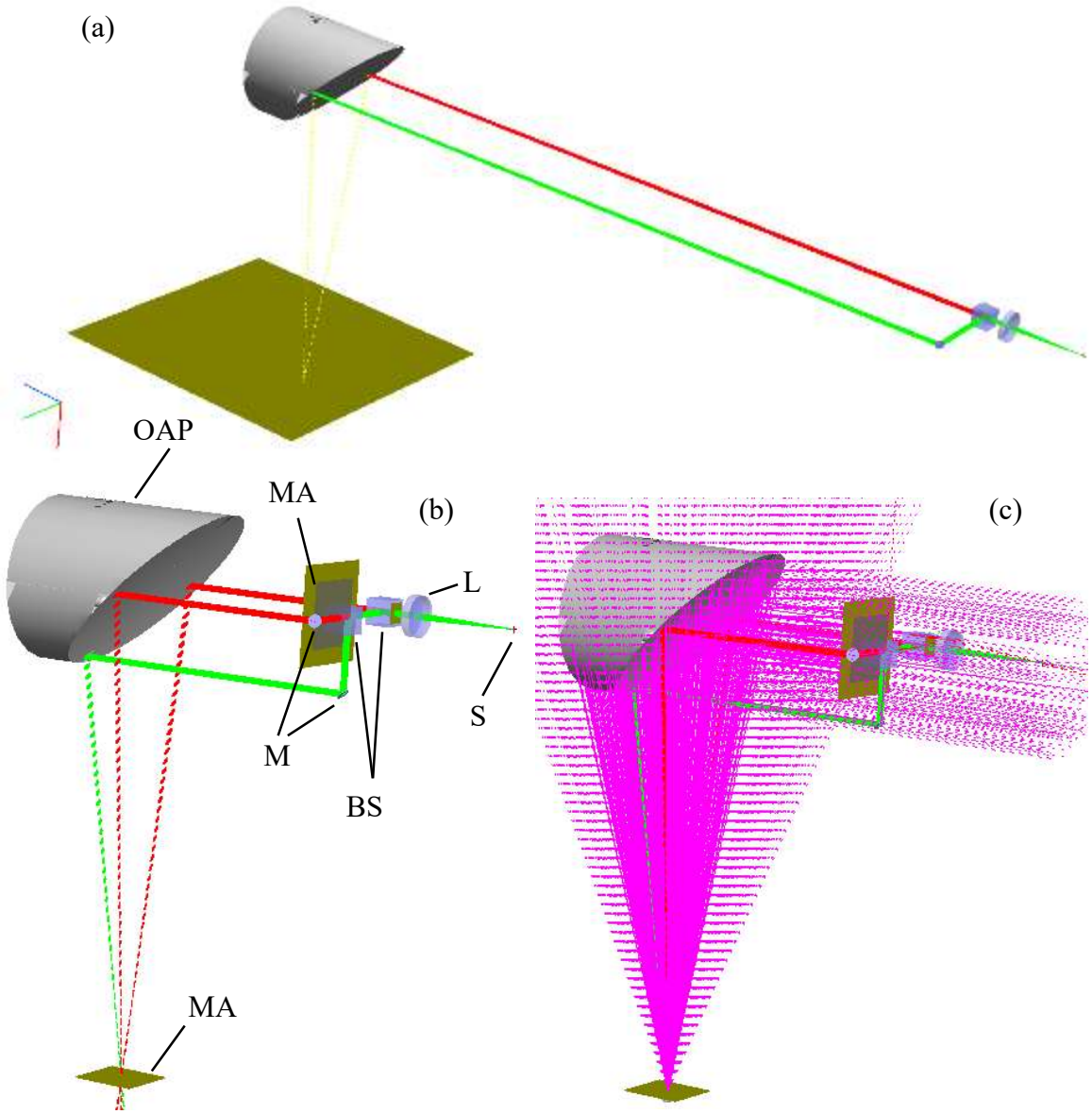

Figure 26: FRED Simulation of the LDV in a two-beam configuration (a), a three-beam configuration (b) and the scattered light of the three-beam configuration (c)

From the punctual laser source *S*, the beam propagates to the collimation lens *L* and is then split 30/70 in two arms by the first beam splitter *BS*. The light of the 30 % arm hits the off axis parabolic mirror *OAP* and is focused on the target, The light of the 70 % arm is divided by a further 50/50 beam splitter *BS* and it also travels over plane mirrors *M* on the off axis parabolic mirror *OAP*, which focuses these beams on the same point of the target as the first beam. The squares in Figure 26 are measurement areas *MA*.

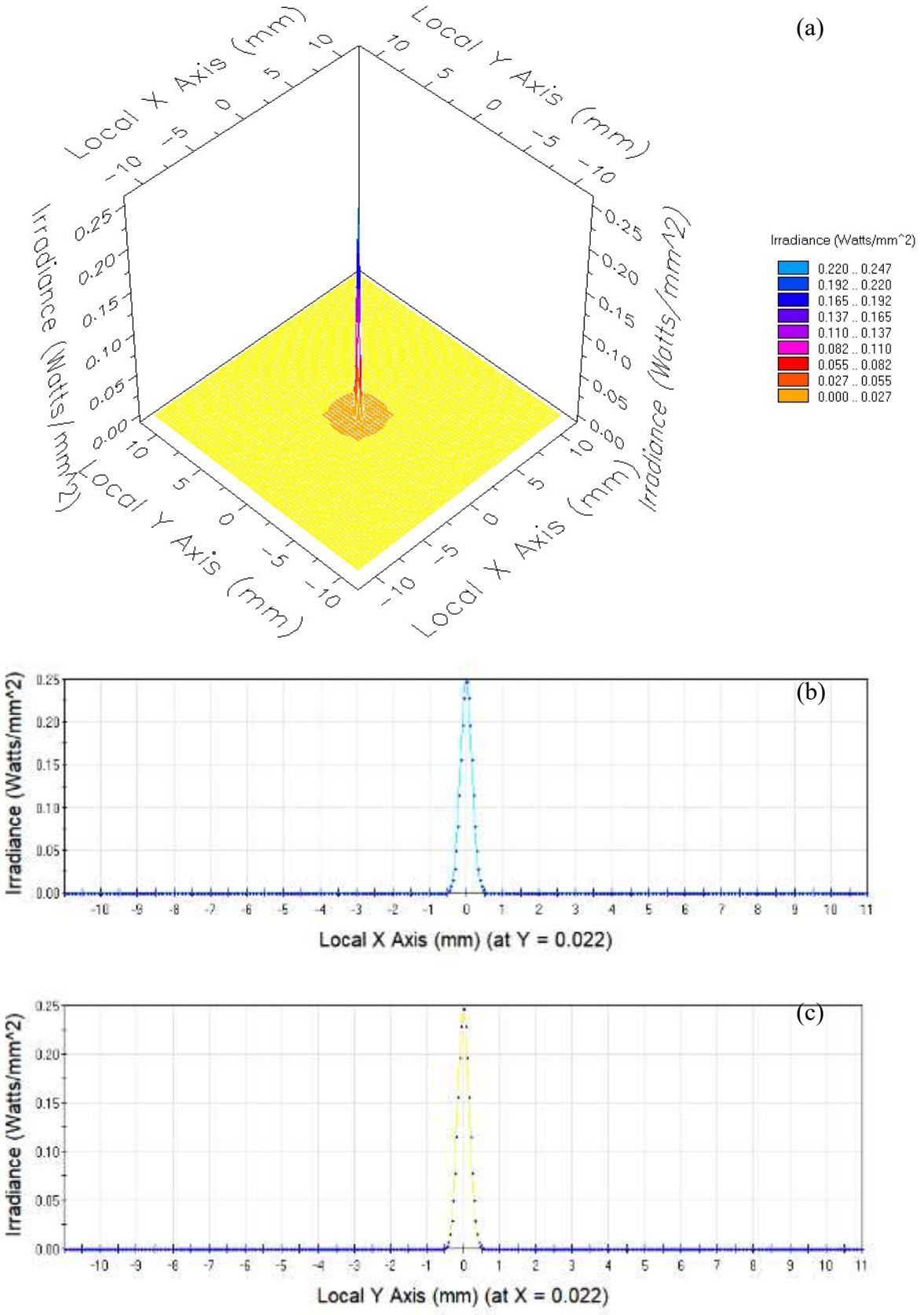

Figure 27: FRED Simulation - Optical power in the measurement area MA of a 200 mW laser source as 3D Model (a), in x-axis (b) and y-axis (c)

Figure 27 shows the result of the measurement area *MA* of Figure 26, using a laser source with 532 nm wavelength and the optical power of 200 mW. In Figure 27 (a), the 3D Model of the optical power of three recombined laser beams in the focal point is shown, whereas in (b) the optical power distribution in x-axis and in (c) the optical power distribution in y-axis are displayed respectively. The results show that the laser beam is not distorted, as the peaks in Figure 27 (b) and (c) have the same shape and the Figure 27 (a) shows an equal power distribution. The maximum reached power is 0,247 W/mm².

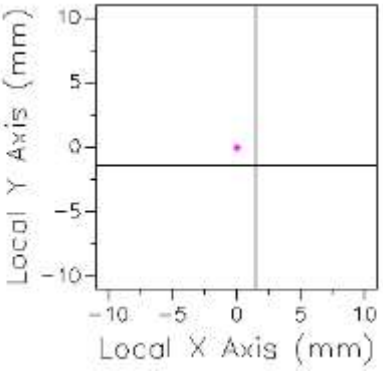

Figure 28: FRED Simulation - Diameter of the crossing beams in the measurement volume

In Figure 28 the diameter of the three crossing excitation beams in the measurement area *MA* is shown. The diameter, and with that, the measurement volume of the cross section is 1 mm, which equals an area of 0,78 mm². With the reached power of 0,247 W/mm² on this area, 192 mW optical power remains from 200 mW irradiance. The losses from the components and the length of the optical pathway are < 4 %. The simulation result of the second measurement area, which measured the scattered light, was 0,000023 W/mm², which would be an optical power of 1,8 mW on the planned sensor.

The simulation shows that enough optical power from the laser source should remain in the measurement area, so that the scattered light should be detectable with the planned LDV sensor, which should be able to detect signal from 2,67 pW (Thorlabs, 2015) .

4 Construction of the prototype

In this chapter, the requirements and specification of the components will be discussed, with special attention to the laser since this is a key component of the LaserEye. Then the construction of the laser Doppler velocimeter (LDV) will be presented, where advantages and disadvantages of the sensors and the target will be discussed, followed by the build of the spatial heterodyne Raman spectrometer (SHRS) and its adjustment. Lastly the construction of the flow channel and its corresponding pumping station, which are used as test equipment will be presented.

4.1 Components

In the beginning a continuous wave (CW) laser diode with λ=532 nm was used and therefore, the simulation was done for this frequency. To determine the frequency the following aspects had been considered:

- Using the LaserEye with "standard" glass for measurement in industry
- Maximum Output Intensity of the Raman light
- The measured objects must be optically active
- The laser should be available at a reasonable price

The Raman intensity I_R is given by (Hazle et al., 1990)

$$I_R = \frac{\pi^2 \cdot c \cdot \bar{\nu}^4 \cdot p_0^2 \cdot sin^2\,\theta}{2 \cdot \varepsilon_0} \quad (22)$$

where c is the speed of light, $\bar{\nu} = \frac{1}{\lambda}$ the absolute wavenumber, p_0 the amplitude of the induced oscillating dipole moment, ε_0 the permittivity of vacuum and θ the angle between the direction of the dipole moment and the direction in which the measurement is done. Since the Raman intensity depends by the 4th power on the wavelength of the laser source, the wavelength of the laser should be as short as possible.

With the above said, the wavelength of the laser is also limited by the glass used in industry, e.g., silicate glass, quartz glass or sapphire glass, since most "normal" glass blocks wavelength under ~400 nm. Therefore, the best wavelength would be 405 nm, 450 nm, 473 nm or 491 nm laser sources which are frequencies standard.

Because of the response spectrum of the Raman Spectroscopy and the divergence angel of the LDV, the laser should fulfil the following specifications, where the lower wavelength limit is due the OAP mirror (450 nm - 20 µm):

- Single Mode Laser
- 450 nm to 491 nm
- 40 mW – 200 mW optical power

The limitation to 200 mW (simulated 0,25 W/mm^2) optical power is reasoned in the damage threshold of the used components (see Table 1).

Table 1: Damage threshold of the used components

Component	**Damage Threshold**	**Suitable for 200 mW Laser**
Beam Splitter (BS)	5 W/mm^2	Ok
Lens (achromatic duplet)	10 W/mm^2	Ok
Lens (singlet)	7,5 W/mm^2	Ok
Plane mirror	1-5 W/mm^2	Ok
OAP mirror	5 W/mm^2	Ok
Edge Filter (dichroic BS)	0,5 W/mm^2	Ok

With the specifications made, the decision for a new custom built laser from Roithner Lasertechnik (Roithner Lasertechnik GmbH, n.d.) was a 473 nm continuous wave (CW) diode laser with 120 mW optical power due its availability and reasonable price. This laser broke after most of the experiments were done and was replacement by a 450 nm CW diode laser with 80 mW optical power from Thorlabs (Thorlabs, n.d.). The used edge filter is an optical high pass/long pass Filter. It reflects all wavelengths below a nominal wavelength, while all wavelengths above the nominal wavelength can pass through with losses under 1 % (depending on the quality of the filter), where the nominal wavelength is the laser wavelength.

The sensor PDA100A2 for the LDV from Thorlabs has low response at 473 nm and 532 nm respectively, therefore, a new senor was built. For maximum flexibility, a transimpedance amplifier was built with the possibility to use different photo diodes.

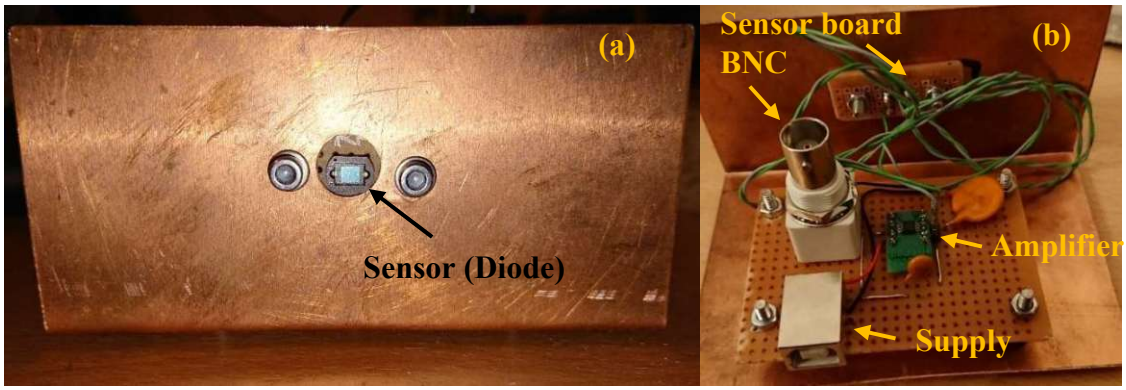

Figure 29: Sensor for LDV - sensor in housing (a), electrical driver circuit (b)

Figure 29 shows the sensor, which is mountable on an optical post, (a) from the front and (b) from the rear. The diode in Figure 29 (a) can be swiftly exchanged by removing the screws left and right of the diode and replacing the sensor board. Figure 29 (b) shows the wired components of the sensor, consisting of the transimpedance amplifier where the diode on the sensor board is connected to, a BNC connector for connecting the sensor to an oscilloscope and an USB connector for the power supply. The wiring diagram of transimpedance amplifier is shown in Figure 30 (a) while the suggested wire diagram from the datasheet of the operational amplifier OPA380 (Texas Instruments, 2007) is shown in Figure 30 (b). C_{STRAY} and C_{TOT} in Figure 30 (b) are compensation capacitors for ideal components and therefore not in the wiring diagram in Figure 30 (a) which was discrete built and uses real, non-ideal components.

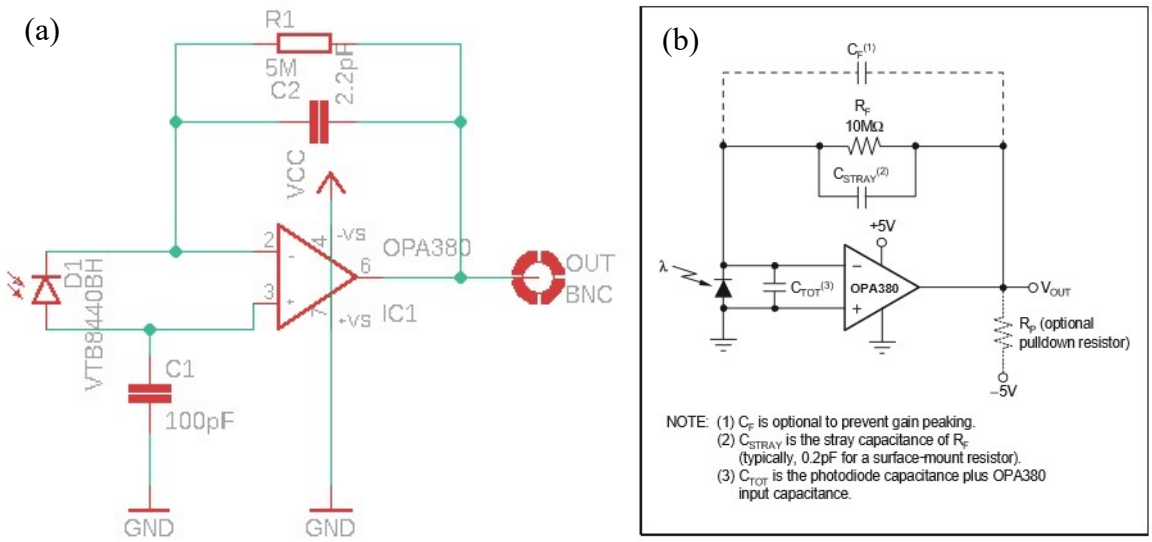

Figure 30: Wiring diagram of the transimpedance amplifier with photo diode (a), transimpedance amplifier wiring diagram from the datasheet of the OPA380 (b) (Texas Instruments, 2007)

With the feedback resistor R_1 (R_F) the transimpedance gain can be controlled and with the feedback capacitor C_2 (C_F) as the frequency response can be controlled. If R_1 (R_F) is adjustable, the signal gain and the amplification of the received signal can be adjusted. With C_2 (C_F), the response frequency, and with this the optimal working bandwidth in accordance with the used photo diode of the amplifier can be set.

The supply voltage VCC is 5 V and is delivered by a linear power supply, since switching power supplies like mobile chargers would have to much noise which overlaps with the measured signal.

The transimpedance amplifier has an ideal input impedance of 0 Ω, which results in a short circuit of the photodiode. If light hits the photo diode, a small current occurs in the short-circuited photo diode. Due to this current, the operation amplifier wants to hold the + and – input on the same level, which means that the operation amplifier must increase its output voltage until the current through R_1 (R_F) is the same current which flows through the photo diode. Therefore, R_1 defines the gain of the circuit through Ohm´s law

$$U_{out} = I_{photo} \cdot R_1 \qquad (23)$$

Since the + and – inputs of the operation amplifier are always at the same potential, a virtual short circuit in the photo diode occurs. This leads to a lack of a voltage change in the photo diode, which means, that the barrier layer capacity has not to be recharged. Due to that, the

barrier layer capacity is no longer a dominant parasitic effect and high frequencies can be achieved.

To change the upper cut-off frequency, C_2 (C_F) must be changed, e.g., for lowering the cut-off frequency, C_2 (C_F) must be increased.

The maximally flat, 2nd-order Butterworth frequency response can be achieved by setting the feedback pole to (Texas Instruments, 2007):

$$\frac{1}{2\cdot\pi\cdot R_1\cdot(C_2+C_{Stray})} = \sqrt{\frac{GBW}{4\cdot\pi\cdot R_1\cdot C_{TOT}}} \qquad (24)$$

Where GBW is the Gain BandWidth product which in case of the OPA380 equals to 90MHz. C_{TOT} is the total input capacitance, consisting of the capacitance of the OPA380 (4,1 pF) and the photo diode capacitance (1 nF for the VTB8440BH). C_{STRAY} is the stray capacitance of the resistor R_1 (R_F), typically 0,2 pF.

The measurement from the datasheet of the responsivity of the photo diode VTB8440BH is shown in Figure 31 (VTB Process, 2000).

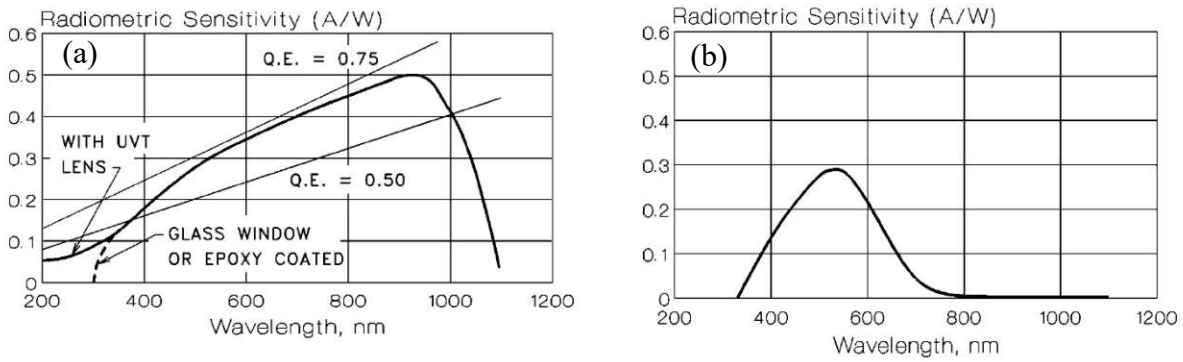

Figure 31: Responsivity of VTB8440BH (VTB Process, 2000)

From the diagram Figure 31 (b) the general responsivity of the diode can be read in searching the wavelength which will hit the diode on the x-axis and by following the plot, get the sensitivity from the y-axis. The sensitivity is needed to calculate the resulting photo current I_{photo} the diode will provide the amplifier circuit. In Figure 31 (a) the responsivity for the diode covered with glass or epoxy is shown.

The current of the photo diode can be calculated with (Hui, 2009)

$$I_{photo} = S_{PD} \cdot P \qquad (25)$$

Where I_{photo} is the resulting current of the photo diode, P is the power of the receiving light and S_{PD} is the wavelength dependent sensitivity of the photo diode. The sensitivity can be read from the responsivity diagram in the datasheet of the photodiode. For 532 nm the sensitivity results to 0,27 A/W and for 473 nm 0,26 A/W. The power of the scattered light was measured to 98 µW. Therefore, the current from the diode is calculated to 26,5µA. With U_{out}=4,5V, R_1 is calculated to 170 kΩ, but a potentiometer was finally mounted to enable for the use of different diodes and optimize the signal. In Figure 32 the measured signals, detected with the (a) Thorlabs sensor PDA100A2 and (b) - (d) the new sensor, using various diodes are shown.

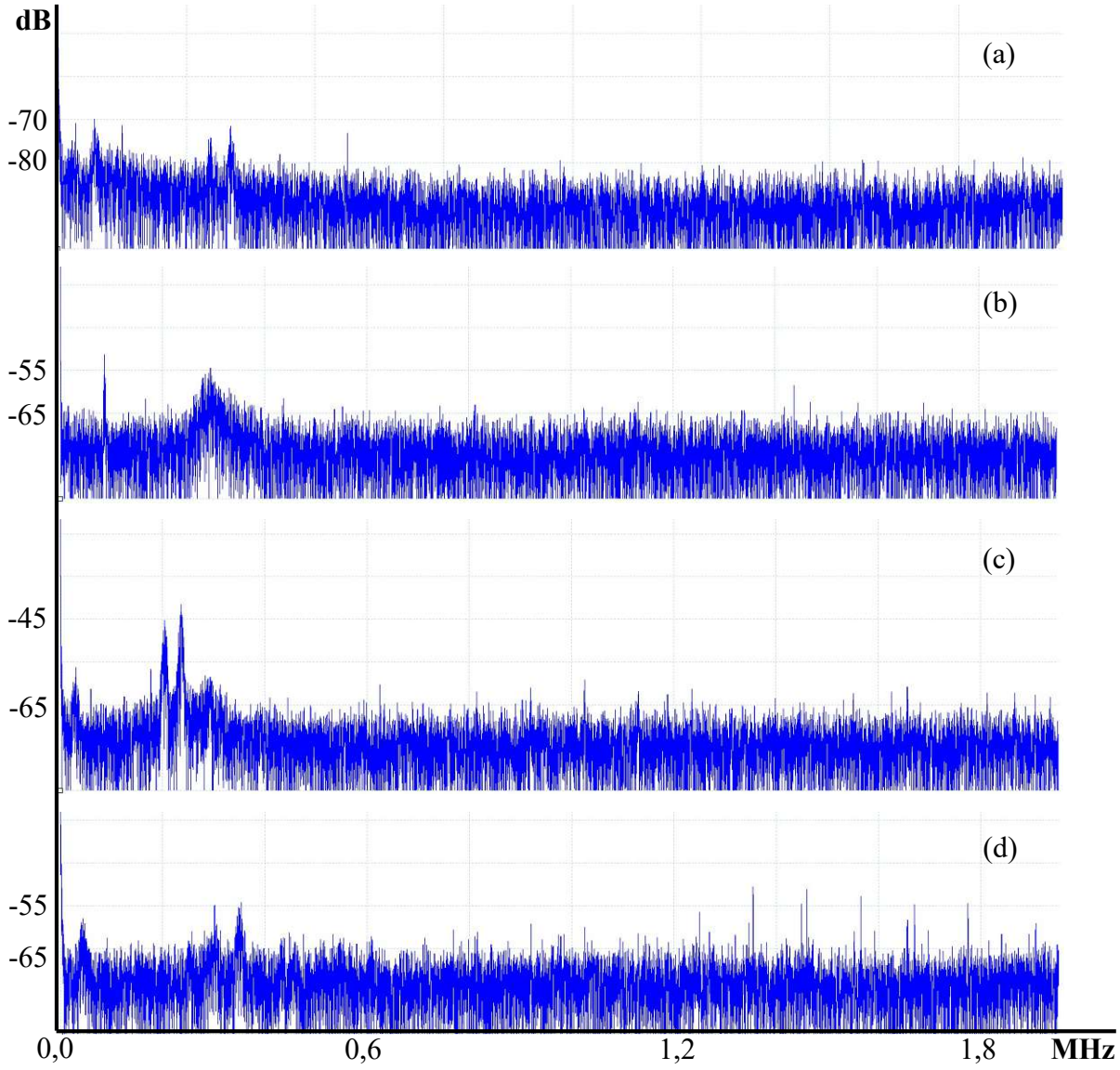

Figure 32: Measurement signal of the 532nm, 40mW laser diode with the new sensor (a) Thorlabs sensor PDA100A2 (b) VTB8440BH (c) Vishay TEMD5510FX01 and (d) Vishay TEMD6200FX01

Figure 32 shows the received signal, where on the x-axis the frequency in Megahertz (MHz) and on the y-axis the signal power in decibel (dB) is measured.

The pseudo decibel, a unit used to characterize the SNR could be obtained by reading the power values out of Figure 32 and calculated using (Gulino et al., n.d.)

$$SNR_{dB} = 10 \cdot \log_{10} \frac{P_{Signal}}{P_{Noise}} \ (dB) \qquad (26)$$

Table 2 shows the calculated SNR of the different sensors. The higher the value of the SNR is, the more signal power can be used and the more accurate the detected signal will be.

Table 2: Comparison of the different diodes of the new sensor and the Thorlabs sensor

Sensor	**SNR (in pseudo decibel dB)**
Thorlabs sensor PDA100A2	0,35 dB
New sensor with VTB8440BH	0,72 dB
New sensor with TEMD5510FX01	1,44 dB
New sensor with TEMD6200FX01	0,72 dB

From the used diodes, the Vishay TEMD5510FX01 showed the best results and will be used as standard diode in the sensor. For the future, a silicon photomultiplier (SIP) is planned as single photon sensor but since the SIP needs another driver circuit, a new sensor must be designed.

Due to the high-power beam of the 473 nm laser diode with 120 mW, which was mainly used during the experiments, the Thorlabs sensor PDA100A2 could be used since the received signal was strong enough with an SNR of up to 1,1 dB, which had the advantage, that the sensor could be nicely integrated into the setup because of its fitting connectors.

4.2 Laser Doppler Velocimeter

In Figure 33 the LDV setup is shown, where (a) shows the setup with only one sensor, which was also used for the following experiments and (b) shows the LDV with two sensors.

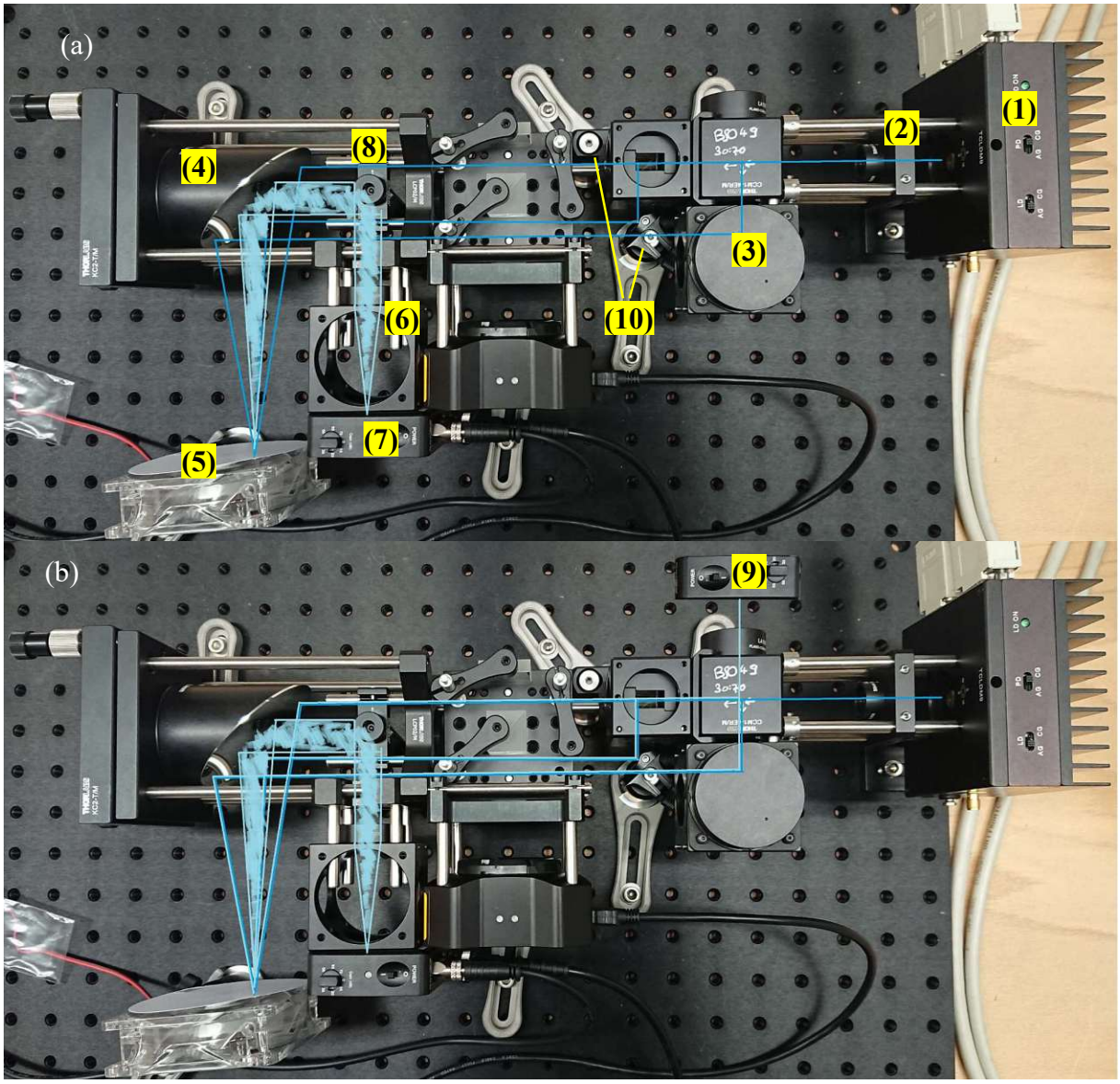

Figure 33: LDV Setup (a) with one sensor, (b) with two sensors

From the laser diode (1) the beam (dark blue) propagates and is collimated with the collimation lens (2). The beam splitter unit (3) divides the collimated beam in three beams and projects theses beams on the off axis parabolic (OAP) mirror (4). Since the Thorlabs cube system was not suitable to build the whole beam splitter unit, the third beam, emitted from under the second beam splitter was guided by mirrors (10) on posts, making the construction less robust against vibrations and bumps. The OAP mirror has a fixed focus length and focus all three beams in

one point on the target (5). The scattered light (light blue) from the target (5) is collected by the OAP mirror and guided to the edge filter (8), which reflects all light under its cut-off frequency to the converging lens (6). The light from the converging lens is then focused on the sensor (7). In Figure 33 (b) the second sensor (9) can be seen after the first beam splitter of the beam splitter unit (3). This sensor analyses the scattered light traveling back the excitation beams. At a later time, a telescope optic was built between the laser diode and the beam splitter, shown in Figure 34, to vary the measurement volume/the cross section by widening or narrowing the beam diameters. With this, a larger area on solids or more (seeding) particles in fluids with lesser irradiance or a smaller area on solids or less (seeding) particle in fluids with higher irradiance can be detected. The diameter of the cross section should depend on the reflectance of solids or the (seeding) particle size and quantity in fluids, e.g., in fluids many small (seeding) particles would scatter more light with higher probability in a bigger cross section with lesser irradiance than in a small cross section with higher irradiance but lesser probability that the (seeding) particle would be hit. In Figure 34 the two lenses (1) and (2) can be moved on the rods and through this the cross section widens or narrows. With an adjustable mirror (3) the beam is guided to the beam splitter.

Figure 34: Telescope optic to vary the size of the cross section

For the LDV Setup the following parts are used from Thorlabs (Thorlabs, n.d.)

Table 3: Used optical components for the first stage of the LaserEye

Laser	532 nm single mode CW laser diode, 40 mW and controller
Collimation Lens	AC127 – 030, 30 mm focus length achromatic lens
Beam Splitter 1	30(R):70(T) Cube beam splitter BS049
Beam Splitter 2	50(R):50(T) Cube beam splitter BS010
Mirrors	silver coated mirrors 1” ME1-P01
OAP Mirror	156mm focal length, 90° off axis silver coated parabolic mirror
edge filter	Longpass Dichroic Mirror DLMP490 (with cut-off frequency of 490nm)
Focus Lens for LDV Sensor	Focus lens 50 mm focal length LA1131-A-ML
LDV detector	Photo Diode PDA100A2

4.3 Spatial Heterodyne Raman Spectrometer

For the integration of the Raman spectrometer into the Lasereye, the spatial heterodyne Raman spectrometer was built.

The following optical components were used:

- Beam splitter 50:50
- Grating 300 grooves/mm
- Mirror
- Line camera

The Littrow angle θ for the gratings/grating and mirror can be calculated by (Nathaniel et al., 2011)

$$\theta = \arcsin(m \cdot \lambda \cdot \frac{1}{2} \cdot d) \qquad (27)$$

Where m is the mode, d is the distance between the grooves of the grating and λ is the wavelength of the laser.

Table 4: Calculation of the Littrow angle

θ (°)	m	λ (nm)	d (mm)
0,067	1	450	0,00333
0,071	1	473	0,00333
0,079	1	532	0,00333

Table 4 shows the values for different laser diodes. Since only the first mode is of interest, m is always set to 1. With that, the Littrow angle results for the 473 nm laser to $\theta_L = 0{,}07°$.

In a first approach, shown in Figure 35 (a), the spatial heterodyne Raman spectrometer (SHRS) was positioned in the middle of the LaserEye to use as little as possible of space and make the LaserEye prototype as compact as possible. Due to problems with the pathway of the laser beams, the SHRS was then position sidewards, shown in Figure 35 (b), and the Raman light was guided with a mirror (1).

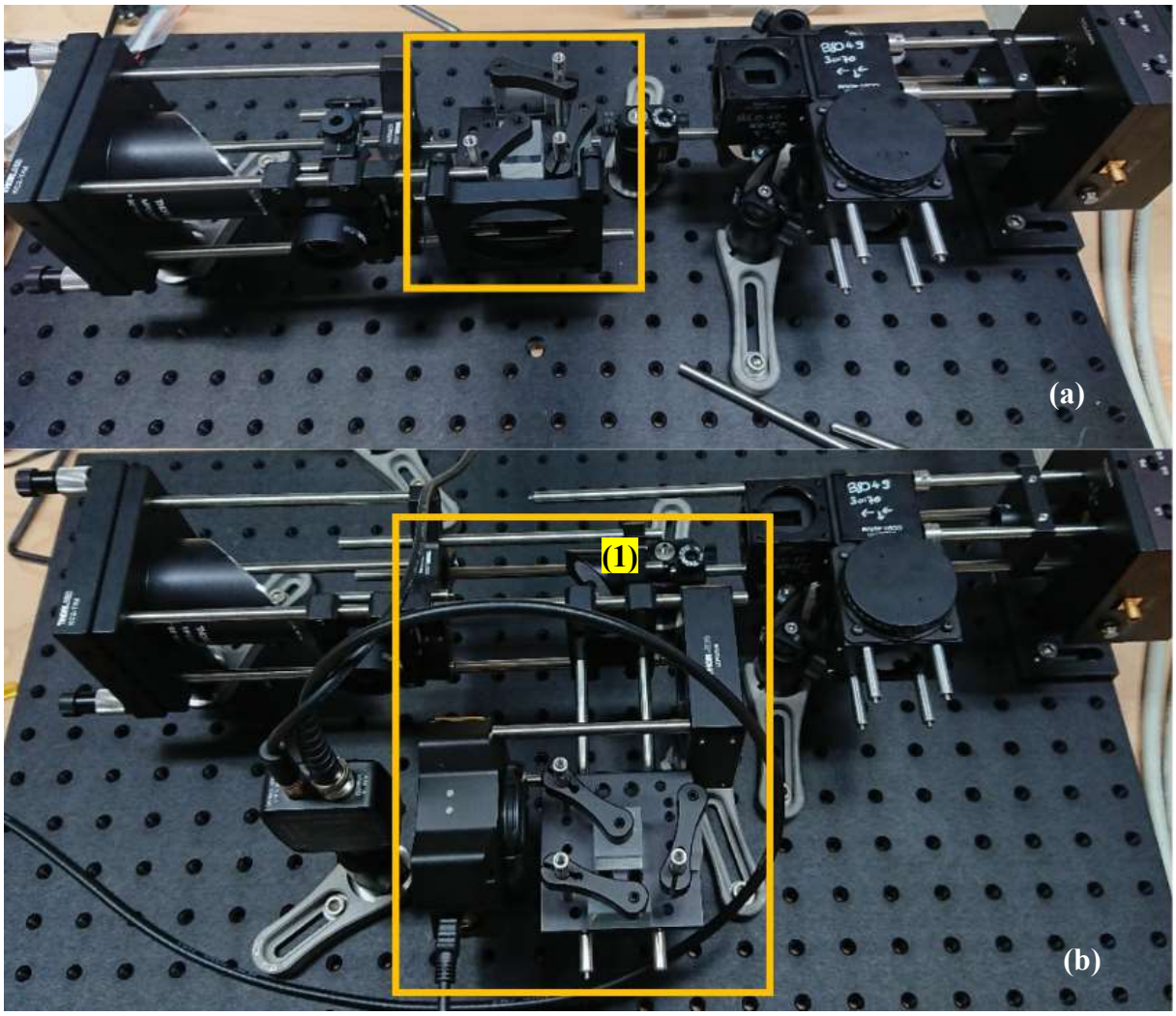

Figure 35: (a) SHRS in the middle of the LaserEye without camera (b) SHRS sidewards connected with rods

Since the platform holding the SHRS (Figure 35 (b)) was not as flexible to handle as wished, a customized platform was built, as shown in Figure 36. With that the mounting of adjustable mirror holders and therefore exact adjusting of the mirrors was possible.

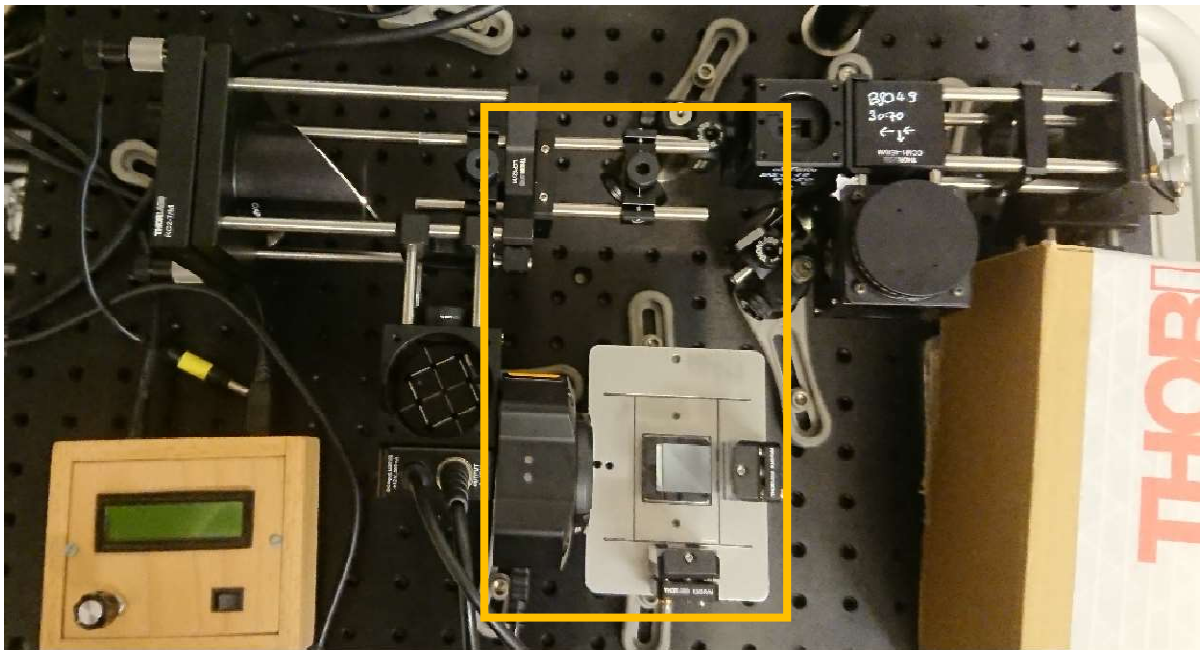

Figure 36: SHRS on customized platform, the cardboard on the laser should prevent unwanted light may leaking from the source

For adjusting the SHRS, a multispectral lamp was built. Therefore, a miniature light bulb (3,6 V) with a tungsten filament and a built-in lens was placed into a light tight housing with a small opening in the front and the possibility to be mounted on an optical post, which is shown in Figure 37. Since the voltage of the power adapter only allows fixed voltages, the operation voltage is 3 V.

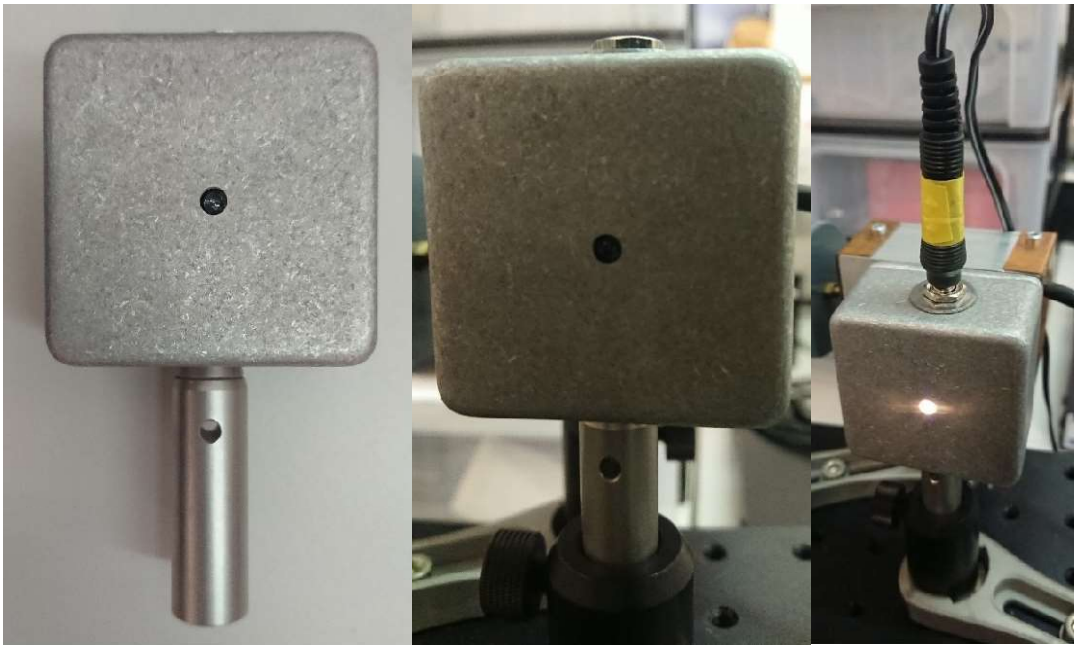

Figure 37: Multispectral lamp for adjusting the SHRS

Using the multispectral lamp, adjustment of SHRS was possible. Figure 38 shows the coarse adjustment from (a) top view, (b) back view from the SHRS in direction of the camera and (c) back view from the SHRS in direction of the camera with a white paper in front of the camera so that the spectral lines are visible.

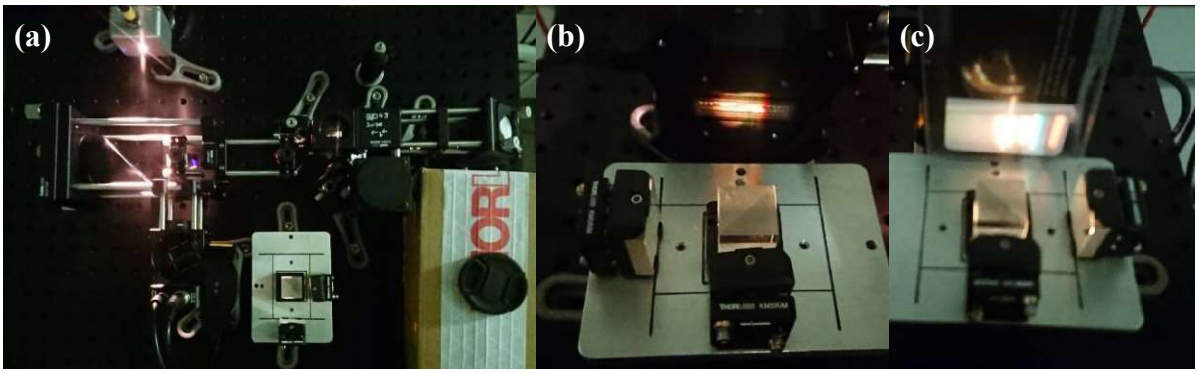

Figure 38: Coarse adjustment of the SHRS from (a) top view, (b) SHRS back view with the spectrum projected on the camera, (c) SHRS back view with the spectrum projected on a paper before the camera

After the coarse adjustment was done, the SHRS was fine adjusted. The spectral lines can be seen in Figure 39, where (b) is a close-up view from (a) and the blue spectral line is missing due to the edge filter.

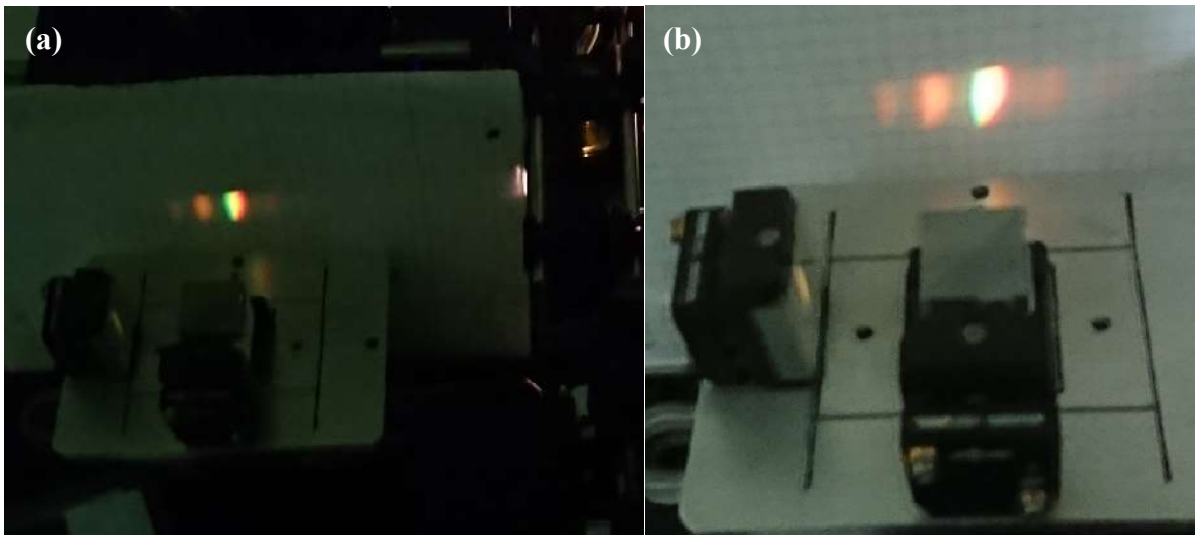

Figure 39: Fine adjustment of the SHRS (a) overview of the SHRS, (b) close-up view of the spectral lines. Light below 473 nm (blue light) is missing due to the edge filter

To get rid of unwanted stray light and gain more accurate results, an aperture was built, shown in Figure 40, so that only the light from the beam splitter should hit the camera.

Figure 40: Aperture for SHRS

The installed aperture is shown in Figure 41 (a) while Figure 41 (b) shows the aperture in the operating SHRS.

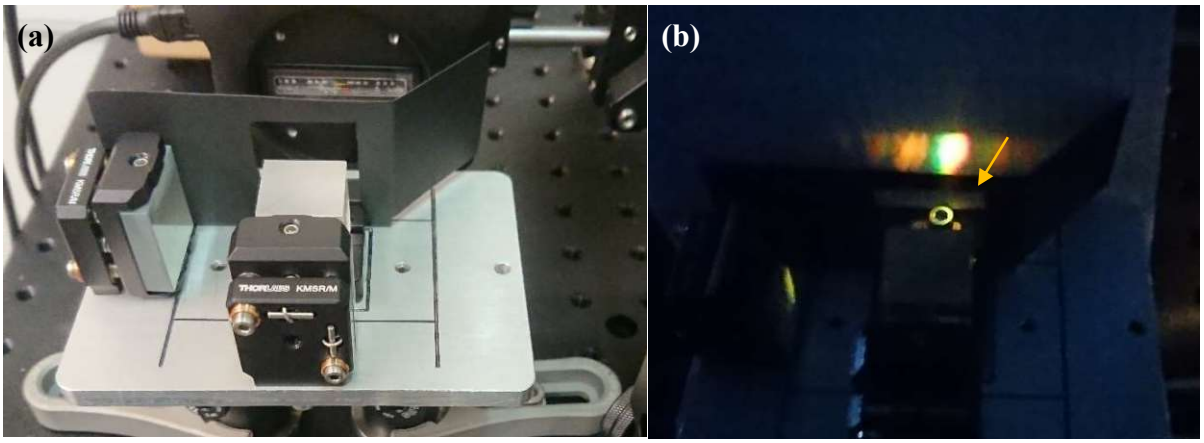

Figure 41: Installed aperture on SHRS (a), working SHRS with installed aperture (b)

4.4 Measurement targets

To be able to measure with the LaserEye, targets are necessary. In the beginning, a fan, normally used in a PC, was used with a plain paper disc sticked on in, which had neither accurate nor reproduceable speed control. Therefore, a controllable spinning disc with velocity feedback was build. Since the LaserEye should work with fluidic process streams, in e.g., chemical plants, a fluid channel was designed and built to evaluate the efficiency of the LaserEye under laboratory conditions.

4.4.1 Target - Spinning disc with micro controller

Since the used fan with the paper disc has the disadvantage, that the speed control is neither reproduceable nor has feedback, a new spinning disc was built using an Arduino Uno which drives a BD6221F H-Bridge (as full bridge) DC brush motor driver and returns the direction, the value of the PWM codeword in bit and the velocity in rpm on a display. The interchangeable spinning discs are made from wood (beech) and PVC. The finished motor with its controller is shown in Figure 42.

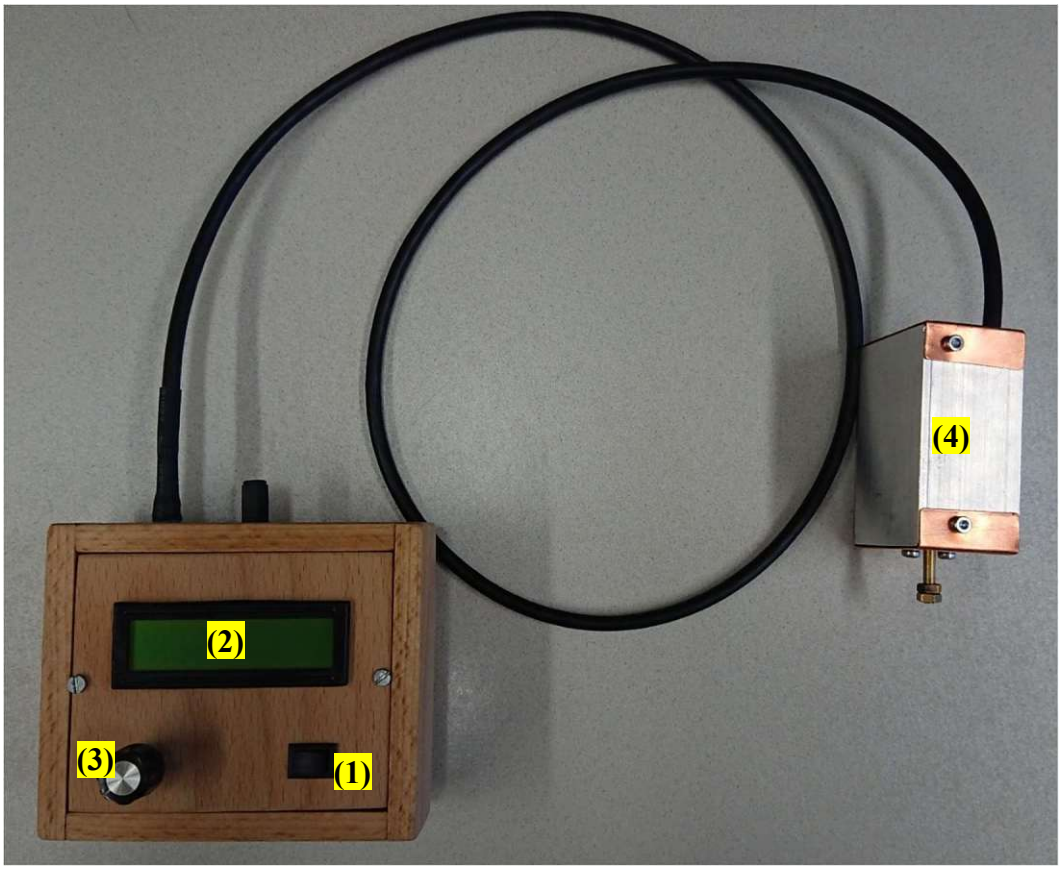

Figure 42: Motor controller with connected motor without disc

The disc can spin clockwise or anti-clockwise by using the switch (1) in Figure 42. The rotation speed (in rpm), the PWM resolution (in bit) and the direction are displayed on the LCD (2). With a rotary potentiometer (3) the rotation speed is adjustable. If the "direction switch" is used, the direction changes while the rotation speed remains the same. The rotations of the disc are measured with a magnet clued on the back of the disc and a Hall sensor mounted at the motor housing (4), which sends a signal to the micro controller of the disc controlling unit every time the magnet passes it. The micro controller counts the rotations in a set period (e.g., one second) and returns the calculated rotation per minute (rpm).

In Figure 43 the different targets are shown, (a) the fan with a paper disc and (b) the beech disc on a controlled motor with feedback.

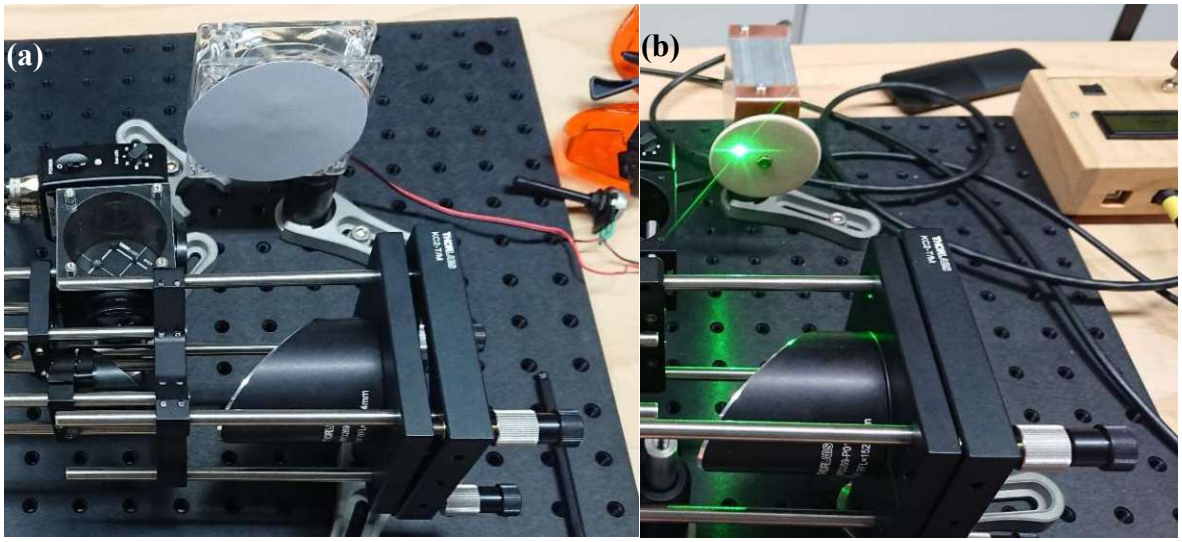

Figure 43: Difference in test equipment – (a) fan with paper disc, (b) µC controlled beech disc

After some experiments with the plain disc, two beech rods had been glued on the disc to simulate "particles". Figure 44 (a) shows the beech disc with the glued beech rods, while Figure 44 (b) shows the laser in its focus point on the vertex of the rods and Figure 44 (c) shows the laser off focus on the beech disc.

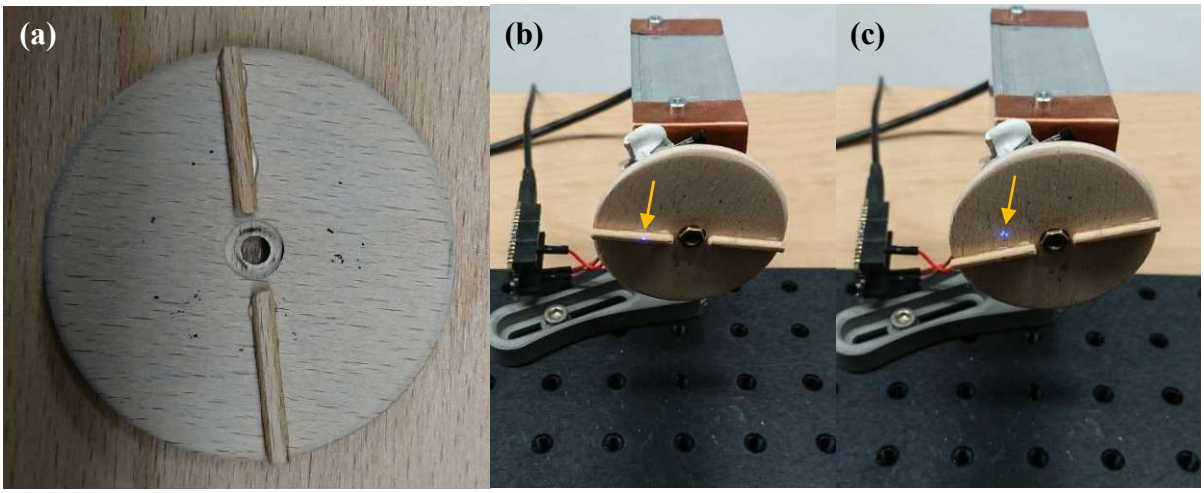

Figure 44: Beech disc with glued beech rods on it (a), beam focused on the rods (measuring) (b), beam off focus on the disc (no measuring) (c)

The simulation of the particles was due to the round geometry of the rods, so that the beams became off focus after hitting the vertex of the rods. With that, two "particles" would pass the measurement volume with each rotation of the disc.

4.4.2 Flow Channel

For using the LDV on the fluid channel, a non-stationary surface where the light can scatter is needed. To obtain such a surface, seeding particle which travels with the flow and are able to scatter the light might be necessary. The flow channel should fulfil the following requirements:

- At least two independent channels (so that only one or both or for future applications more channels can be used)
- stackable (e.g., with magnets)
- diameter of channel d=1-10 cm, so that the channel can be easy handled on the optical table (not bulky, no stiff tubes, channel easy to move and tilt, no tension on channel, no vibrations, the use of seeding particles won´t clog the channel, fixation of channel with M4 or M6 on an optical post)
- fluid velocity v=0-10 m/s, so that with high fluid velocity a turbulent flow would be formed, and mixing effects could be observed

The requirement for at least two channels is in this stage for easy switching between two fluids without cleaning the channel (and pumping station). A small fluid channel could also be used

for future experiments or presentation on e.g., a fair. The fluids for calibrating the SHRS should be

- An ethanol/water mix
- Water with Sodium sulphate or Ammonium sulphate, where the active component for calibrating the SHRS is sulphate due its unique and well known spectral line. Therefore, sodium sulphate is the better choice since it is a neutral salt and won´t cause troubles with the materials

The channels are made from aluminium and glass in a basic design. To calculate the volume flow through the channel and decide on the tube size and connectors equation 28 was used

$$V_f = A_C \cdot v \cdot 3600 \frac{s}{h} \cdot \frac{1l}{0{,}001\, m^3} = \frac{d_i^2}{4} \cdot \pi \cdot v \cdot 3600 \frac{s}{h} \cdot \frac{1l}{0{,}001\, m^3} \qquad (28)$$

Where A_c is the cross section of the channel and v is the fluid velocity. The channel itself has a rectangular shape, but the tubes and connectors have round shape, therefore in equation 28 the cross section of the inner diameter of the tube was used.

Table 5: Decision table for tube and connector size dependent on the volume flow

d_i	**v**	**V_f**	**V_f**
9 mm (~G1/8”)	5 m/s	287 l/h	4,8 l/min
9 mm (~G1/8”)	10 m/s	573 l/h	9,6 l/m
12 mm (~G1/4”)	5 m/s	509 l/h	8,5 l/min
12 mm (~G1/4”)	10 m/s	1017 l/h	17 l/min
20 mm (~G1/2”)	10 m/s	2828 l/h	48 l/min
24 mm (~G3/4”)	5 m/s	2036 l/h	34 l/min
24 mm (~G3/4”)	10 m/s	4072 l/h	68 l/min

With the gathered data from the calculation and the requirements, the flow channel was designed as shown in Figure 45 and manufactured.

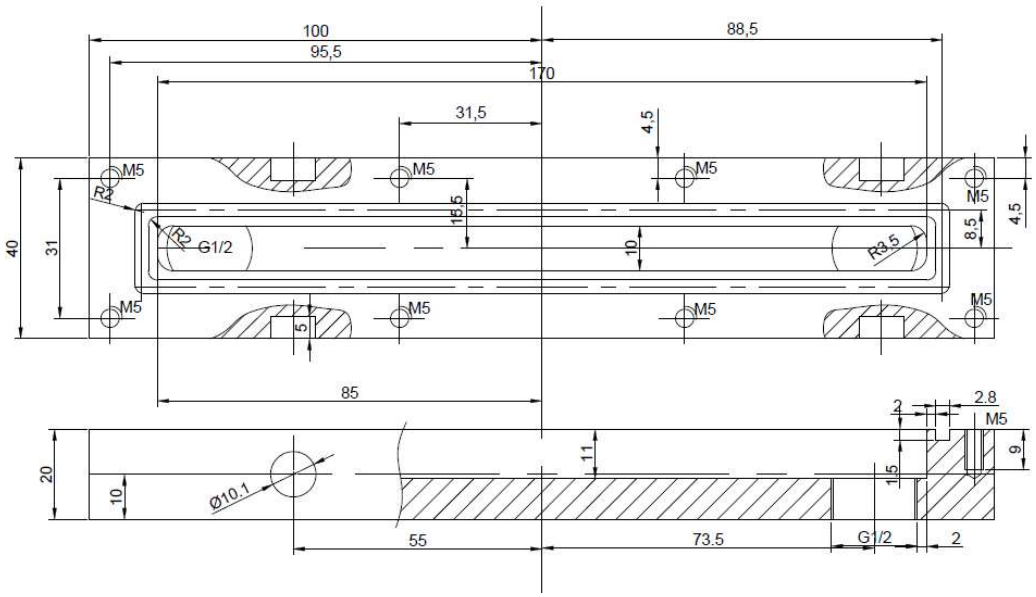

Figure 45: Drawing of the flow channel

The finished flow channel is shown in Figure 46, where (a) shows one flow channel from the side with the magnets to stack the flow channels. Figure 46 (b) shows both flow channels from different perspectives and the base plate which can be mounted on a post and holds the flow channels with magnets. The magnets have different polarisation, so that there is only one way the flow channels can be stacked. In Figure 46 (c) the flow channels are shown from the front were the LaserEye will measure through the quartz glass.

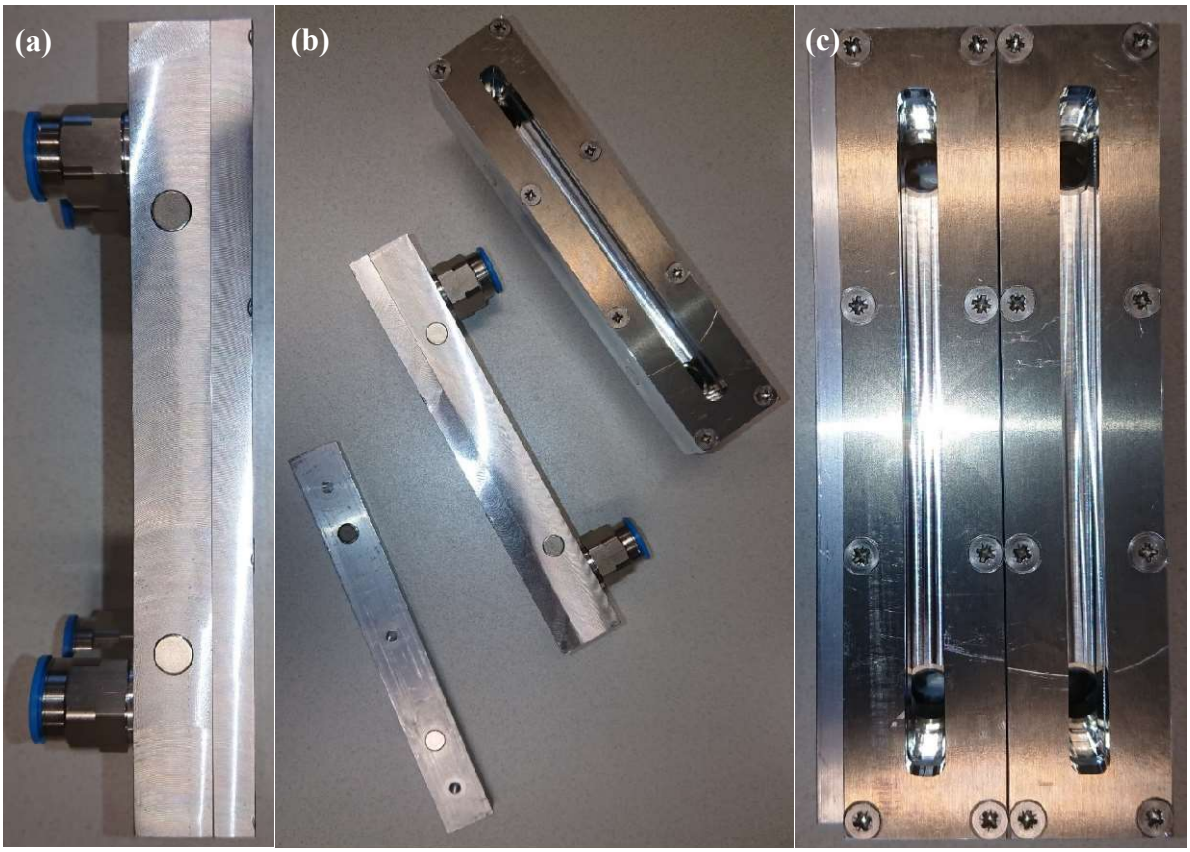

Figure 46: Manufactured flow channel, flow channel from above (a), both flow channels and mounting base (b), both flow channel frontal (c)

4.4.3 Pumping station

To be able to operate the flow channel, pumps are necessary. With the requirements of the flow channel, suitable pump, normally used in heating system, had been found, with the advantage that small particles can be pumped, the speed controller is built in and all materials are resistant to the chemicals planned to use. The P&I flowchart of pumping station is shown in Figure 47. It consists of an adjustable pump, a digital flowmeter (with a range of 1 m/s to 10 m/s), a 1 l tank for storing the fluids and seeding particle, a ball valve for emptying the system, and a throttle, which was built in at a later point for reducing the flow.

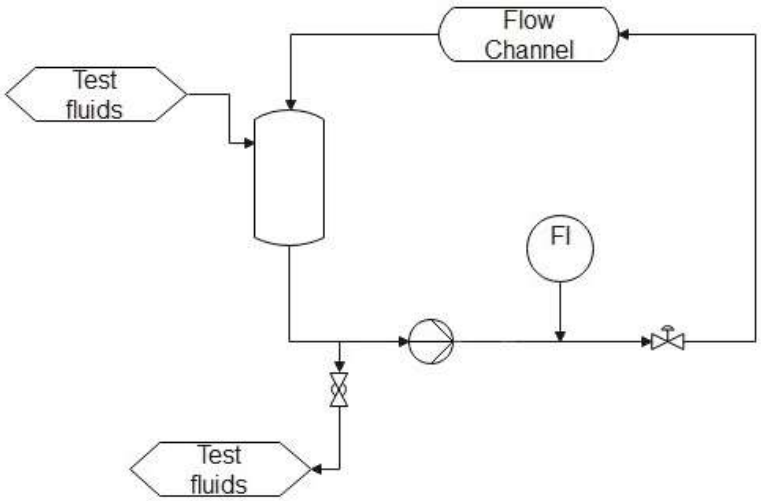

Figure 47: P&I flowchart of the pumping station

All components were mounted on a rack, built from aluminium profile rods, which can be seen in Figure 48. Since it was planned to use two flow channels simultaneous, two pumping station had been built. Figure 48 (a) shows the finished pumping station, while Figure 48 (b) shows the pumping station integrated in the experimental setup of the LaserEye with connected flow channel.

The pumping station in Figure 48 (a) consists per channel of an adjustable pump (1) Wilo Stratos PICO plus for heating systems which is tolerant to small particles and to the planned chemical, a digital flowmeter (2) which indicates the flow and a 1 l tank (3), mounted on the backside of the rack. In Figure 48 (a) the connectors (4) for the flow channel are still open while in Figure 48 (b) the flow channel (7) is connected. Under the pump (1), a ball valve (6) is mounted to empty the system. On top of the vessel a tee with removeable end stop is installed to fill the system with the wanted fluid and particle through a funnel. In Figure 48 (c) the throttle (8) and end stop (9) are shown.

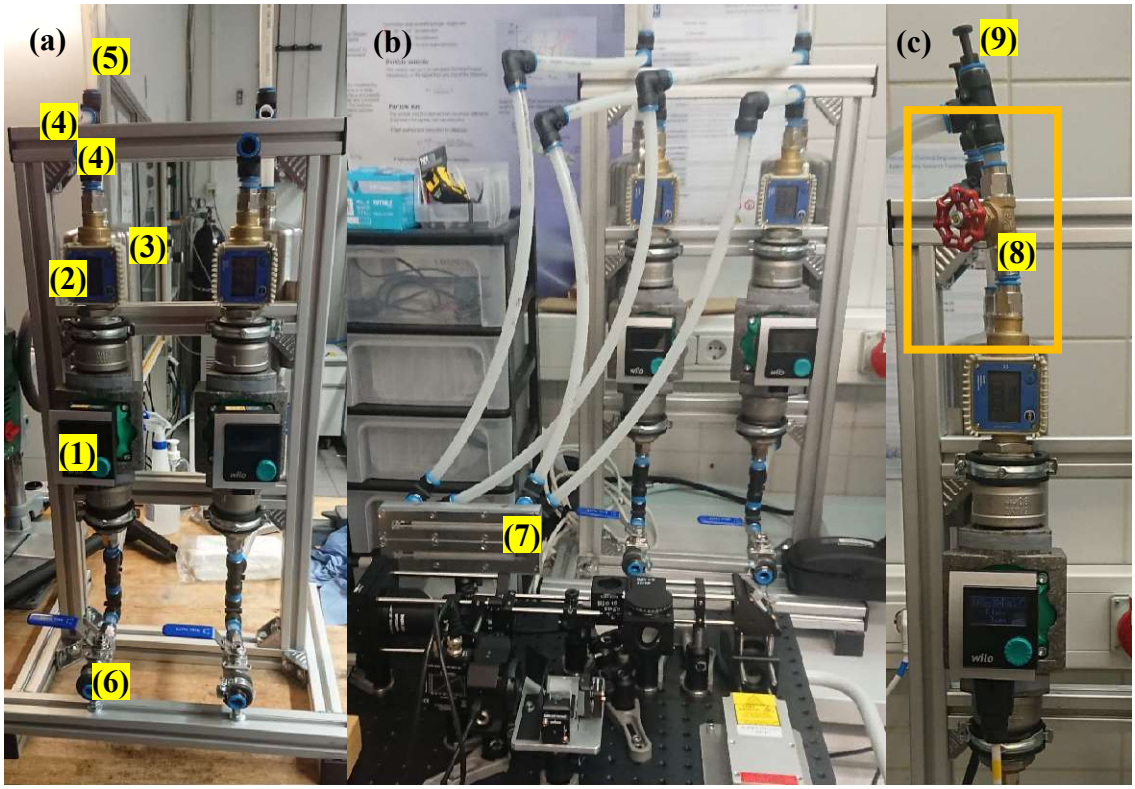

Figure 48: Pumping station without flow channel (a), pumping station with connected flow channel in the experimental setup (b) and installed throttle and end stop (c)

The used tubes are very stiff and difficult to handle. Therefore, the connection between flow channel and outlet/inlet of the pumping station had been replaced with soft silicon tubes.

Figure 49 gives some impression how the flow channel was used in the experiment.

Figure 49: Flow channel in front of the LaserEye

5 Results and Discussion

In this chapter the measurement results will be presented and discussed. First, the results of the measurement of the LDV, then the SHRS and last the combination of the LDV and SHRS, using the spinning disc will be shown. Then the results of the measurement in the flow channel will be discussed, again first for the LDV and then for SHRS. Lastly an outlook will be given.

5.1 Measuring on solids

The measurement results presented here were done with a fan covered with paper disc and with the spinning beech disc, respectively, using a 532 nm laser diode with 40mW optical power in the beginning and a 473 nm laser diode with 120 mW optical power later. With the high optical power of the 473nm laser diode, the Thorlabs sensor PDA100A2 was applied due the convenience of the compatibility of the whole mechanical system used. The analysis of the signal delivered by the Thorlabs sensor PDA100A2 was done with an oscilloscope from Pico Technology, PicoScope 2000 series. The computer software for the oscilloscope from Pico Technology (Pico Technology, 2022) is able to apply fast Fourier transformation (FFT) on the received signal in the time domain to transform it into an output signal in the frequency domain.

5.1.1 LDV measurement

Some measurement results from the LDV sensor can be seen in Figure 50 and Figure 51. On the x-axis the frequency (MHz) of the received signal is plotted while on the y axis, the signal strength (dB) can be seen. The stronger the signal power in relation to the noise power, the SNR (signal to noise ratio) is, the easier and better the correct signal can be detected. More detailed work on this topic was done by (Buchner et al., 2021) for diodes which are here used as LDV detector and (Nissinen et al., 2017) for improved Raman signals. Figure 50 shows the FFT transformed signal of the sensor when the target (fan) is turned off, which correspond to the noise of the sensor, while Figure 51 shows the FFT transformed signal of the sensor when the target (fan) is turning.

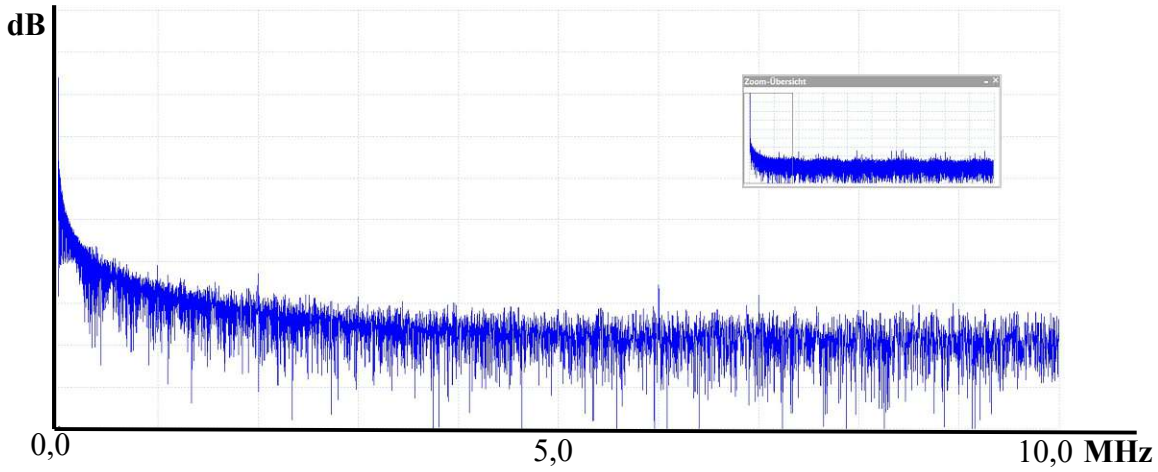

Figure 50: Frequency measurement when fan turned off

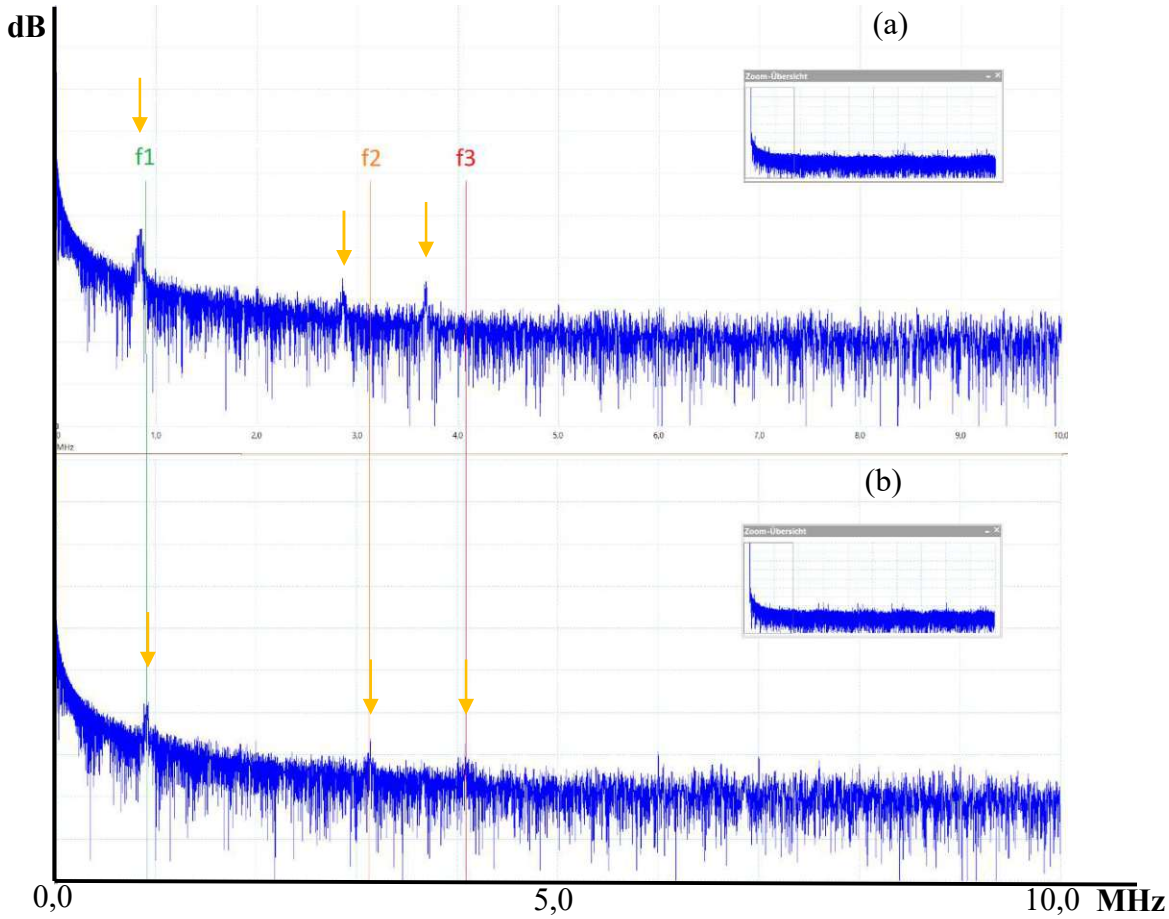

Figure 51: Frequency measurement when fan turned on for (a) low velocity and (b) high velocity

The occurring peaks in Figure 51 are marked by arrows. While in Figure 50 the fan doesn´t turn and therefore no frequency peak is detected, Figure 51 shows the peaks in the frequency spectrum when the fan is turning. In the Figure 51 (a) the fan turns with lower rotation per minute (rpm), while in Figure 51 (b) the fan turns at higher speed. With the coloured lines in Figure 51 the shifts of the frequency peaks dependent on the rotational speed of the fan can be seen. The three different peaks occur due to the different angles of the excitation beams but also represent three 2-beam LDV. Therefore, each frequency presents one direction, x, y, and z, put up through the three 2-beam LDV´s. With this said, the frequency shift of f_1 for the z-axis which is in direction of the OAP mirror is only caused by wobbles of the paper disc, since the fan was in a fixed position. The shifts of f_2 and f_3 are equal since the x and y direction of the paper disc are coupled. The direction dependency is shown in Figure 52.

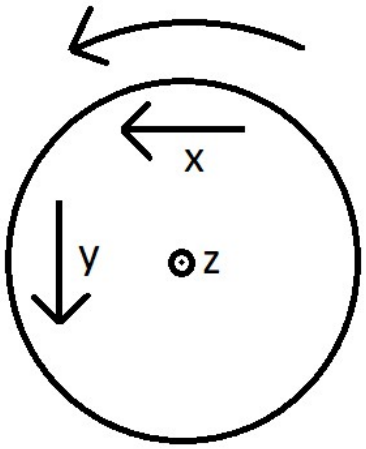

Figure 52: Direction dependency on spinning disc

The occurring frequencies are plausible with the following approximation:

The speed of the fan at 12 V (maximum speed) is nominal 2500 rpm. The excitation beams (532 nm) hit the disc 3,5 cm away from the centre, which results in an effective diameter of 0,07 m. Therefore, the velocity at the measurement point is

$$\frac{0{,}07\ m \cdot \pi \cdot 2500\ min^{-1}}{60} = 9{,}16\ m/s \qquad (29)$$

The velocity for a 2-beam LDV can be calculated by (Morita et al., 2016)

$$v = \frac{f_d \cdot \lambda}{2 \cdot \cos \Delta\theta} \qquad (30)$$

And therefore

$$f_d = \frac{v \cdot 2\,co}{\lambda} \qquad (31)$$

With the tangent function the angle can be calculated to

$$\Delta\Theta = 90° - tan^{-1}\left(\frac{mirror\ diameter \cdot \frac{1}{2}}{focal\ lengt\quad OAP\ mirror}\right) \sim 81° \quad (32)$$

With this, the expected doppler frequency f_d would be 5,3 MHz at maximum speed of the disc under the condition that the excitation beam hits the OAP mirror orthogonal. Since the excitation beams are tilted to the OAP mirror, the signal will occur at lower frequency. Also, the measurement of the distance between the focus points of the laser and the centre of the disc is not 100 % accurate due to the given equipment and the velocity of the fan was taken from the datasheet. Therefore, the highest occurring frequency f_3 of 4,1 Mhz is a plausible result.

Since the detected signals are weak (the signals in Figure 51 are the best results with the given components) due the low response of the commercial detector, a new sensor, described in chapter 4.1, was built with a higher sensitivity and lower SNR. Since the stronger 473 nm diode laser was used early in the prototype build, the Thorlabs sensor PDA100A2 was used for the measurements presented in this chapter.

The oscilloscope software from Pico Technology offers to measure an averaged signal and a live signal. While the averaged signal has the disadvantage of a certain delay time, which can be freely chosen, until the signal peak is formed, it has the advantage, that noise is reduced which increase the SNR and therefore makes it easier to detect the signal peaks, shown in Figure 53 for the plain disc (a) and rods on the disc (b). The lower peaks in Figure 53 (b) are due the lower scattered light, since the rods have a smaller surface area than the plain disc.

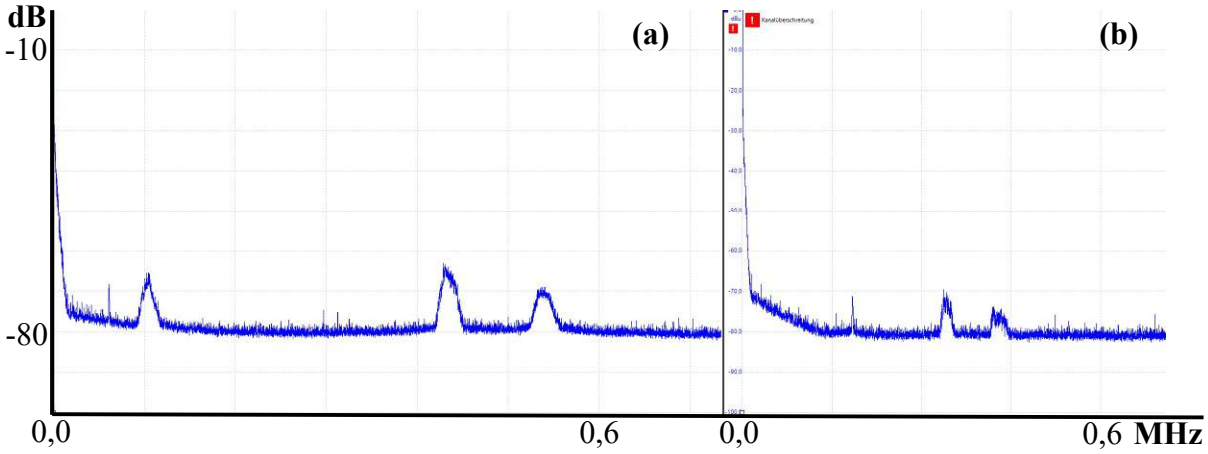

Figure 53: Averaged signal of (a) the spinning plain disc (b) the spinning disc with rods

On the other hand, the live signal can be measured, which holds the advantage, that the signal is updated in real-time (depending on the Sample rate of the oscilloscope), and changes can be recognized immediately but it has high noise which makes the peak detection more difficult. The live signal of a spinning plain disc is shown in Figure 54. Another advantage of the live signal is, that the peaks are sharper since small fluctuations leads to fluctuating peaks and not to widening of the average peak.

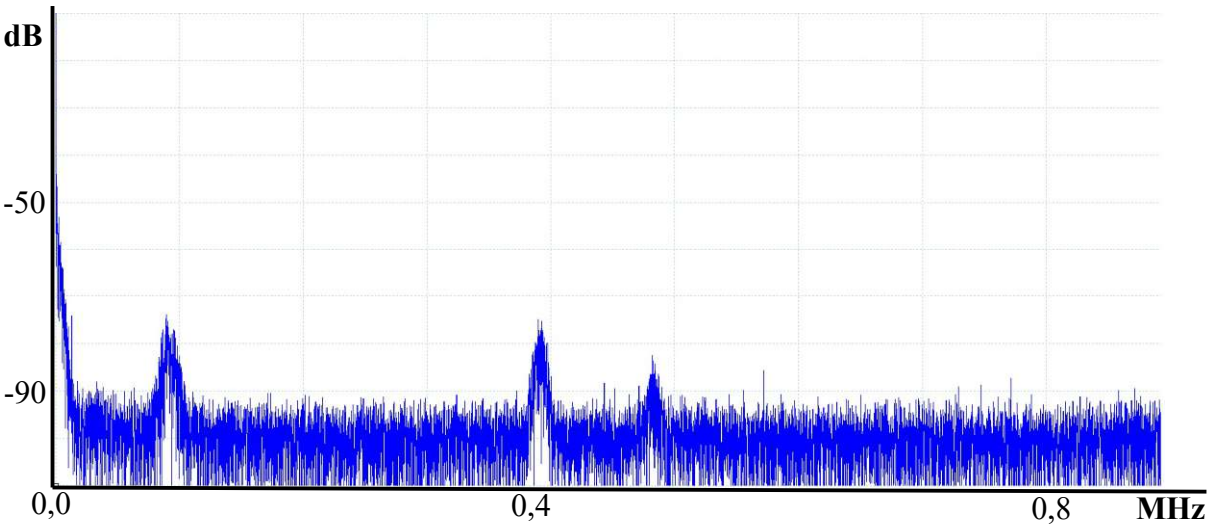

Figure 54: Live signal of spinning plain disc

The received signals in the frequency domain from the LDV for a spinning disc correlate linearly with the measured velocity. Since both spinning directions returned the same

frequencies at the same velocities, only the clockwise spinning direction is shown and discussed in Figure 55 and Figure 56. Figure 55 shows the corresponding measured frequency to the velocity of a plain spinning disc. While f_2 (orange) and f_3 (grey) are the graphs for the x- and y-axis of the disc, f_1 (blue) represents the z-axis which tumbles due to missing bearings and high tolerances of the disc. The different slope of f_2 and f_3 results from the different excitation beam angles.

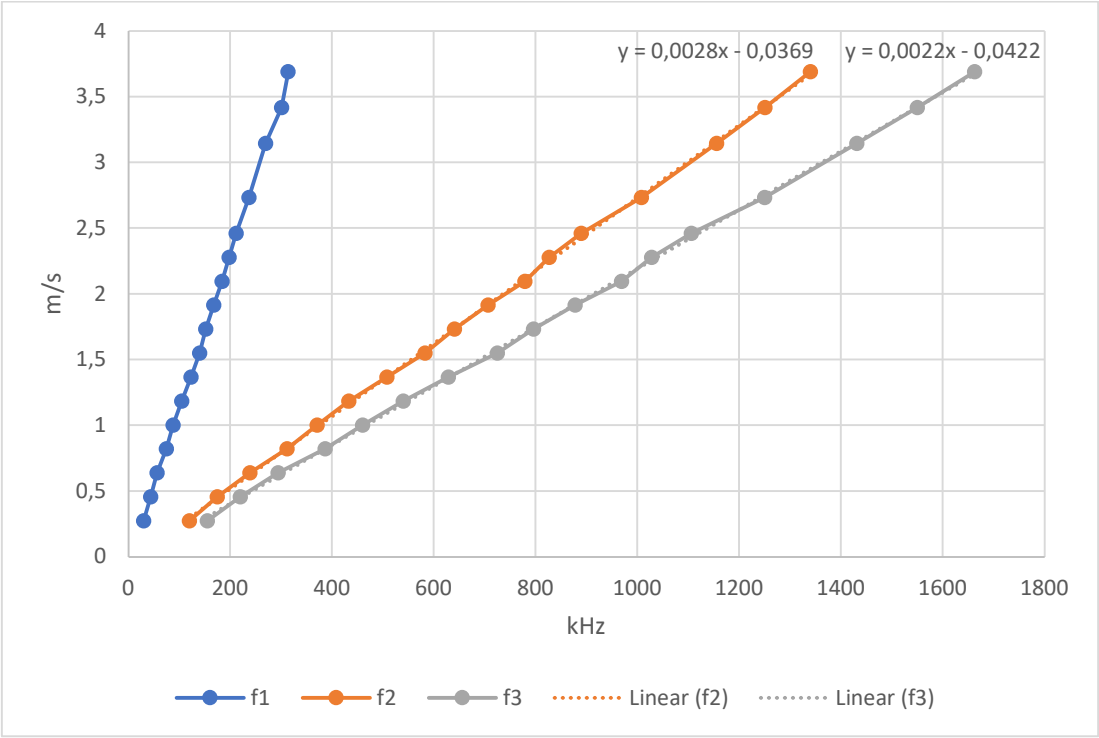

Figure 55: Measurement of the frequency and velocity of a spinning plain discs

Figure 56 shows the corresponding measured frequency to the velocity of a spinning disc with rods, where the focus was on the rods to simulate small particles.

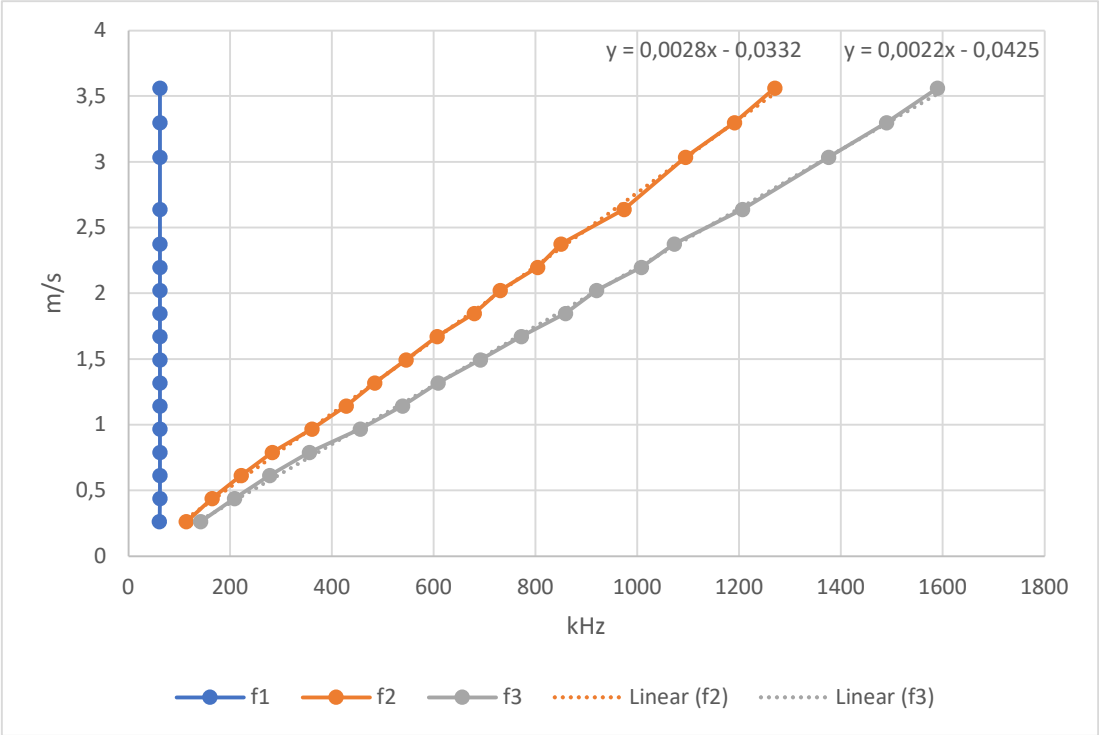

Figure 56: Measurement of the frequency and velocity of a spinning disc with rods

In Figure 56, f_2 (orange) and f_3 (grey) are the graphs for the x- and y-axis of the disc and f_1 (blue) represents the z-axis. The z-axis graph in Figure 56 is constant due to the focus of the measurement volume on only one rod through a slight tilt of the disc as shown in Figure 57. In Figure 57 (a) the off focus of the measurement volume (three beams are visible and no signal can be measured) on the plain disc at the first rod (1) is shown. In Figure 57 (b) the focus of the measurement volume (all three beams appear as one beam and a signal can be measured) on the rod (1) is shown, while in Figure 57 (c) and (d) the off focus of the measurement volume on the plain disc and the rod (2) is shown. This leads to only one focus point on a rod and therefore get rid of the tumble of the disc and only general vibration of the motor/disc unit could affect the measurement. Another advantage of the focus on only one rod is to simulate a small particle and see if enough light would be scattered.

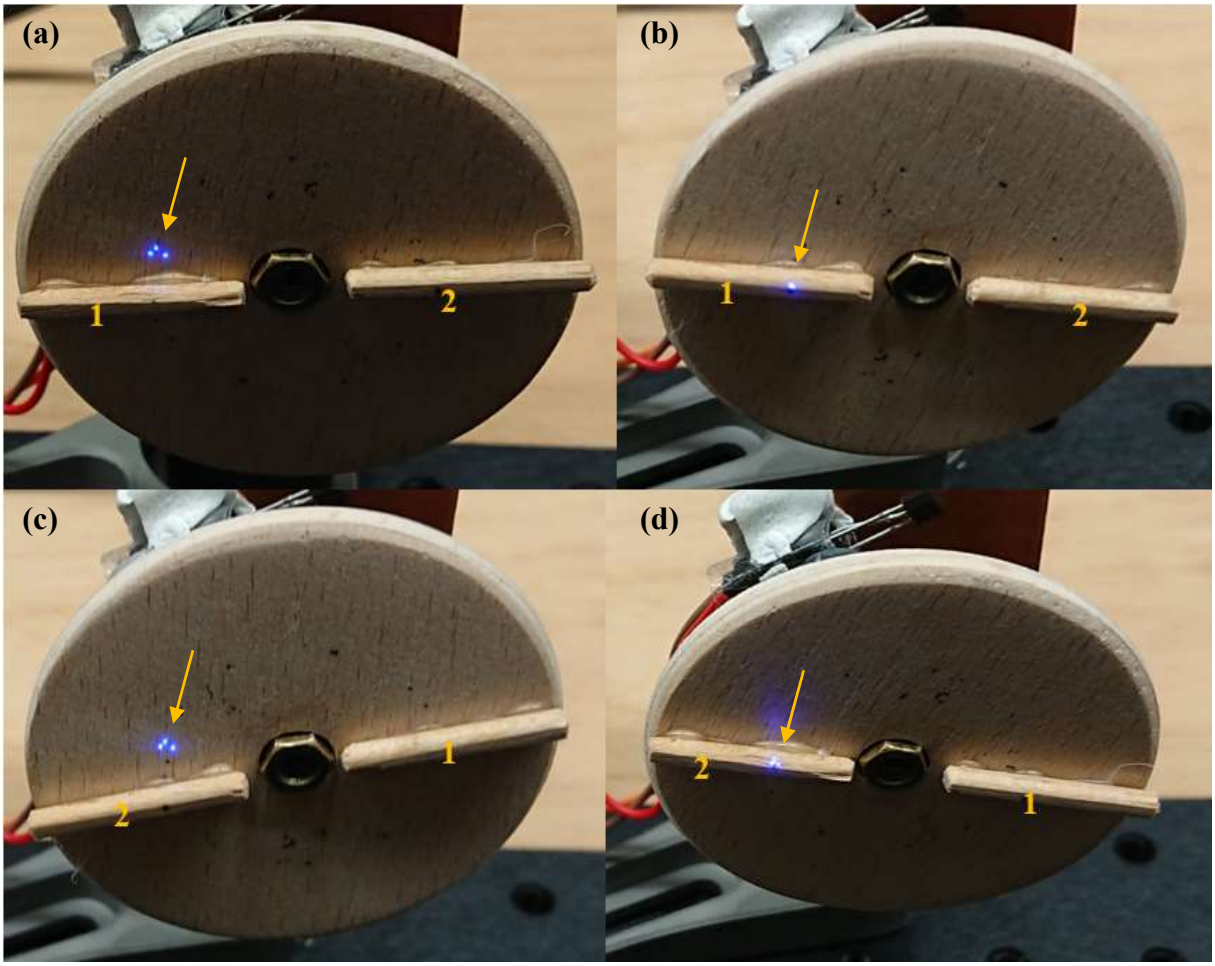

Figure 57: Measurement volume is off focus on plain disc (a), measurement volume is focused on rod 1 (b), measurement volume is off focus on plain disc (c), measurement volume is off focus on rod 2 (d)

To verify that the measurement of the frequency correlating to the rotations per minute is the same for the plain disc and the simulated particle the slopes of f_2 and f_3 from Figure 55 and Figure 56 must be equal. Table 6 shows the result of the comparison of the slopes of the meausrement curves.

Table 6: Slope of graph f_2 and f_3 for plain disc and disc with rod

	Slope f_2	Slope f_3
Plain disc	$2{,}766 \cdot 10^{-6}$	$2{,}23 \cdot 10^{-6}$
Disc with rod	$2{,}789 \cdot 10^{-6}$	$2{,}24 \cdot 10^{-6}$

As ist can be seen, the slopes in Table 6 are in excellent agreement with respect to the acceptable measurement errors due to analog digital conversion (ADC), truncation errors and noise.

The component velocity of the x-, y- and z-axis can be calculated with the formular for the 2-beam LDV (Morita et al., 2016), using for each corresponding beam pair i (i=1,2,3) the measured frequencies f_1, f_2 and f_3

$$v_i = \frac{f_i \cdot \lambda}{2 \cdot cos\, \Delta\theta_i} \qquad (33)$$

The overall velocity can be calculated with (Mikami & Fujikawa, 2016)

$$V = \sqrt{v_1^2 + v_2^2 + v_3^2} \qquad (34)$$

While adjusting the excitation beams on the target and looking for changes due to changes in direction of rotation always one excitation beam was covered. While using the same speed but different direction, it was discovered, that the received signals change their amplitude depended on the spinning direction of the disc. When all three beams are hitting the target, all received signal had the same amplitude, independent of the spinning direction.

In Figure 58 and Figure 59 the measured peaks of the disc turning clockwise (Figure 58) and counter-clockwise (Figure 59) with the same constant rotational speed are shown.

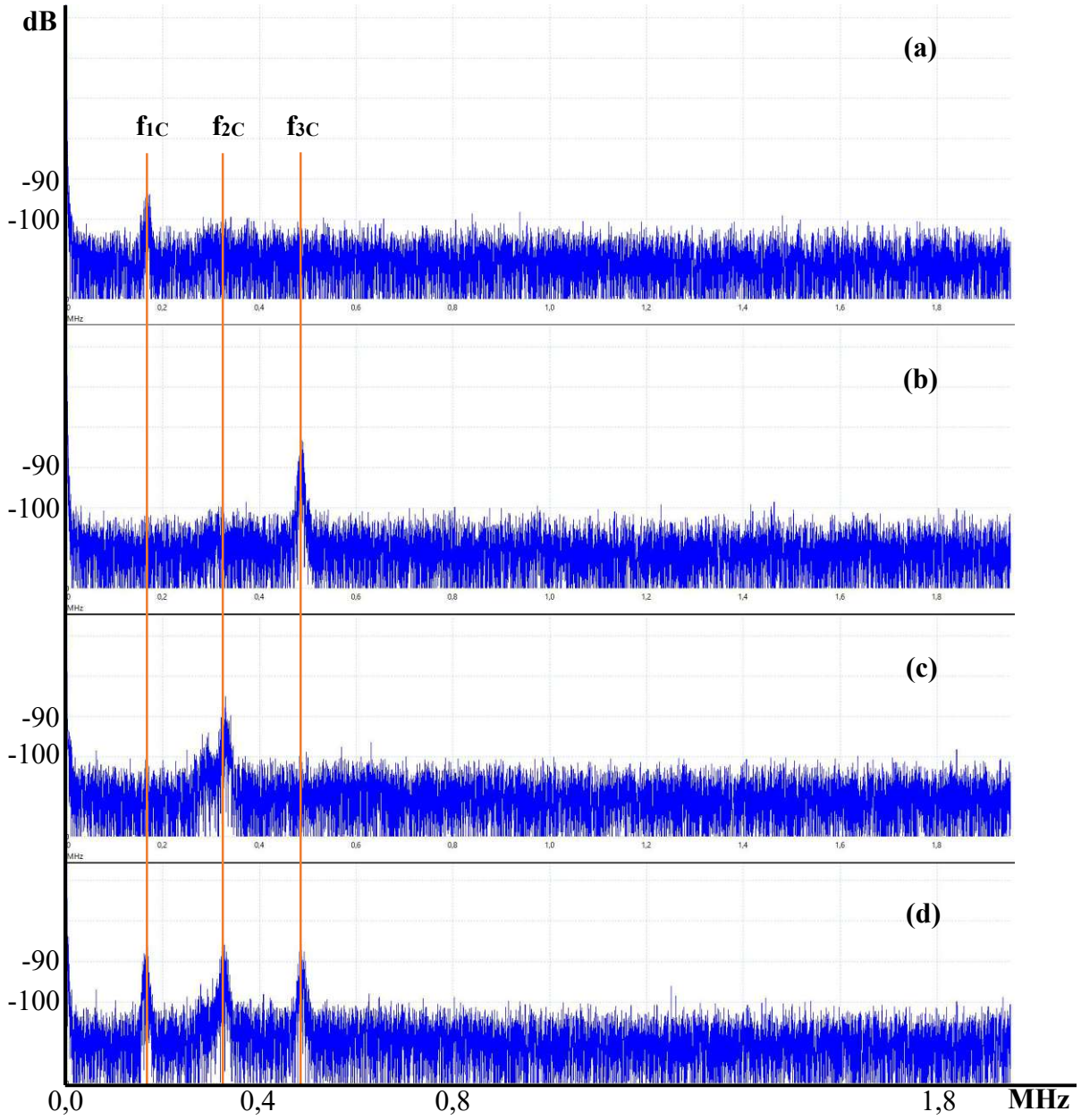

Figure 58: Direction clockwise (a) first beam covered, (b) second beam covered, (c) third beam covered, (d) no beam covered

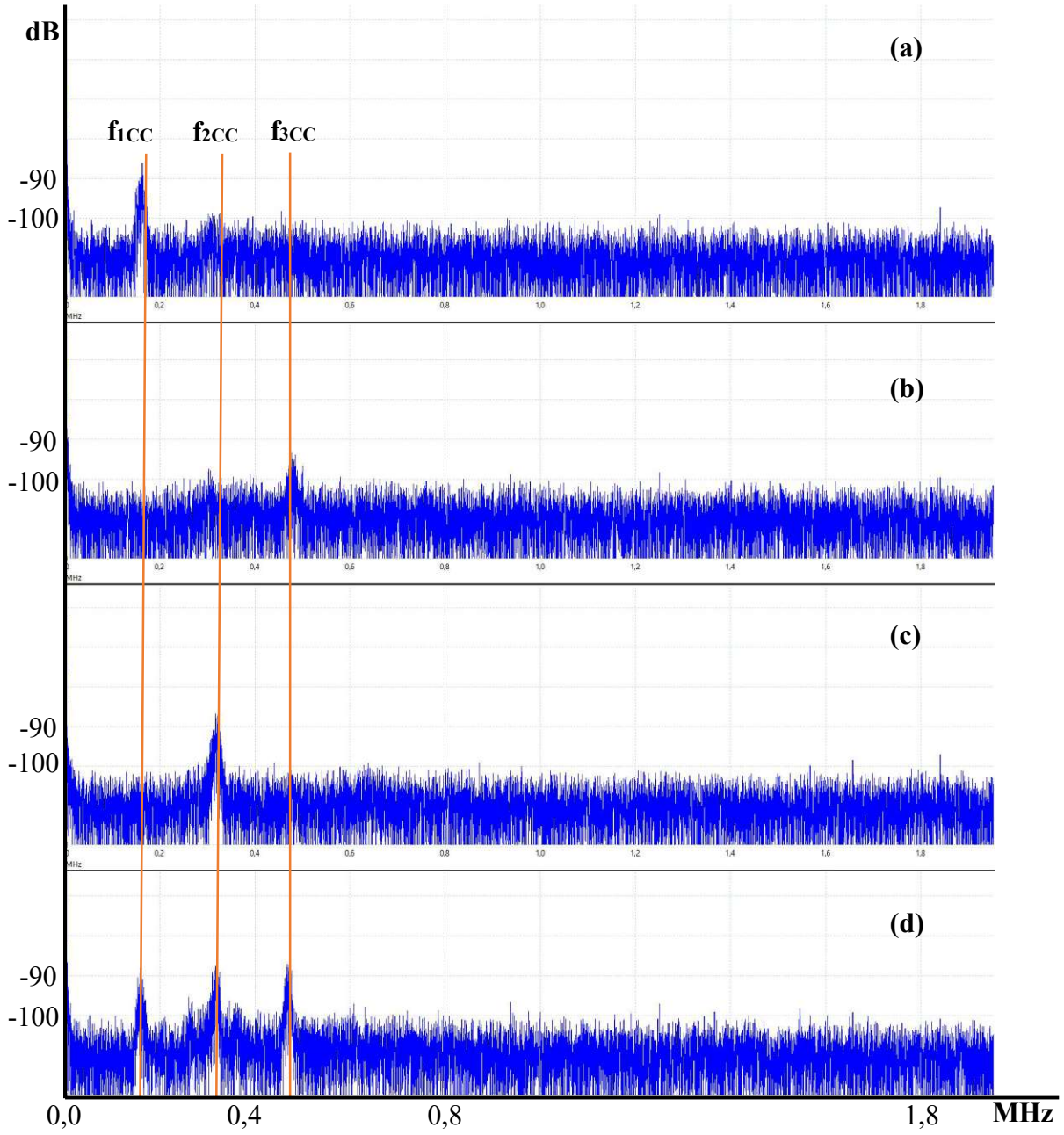

Figure 59: Direction counter-clockwise (a) first beam covered, (b) second beam covered, (c) third beam covered, (d) no beam covered

Figure 58 and Figure 59 both show in (a) the first beam covered, so that beams 2 and 3 hit the target, (b) the second beam covered, so that beams 1 and 3 hit the target, (c) the third beam covered, so that beams 1 and 2 hit the target, and (d) no beam covered, so that all beams hit the target. The resulting frequencies are marked with $f_{1\text{-}3C}$ and $f_{1\text{-}3CC}$, where C means clockwise and CC means conter-clockwise. The frequencies are summarized in Table 8 and are the same for

clockwise and counter clockwise soinning of the disc, since the rotation per minute did not change.

Table 7: Comparison of the peak frequency, dependent on the beams forming the cross section

Beam	Frequency - Clockwise rotation	Frequency - Counter clockwise rotation
1-2 (f_{2C}, f_{2CC})	0,32 MHz	0,32 MHz
2-3 (f_{1C}, f_{1CC})	0,18 MHz	0,18 MHz
1-3 (f_{3C}, f_{3CC})	0,48 MHz	0,48 MHz

Figure 60 summarizes the measurement result of Figure 58 and Figure 59 with the target moving in different directions but with the same constant velocity in each direction and compares the signal strength of the clockwise and counter-clockwise spinning disc. Figure 60 (a) shows the measured frequencies and signal strength when one beam is covered. In Figure 60 (a) (1) the second beam is covered, in (2) the third beam is covered and in (3) the first beam is covered. The signal strength of the higher peak of the two peaks serves for comparison. The left spectrum (l) displays the counter-clockwise spinning direction and right spectrum (r) displays the clockwise spinning direction. Figure 60 (b) shows the frequencies and signal strength when all beams are hitting the target, where (4) shows the counter-clockwise spinning disc and (5) shows the clockwise spinning disc.

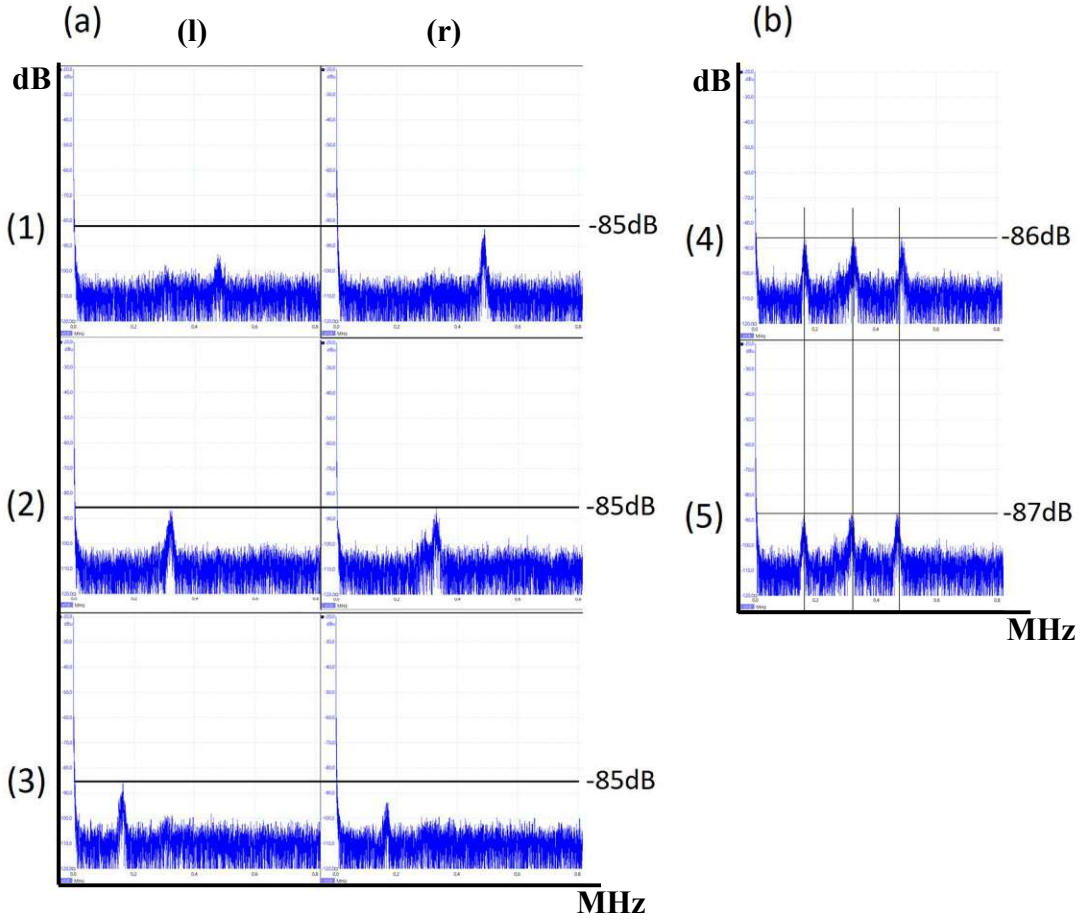

Figure 60: Measurement result of cross section 3-beam LDV with target moving in 2 different directions but same velocity. (a) frequencies and signal strength with always one beam (1-3) covered; left spectrum (l) counter-clockwise turning; right spectrum (r) clockwise turning; (b) frequencies with all beams hitting the target, (4) counter-clockwise turning disc, (5) clockwise turning disc

With these findings, a new method to measure the component velocity of a particle/target and its direction in three dimensions with only one laser, one sensor and without frequency shift as used in (Gooding & Key, 2019) was developed. Therefore, the known angles of the excitation beams must be different to each other, which leads to three different frequencies if all beams hit the particle/target. The amplitude of the occurring frequency when one beam is blocked must be compared to the amplitude of the same frequency when no beam is blocked. The difference in the amplitude gives the direction of the particle/target. If the amplitude is slightly lower than the "base"-amplitude, the particle moves from the measuring beam pair of LaserEye, if it is steep lower, the particle moves to the measuring beam pair of the Lasereye and if it is equal the "base"-amplitude it moves orthogonal to the measuring beam pair of the Lasereye.

The amplitude holds the directional information of the particle, while the frequency holds the velocity information. This behaviour is shown in Figure 60 and was reproducible.

Therefore, a new measurement method was developed:

1. Measuring with three beams to get the reference amplitude and all frequencies
2. Measuring beam 1-2 (beam 3 covered) to get the amplitude of the now occurring single peak as well as the frequency
3. Comparing the amplitude from the first and the second measurement (the frequency should stay the same)
4. Repeating this cycle with the other beams (1 and 2) covered

For this measurement cycle, a shutter system would be preferable and further research for safe distinguishing between moving from or to the measuring beam pair of the LaserEye and orthogonal moving to the measuring beam pair of the LaserEye of the particle will be necessary.

5.1.2 Raman measurement

The measurement with the spatial heterodyne Raman spectrometer (SHRS) returns an interferogram as it could be seen in Figure 61 for the beech disc. The interferogram shows the intensity (y-axis) over the pixel (x-axis) of the line-camera sensor. On the x-axis, the pixel from 1 to 2048 are shown, while on the y-axis the intensity from 0 to 100 % is displayed.

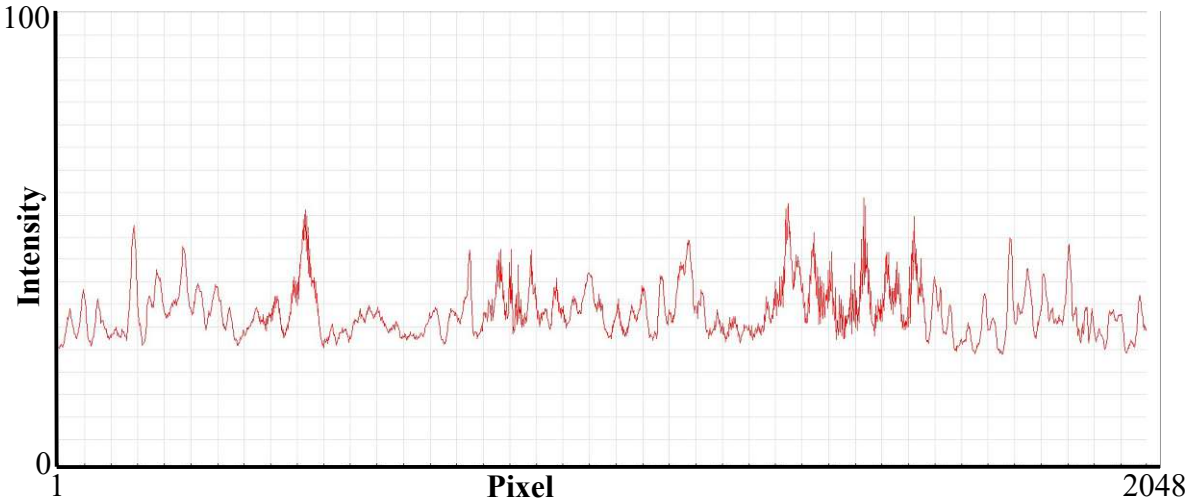

Figure 61: Interferogram of beech disc

In Figure 61 the x-axis shows the pixel number and the y-axis the intensity of the irradiation in percent. If a FFT operation is performed on the interferogram, the spectrum of the irradiation can be recovered (Barnett & Angel, 2017), which can then be transformed into the wavenumber σ (in cm^{-1}) using (Nathaniel et al., 2011)

$$\sigma = \frac{1}{\lambda} \qquad (35)$$

To calculate the Raman shift the measured wavenumber has to subtracted from the laser wavenumber (Nathaniel et al., 2011)

$$\sigma_{Raman\ shift} = \sigma_{Laser} - \sigma_{Measure} \qquad (36)$$

To obtain the correct frequency and intensity, the camera must be calibrated a test fluid with a well-known spectrum (e.g., sulphates or ethanol) or a special lamp (e.g., a mercury-argon lamp) (Jakubek & Fries, 2020). Typical substances with their Raman shifts are shown in Figure 62 (Nathaniel et al., 2011)

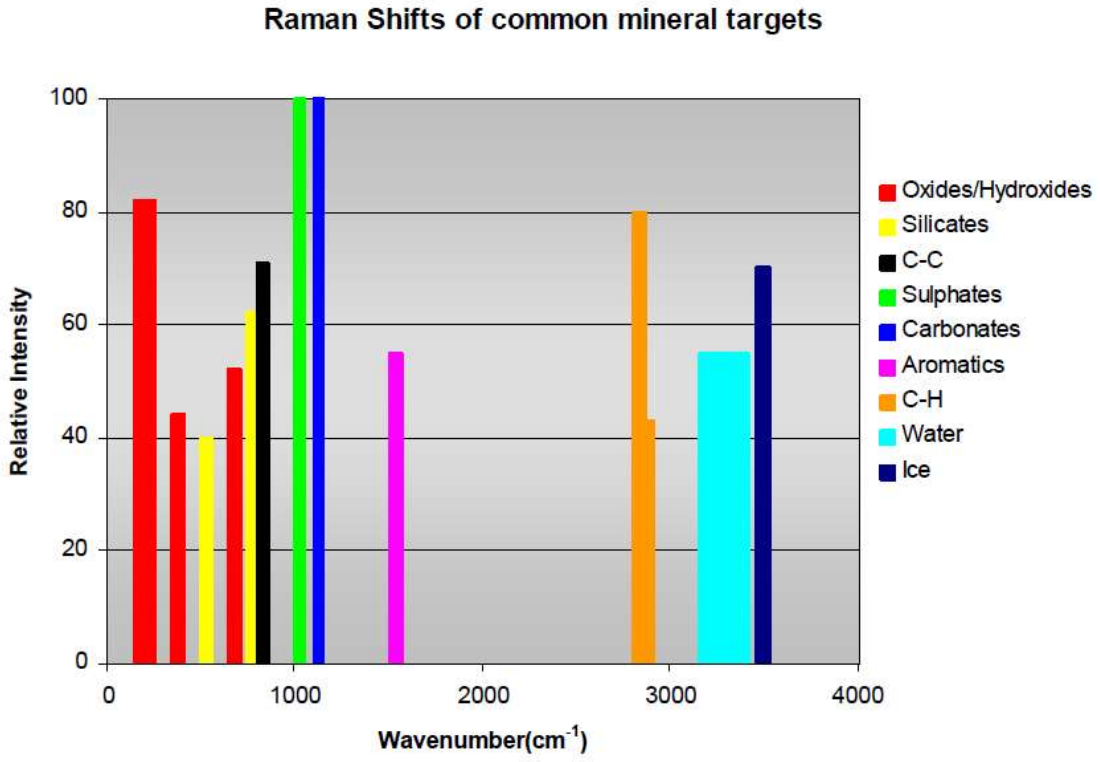

Figure 62: Raman shift of well-known substances (Nathaniel et al., 2011)

In the beginning of the measurement, it was not clear if the interferogram of the beech disc is plausible or not. Therefore, as a quick solution, a PVC disc was made and its interferogram was

compared to that of the beech disc. Figure 63 shows the overlay of the beech (red line) and the PVC (blue line) interferogram, which have different peaks.

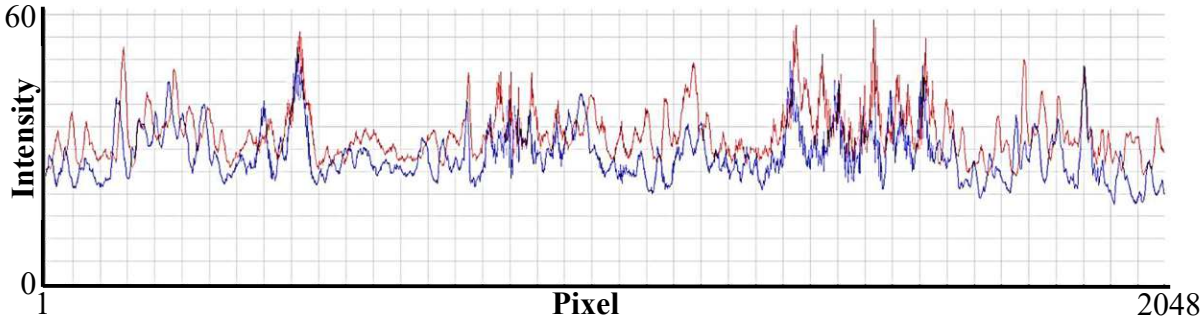

Figure 63: Comparison of PVC (blue) and beech wood (red) interferograms (overlayed)

Eventually, the SHRS returns different interferograms for different materials, but there is no evidence, that the same material will return the same interferogram over time. Therefore, the PVC disc was measured twice in a period of 48 hours while other experiments with the LaserEye had been performed. As result of this measurement, shown in Figure 64, it can be said, that the SHRS returns reproduceable interferograms.

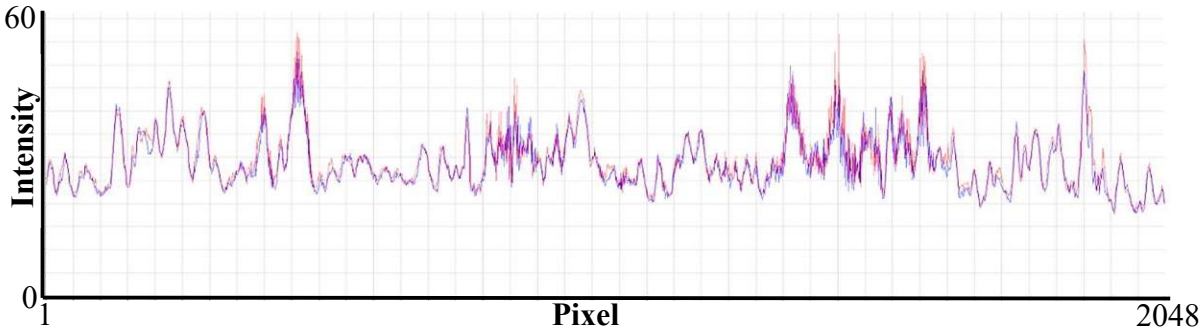

Figure 64: Overlayed interferograms of PVC, measured in a 48-hour period

5.1.3 Combined LDV-Raman measurement

Finally, the measurements of the LDV and SHRS were done simultaneous, shown in Figure 65. In Figure 65 a screenshot of the split screen is shown, where both measurement software are running in parallel. These simultaneous measurements were repeated several times for the beech disc and PVC disc, where the interferogram stayed always the same for the beech respectively the PVC disc but the frequency changed with the rotation per minute of the disc.

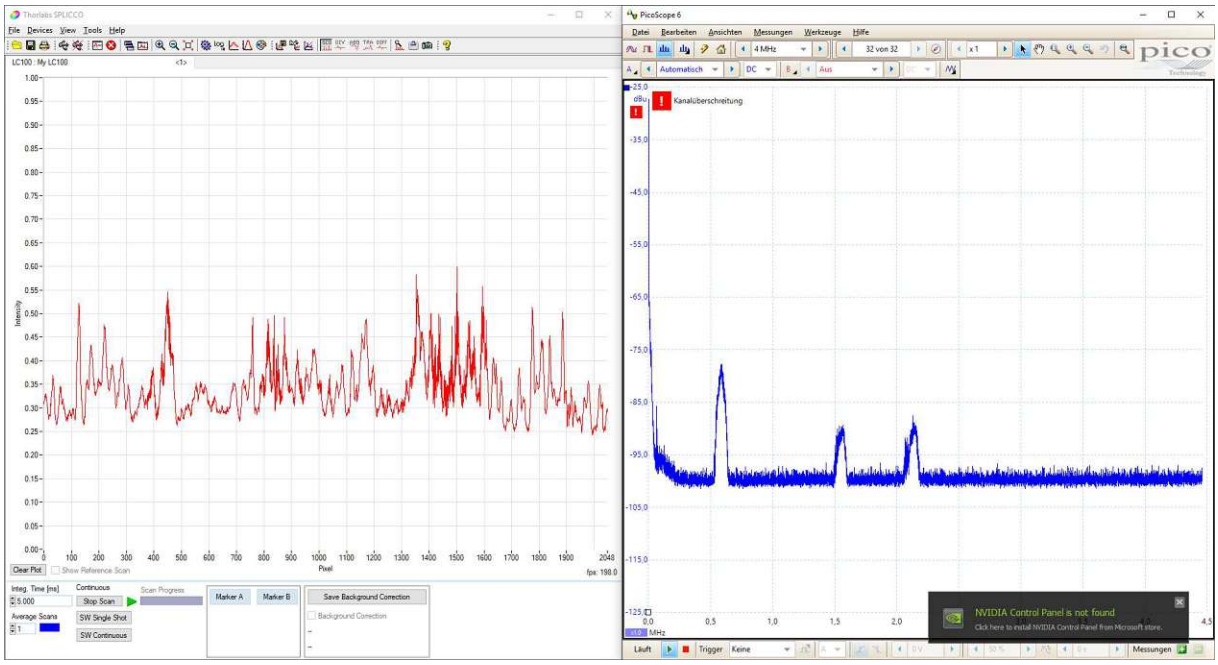

Figure 65: Screenshot of the interferogram and frequency peaks for the spinning beech disc

To gain the spectrogram, a FFT operation must be done on the interferogram. For PVC, the interferogram and spectrogram calculated with MATLAB out of the raw data from the camera sensor are shown in Figure 66 and Figure 67.

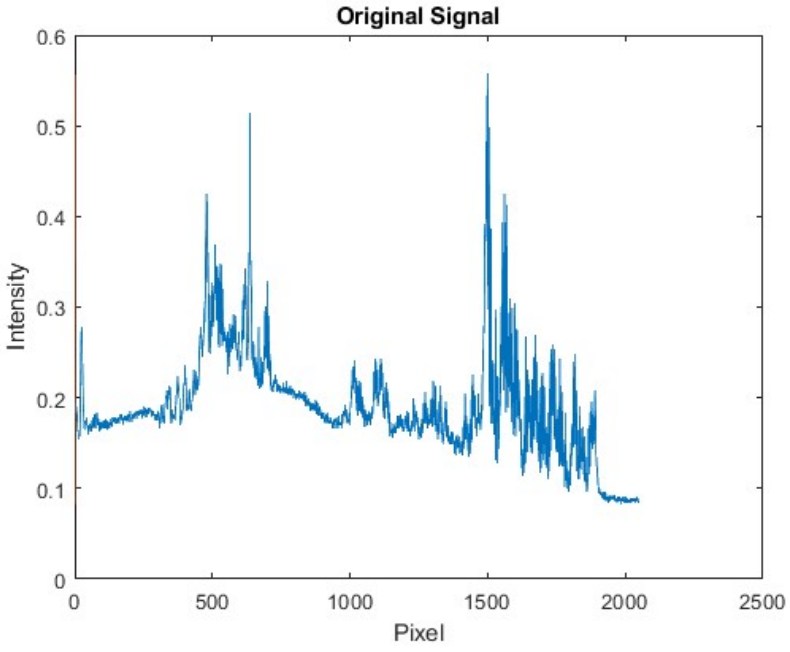

Figure 66: Interferogram PVC plotted with MATLAB

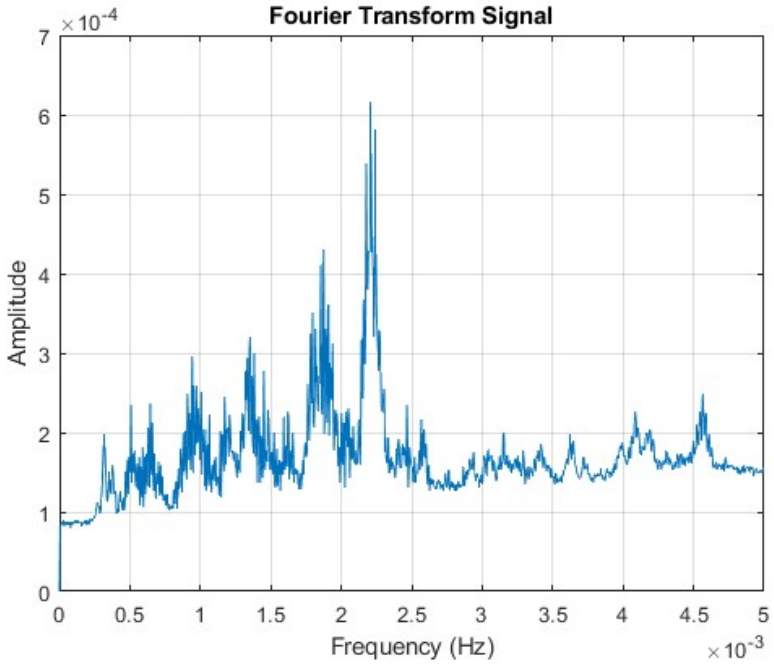

Figure 67: Spectrogram using FFT on interferogram, plotted with MATLAB

The frequency in the spectrogram, plotted on the x-axis in Figure 67 is a placeholder since for the correct frequency a calibration is needed which was not done due time issues. Therefore, it is not sure if the SHRS delivers a Raman spectrum or not. A Raman spectra of PVC, PVC gel and dioctyl terephthalate (DOTP) from the work of (Cheng et al., 2018) is shown in Figure 68 as a reference.

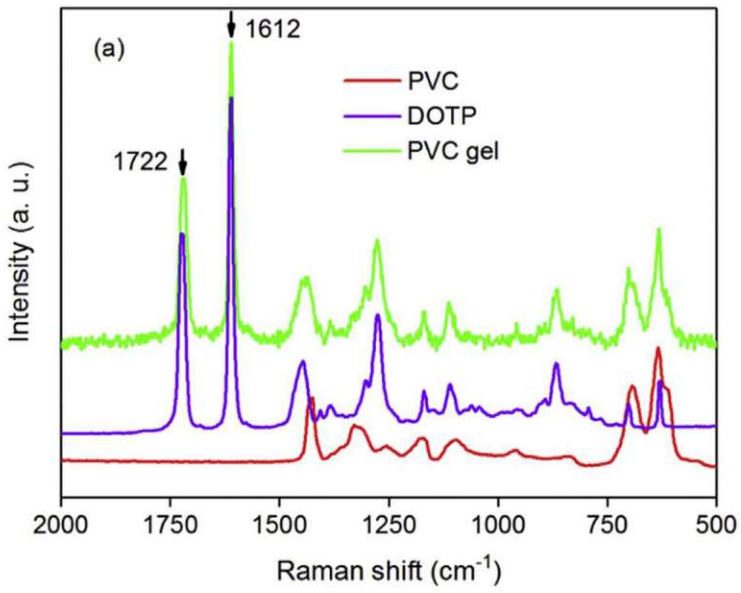

Figure 68: Raman spectra of PVC, DOTP and PVC gel (Cheng et al., 2018)

5.2 Measuring in flow channel

For the measurement of the LDV in the flow channel, seeding particles are necessary to scatter light. Therefore, the following seeding particles were used:

- Spherical Polyamide particles 20 µm
- Spherical Polyamide particles 55 µm
- Spherical Glass hollow spheres 9-13 µm
- Random broken Aluminium particles 45 µm

For the experiments with the LDV, the seeding particle were mixed with tap water in different concentrations. Figure 69 shows the first LDV measurement, where in (a) the whole LaserEye while measuring is shown and (b) a close-up of the three laser beams measuring through the glass is shown. In Figure 69 (b) the focus point in the fluid is not visible but the laser beams in the glass.

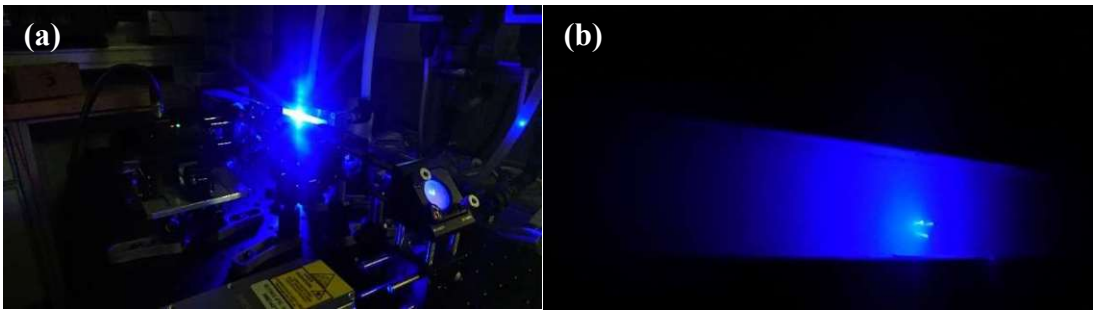

Figure 69: Velocity measurement in flow channel

With the initial settings from the spinning disc, no signal could be found. Also, the variation of the seeding particles and the change to different seeding particles and different flow velocities did not return a LDV signal.

To find the weak signal, the expected frequency corresponding to the particle moving with the flow velocity in the channel was calculated with the cross section of the flow channel of $A_{flowchannel}$=0,00011 m² and the different mass flows (with 1 l/min=0,0000166 m³/s) in accordance with the data from the spinning disc. Table 8 shows the flow corresponding to velocity and expected frequency.

Table 8: Corresponding flow to frequency

flow (l/min)	velocity (m/s)	frequency (MHz)
9	1,3	0,5
10	1,5	0,7
13	1,96	0,8
18	2,7	1,5

Since no signals could be found at the expected frequency, the influence of the glass from the flow channel was investigated, since the possibility of high damping of the excitation beams or the scattered light or a shift of the focus point could occur. By using the same glass used in flow channel, between the LaserEye and the spinning disc the influence of the glass was investigated. The setup is shown in Figure 70, where (a) shows the mounting of the glass and (b) the whole setup of the glass (1) 5 cm away of the spinning disc.

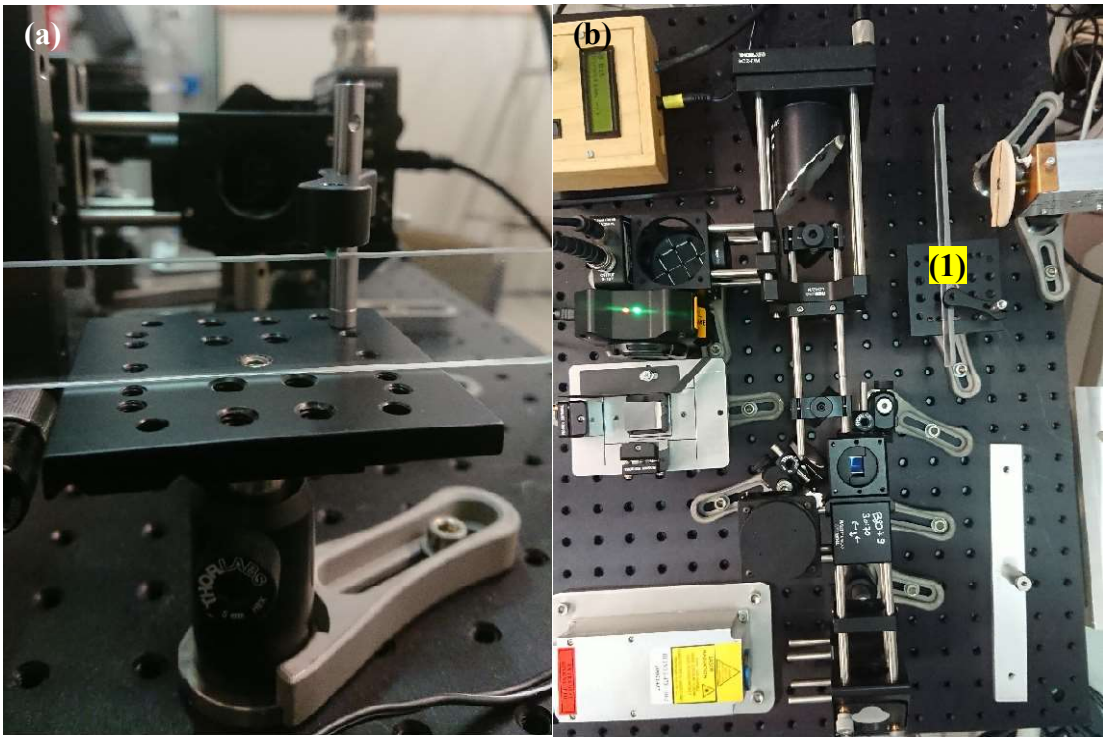

Figure 70: Setup to investigate the influence of the glass

Figure 71 shows the signal from the spinning disc with no glass (a), glass normal to the disc (b) and slightly tilted glass (c). When the signal went through the glass damping occurs, where significant damping of 50 % of the original signal strength when the signal went through the

glass, orthogonal to the LaserEye and very high significant damping of 90 % of the original signal strength when the glass was tilted around the optical post in a range of 1° – 3°.

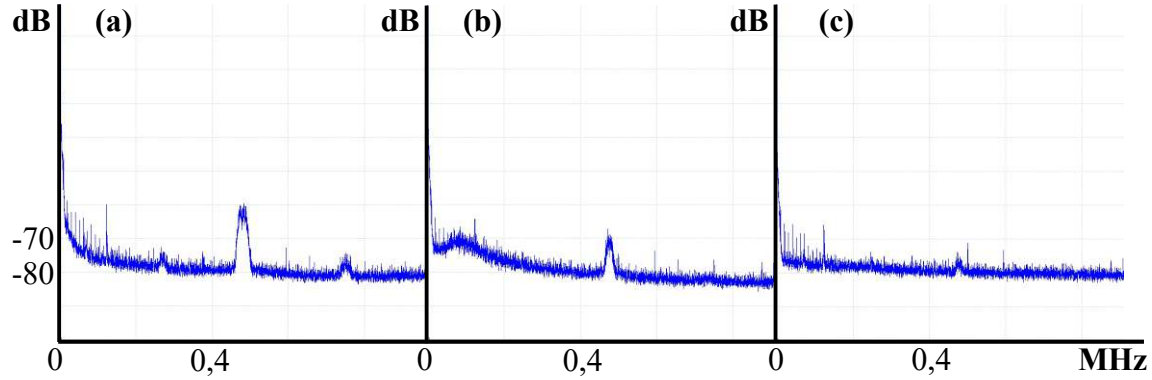

Figure 71: Signal without glass on disc (a), signal through glass normal to disc with same settings (b), signal through glass slightly shifted to disc with same settings (c)

If the glass was tilted more than ±3° around the optical post, no signal could be detected. The signal loss due tilted glass was caused by losing the focus point on the disc due the shift of the excitation beams caused by the different refractive index of glass and air. Also, the influence of the optical power was examined. Therefore, a power meter was used to measure the scattered light reaching the LDV sensor and the excitation beams hitting the target. Figure 72 (a) shows the setup of the power measurement with the sensor head of the power meter (1) in place where normally the LDV sensor would be. Figure 72 (b) is a close-up of said sensor head (2) with the scattered light focused on it. For measuring the excitation beams, the sensor head of the power meter replaced the spinning disc.

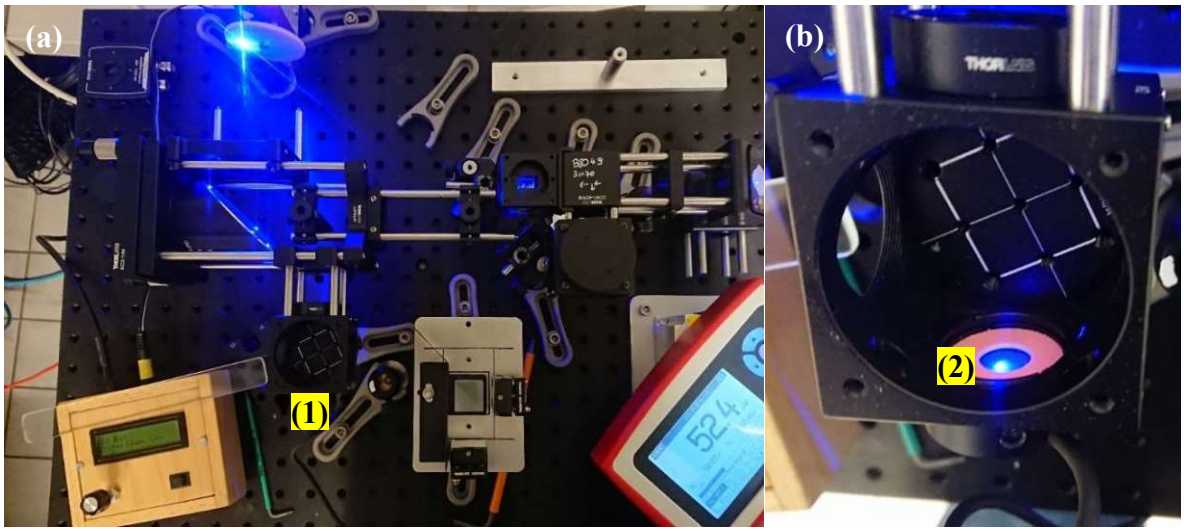

Figure 72: Measurement of the optical power, using a power meter instead of the LDV sensor

The results of the optical power measurement with and without glass between the LaserEye and the spinning disc are shown in Table 9.

Table 9: Optical power with and without glass

Setup	Optical power
excitation beams without glass	74,1 mW
excitation beams with glass	64 mW
scattered light without glass	47,8 µW
scattered light with glass	40 µW

The results in Table 9 show, that damping occurs, but that the damping should not prevent signal detection.

Also, the influence of the distance of the glass to the spinning disc was examined. This experiment should show if there is an influence on the different angle of the excitation beams with different distance to the target (e.g., one beam is displaced so it does not hit the measurement volume in the focal point anymore). The measurement was performed with the room light on, which take effect in a slightly higher noise level and accurate adjustment of the excitation beams. For accurate alignment of the glass, additional rods where installed (normal to the parabolic off axis mirror) which enabled the positioning of the glass through distance

measurement. In Figure 73 the measurement of the signal without glass (a), with the glass in a distance of 5 mm to the target (b) and the setup (c) is shown.

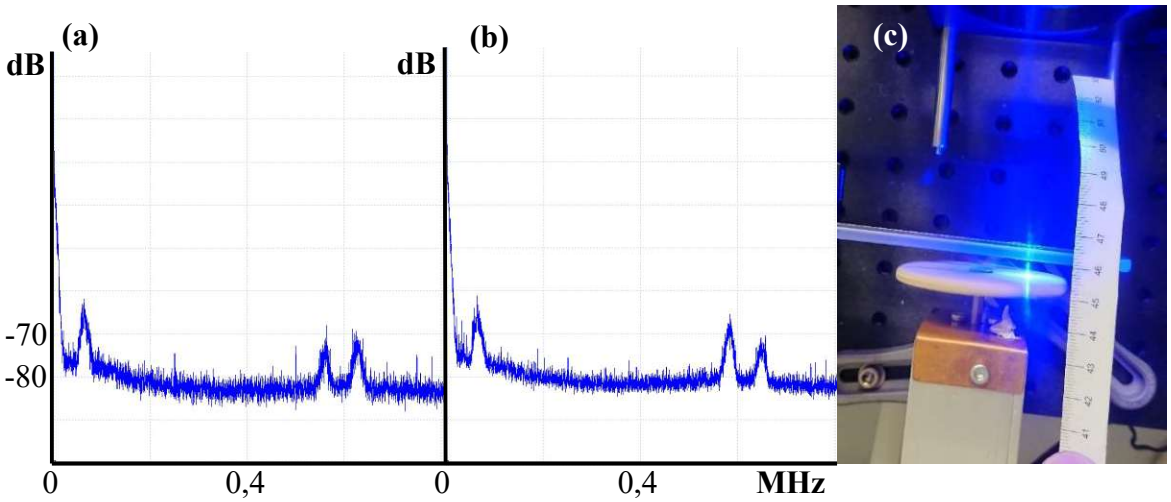

Figure 73: Signal without glass (a), signal with glass 5mm away from the disc (b) and setup (c)

The signal damping due the glass was not noticeable, opposite the previous experiment where the signal damping seemed a lot stronger. Since the results of the experiment shown in Figure 73 are in accordance with the measurement done in Table 9, the signal damping due the glass can be excluded as a dominating reason for not finding a signal.

Further thoughts about the different material properties[5] like signal damping and refraction index of air, glass and water lead to the next experiment where a water filled glass cuvette was brought between the spinning disc and the LaserEye, as shown in Figure 74.

[5] For more detailed analysis, also temperature- and wavelengths-dependency of these properties may need to be considered

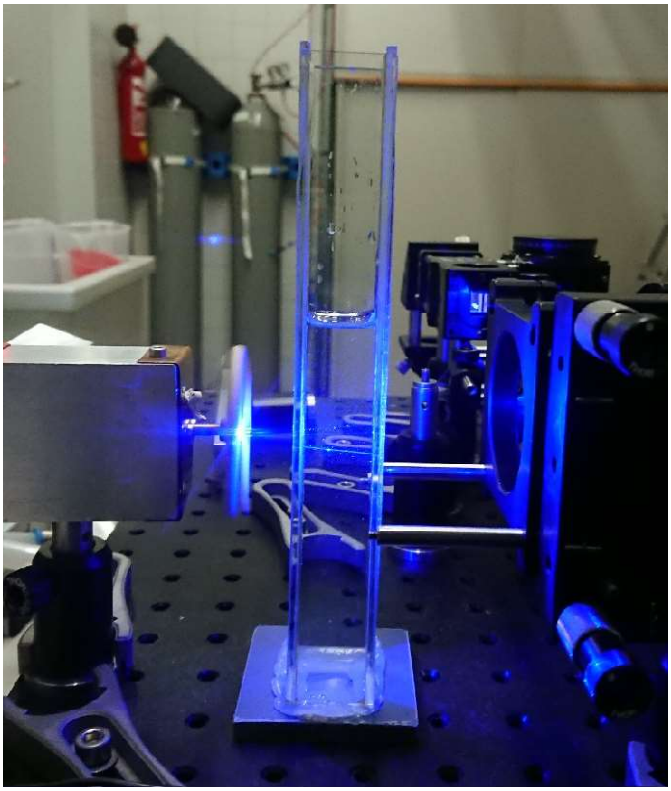

Figure 74: Water filled cuvette between spinning disc and LaserEye

The cuvette had a cross-section of 2,5 x 25 cm and was placed in 3 cm to the spinning disc between spinning disc and LaserEye. The goal of this experiment is to determine if the combination of water and glass will lead to excessive damping or other phenomena which causes signal loss. In Figure 75 the results of the measurement are shown. Figure 75 (a) shows the signal without the cuvette between the target and the LaserEye, Figure 75 (b) shows the signal with the empty cuvette between the target and the LaserEye and Figure 75 (c) shows the waterfilled cuvette between the target and the LaserEye.

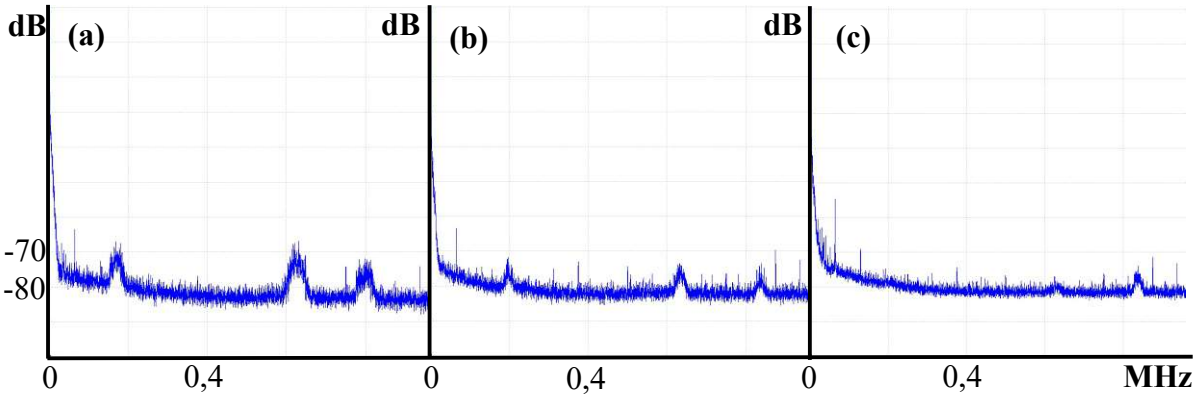

Figure 75: Signal without cuvette (left), with empty cuvette (middle) and waterfilled cuvette (right)

The signal damping in Figure 75 (b) was expected since the light goes through two glass plates. The signal damping in Figure 75 (c) was unexpected, but through further investigation it was found out, that the signal loss occurred due a shift of focus point, which was found to be 1cm from the LaserEye away. With the repositioning of the target, the signal damping was of the level of the empty cuvette, as shown in Figure 76.

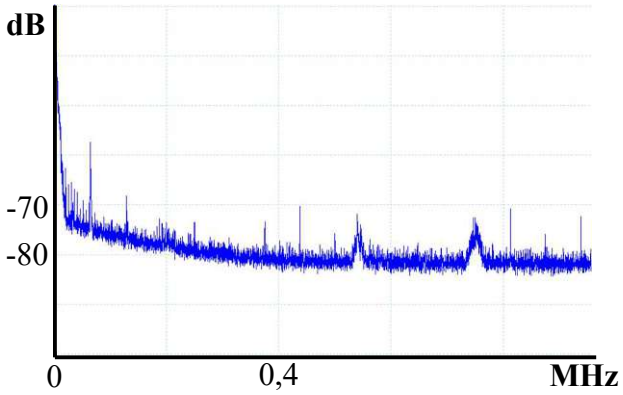

Figure 76: Signal with waterfilled cuvette and repositioned target

Therefore, the damping of the glass-water system alone should not lead to full signal loss. Since the flow channel was adjusted by tracking the focus point in the fluid, the shift of the focus point can be excluded as reason for not finding a signal.

Another reason why no signal was found while measuring the flow channel could be, that the flowrate is too high since the signal becomes weaker the higher the particle velocity is because less light is scattered. Therefore, the throttle was installed in the pumping station. Also, the telescope optic was installed to adjust the beam diameter and with that the measurement volume, so that on one hand with a bigger measurement volume more particle scatter light. On the other hand, if destructive interference occurs due to particles in different depth and may velocity offsets, a smaller measurement volume is preferable.

At the time the work on the thesis stopped, these measures did not produce a reproducible signal when measuring the fluid channel.

An interferogram of a test fluid consisting of tap water and polyamide seeding particles was recorded in the flow channel to verify if the SHRS works with the flow channel. Figure 77 shows the interferogram of the mix of tap water, polyamide, some residuals like iron from pump and the glass where the laser pass through. Since water is not Raman active it should not be visible in the interferogram but, since the SHRS was not calibrated, it is unknown what the spectrum in Figure 77 exactly shows.

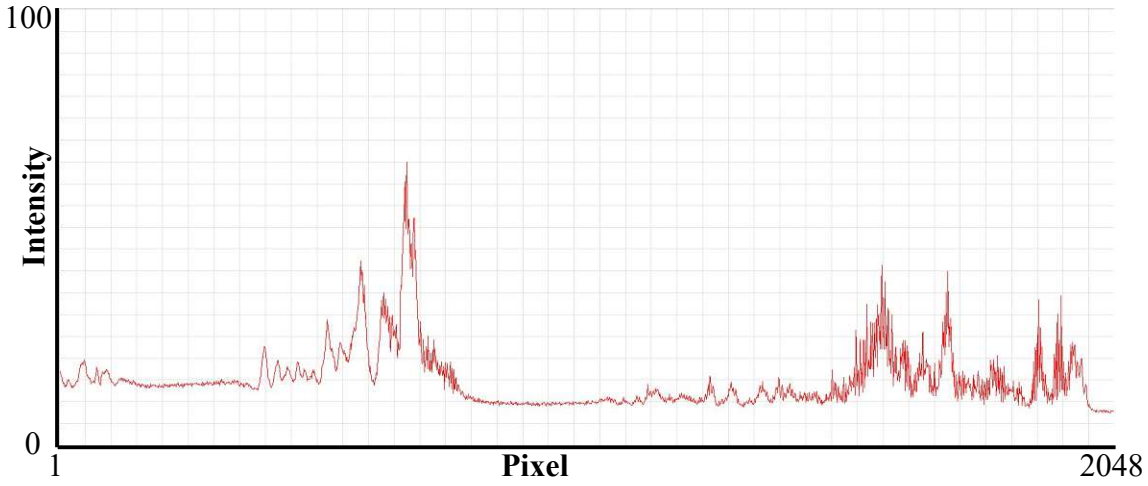

Figure 77: Interferogram of the test fluid from the flow channel. consisting of a mix of tap water, polyamide, some residuals like iron from pump, etc., the influence of the glass from the channel is unknown

5.3 Outlook

In this thesis, the LaserEye was working for solids, but it was not providing interpretable signals with the used fluids respectively the flow channel. For the flow channel, the LaserEye had been split functionally in a LDV part and a spectrometer part. Since the LDV part failed working until the end of this project, the spectrometer was not tested/calibrated with pure substances due lack of time.

One of the issues is the lack of optical power when measuring small particles in an environment where quite strong damping occurs. Therefore, another laser with higher optical output and a more sensitive sensor, e.g., a silicon photomultiplier (SIP) is recommended. To gain better signal quality, signal processing techniques, e.g. chromatic coding (Czarske, 2001) or pulse compression in combination with matched filters (Kashmiri et al., 2020) can be used.

For better usability, a software should be written, which combines the LDV and Raman measurement results and returns the velocity instead of the frequency.

To use the new developed measurement method to gain directional information over the signal strength, a shutter system should be installed.

6 Conclusion

The LaserEye is a measuring device, capable of measuring velocity, direction, composition, and component concentrations of a process stream simultaneously. It consists of a laser source, a telescope optic to adjust the measurement volume, a beam splitter unit which divides the incoming excitation beam in three beams with equal optical power, an off axis parabolic mirror, which not only focuses the three excitation beams on the target but also collects the scattered light, an edge filter, which divides the scattered light in high frequeny light used for LDV measuring and low frequency light used for Raman spectroscopy, a LDV sensor, which delivers the velocity and the direction of the particle which scattered the light, and a Raman spectrometer, which returns the composition and the concentration of the substances in the measurement volume.

The LaserEye was built in two major stages, which had been divided in smaller stages. In the first major stage, the LDV was built for measuring solids, in particular a spinning disc. After the LDV was working, the Raman spectrometer was built and tested on different discs, like beech wood and PVC. In the second major stage the flow channel with a pumping station was built, with the goal to measure the actual fluid flow with the LaserEye.

The LaserEye works well on solid materials and a new measurement method was found to gain the velocity and the direction information of the 3-dimensional target/particle movement with only one laser source and one sensor. These findings have been used for a patent application (Wedl G., Jordan C., Haddadi B., Harasek M., 2021).

The second major stage was not that successful as the findings in the first major stage, since no LDV signal from the flow channel could be found. This could be due the lack of excitation laser power or to the low sensitivity of the LDV sensor. Also, signal processing techniques might help to receive reproducible signals. For the Raman spectrometer further research must be done since the spectrometer is not calibrated yet. As a third major stage the possibilities to use the LaserEye in gaseous process streams should be researched.

List of References

Ang, M. I. N. G. W. (2017). *Self-mixing birefringent dual-frequency laser Doppler velocimeter*. *25*(2), 4423–4429.

Barnett, P. D., & Angel, S. M. (2017). Miniature Spatial Heterodyne Raman Spectrometer with a Cell Phone Camera Detector. *Applied Spectroscopy*, *71*(5), 988–995. https://doi.org/10.1177/0003702816665127

Bin Muhamad, A. L., Ugajin, A., Mikami, O., Okazaki, T., & Yoshikuni, Y. (2011). Two-beam fiber laser Doppler velocimeter enabling velocity distribution measurement of liquid flow. *21st International Conference on Optical Fiber Sensors*, *7753*, 77536G. https://doi.org/10.1117/12.885883

Buchner, A., Hadrath, S., Burkard, R., Kolb, F. M., Ruskowski, J., Ligges, M., & Grabmaier, A. (2021). *and Single-Photon Avalanche Diodes*. 1–18.

Chan, C. A., Lu, M. C., Tsai, F. W., Zhong, Y. L., Tsai, T. Y., Hsu, C. S., Li, B. Y., Zheng, Z. X., Hsu, T. F., Liu, C. J., & Ho, M. C. (2019). Experimental Observation of Dynamical Behavior of Self-mixing by Doppler Feedback in Microchip Nd:YAG Laser. *Sensors and Materials*, *31*(8), 2433–2439. https://doi.org/10.18494/SAM.2019.2213

Chen, G., Lu, D., Guo, L., Zhao, W., Wang, H., & Zhao, L. (2018). Dual-frequency Laser Doppler Velocimeter based on Integrated Dual-mode Amplified Feedback Laser. *Asia Communications and Photonics Conference, ACP*, *2018-Octob*, 1–3. https://doi.org/10.1109/ACP.2018.8596305

Cheng, X., Yang, W., Zhang, Y., Kang, Y., Ding, Y., & Jiao, Z. (2018). Understanding the electro-stimulated deformation of PVC gel by in situ Raman spectroscopy. *Polymer Testing*, *65*(September 2017), 90–96. https://doi.org/10.1016/j.polymertesting.2017.11.013

Czarske, J. (2001). Laser Doppler velocity profile sensor using a chromatic coding. *Measurement Science and Technology*, *12*(1), 52–57. https://doi.org/10.1088/0957-0233/12/1/306

Egan, M. J., Acosta-maeda, T. E., & Angel, S. M. (2020). *One-mirror , one-grating spatial*

heterodyne spectrometer for remote-sensing Raman spectroscopy. *September 2019*, 1–8. https://doi.org/10.1002/jrs.5788

Englert, C. R., Harlander, J. M., & Roesler, F. L. (2010). *Spatial Heterodyne Spectroscopy : An Emerging Optical Technique for Heliophysics and Beyond 1 . This is how SHS works*. *October*.

Geusic, J. E., Marcos, H. M., & Van Uitert, L. G. (1964). Laser oscillations in nd-doped yttrium aluminum, yttrium gallium and gadolinium garnets. *Applied Physics Letters*, *4*(10), 182–184. https://doi.org/10.1063/1.1753928

Gooding, W. J., & Key, N. L. (2019). Leveraging LDV techniques for the investigation of unsteady turbomachinery flows. *Aeronautical Journal*, *123*(1270), 1919–1937. https://doi.org/10.1017/aer.2019.28

Gulino, M., Vangi, D., & Virga, A. (n.d.). *SIGNAL-TO-NOISE RATIO OPTIMIZATION FOR LOW-POWER LASER GENERATED ULTRASOUND*. *00*, 1–4.

Haddadi, B., Gasser, C., Jordan, C., Harasek, M., & Lendl, B. (2018). Simultaneous Laser Doppler Velocimetry and stand-off Raman spectroscopy as a novel tool to assess flow characteristics of process streams. *Chemical Engineering Journal*, *334*(August 2017), 123–133. https://doi.org/10.1016/j.cej.2017.10.027

Hariharan, P., & Hariharan, P. (2007). *3 - Two-Beam Interferometers*. 13–22. https://doi.org/https://doi.org/10.1016/B978-012373589-8/50005-5

Harris, H. H., Mohr, C., Spencer, C. L., & Hippler, M. (2010). *Inexpensive Raman Spectrometer for Undergraduate and Graduate Experiments and Research*. *87*(3).

Hazle, M. A., Mehicic, M., Gardiner, D. J., & Graves, P. R. (1990). Practical Raman Spectroscopy. *Vibrational Spectroscopy*, *1*(1), 104. https://doi.org/10.1016/0924-2031(90)80015-v

Hui, R. (2009). Fiber optic measurement techniques. *Fiber Optic Measurement T*, *ISBN 1-282-28689-7*, 1 online resource (671 p.).

Ibrahim, A. A., Ambran, S., Ahmad, F., Mikami, O., & Fujikawa, C. (2018). Velocity Measurement by Self-Mixing Laser Diode Using Direct Modulation. *2018 IEEE 7th International Conference on Photonics, ICP 2018*, *1*, 1–3. https://doi.org/10.1109/ICP.2018.8533200

Jakubek, R. S. S., & Fries, M. D. (2020). Calibration of Raman wavenumber in large Raman images using a mercury-argon lamp. *Journal of Raman Spectroscopy*, *51*(7), 1172–1185. https://doi.org/10.1002/jrs.5887

Kajava, T. T., Lauranto, H. M., & Salomaa, R. R. E. (1993). *Fizeau interferometer in spectral measurements*. *10*(11), 1980–1989.

Kashmiri, M., Behroozpour, B., Petkov, V. P., Wojciechowski, K. E., & Lang, C. (2020). A 4-GS/s 80-dB DR Current-Domain Analog Frontend for Phase-Coded Pulse-Compression Direct Time-of-Flight Automotive Lidar. *IEEE Journal of Solid-State Circuits*, *55*(12), 3131–3145. https://doi.org/10.1109/JSSC.2020.3022658

Li, Z., Deen, M. J., Kumar, S., & Selvaganapathy, P. R. (2014). *Raman Spectroscopy for In-Line Water Quality Monitoring — Instrumentation and Potential*. 17275–17303. https://doi.org/10.3390/s140917275

Maru, K. (2011). Axial scanning laser Doppler velocimeter using wavelength change without moving mechanism in sensor probe. *Optics Express*, *19*(7), 5960. https://doi.org/10.1364/oe.19.005960

Michelson, A. A. (1910). *ART . XXI . --The relative motion of the Earth and the Luminiferous ether ;*

Mikami, O., & Fujikawa, C. (2016). 3-Beam laser Doppler velocimeter for 3-D velocity measurement. *2016 IEEE 6th International Conference on Photonics, ICP 2016*, *1*, 1–3. https://doi.org/10.1109/ICP.2016.7510010

Morita, N., Nogami, H., Higurashi, E., Ito, T., & Sawada, R. (2016). Development of a Built-In Micro-Laser Doppler Velocimeter. *Journal of Microelectromechanical Systems*, *25*(2), 380–387. https://doi.org/10.1109/JMEMS.2016.2518691

Nathaniel, T. A., Underwood, C. I., & Surrey Space Centre. (2011). Spatial Heterodyne Raman Spectroscopy. *42nd Lunar and Planetary Science Conference 2011*, *September*, 1045.

Nevie, M., Popov, E., Bojhkov, B., Tsonev, L., & Tonchev, S. (1999). *High-accuracy translation – rotation encoder with two gratings in a Littrow mount*. *38*(1), 67–76.

Nissinen, I., Nissinen, J., Keränen, P., & Kostamovaara, J. (2017). Sensors and Actuators B : Chemical On the effects of the time gate position and width on the signal-to-noise ratio for detection of Raman spectrum in a time-gated CMOS single-photon avalanche diode

based sensor. *Sensors & Actuators: B. Chemical*, *241*, 1145–1152. https://doi.org/10.1016/j.snb.2016.10.021

Petry, R., Schmitt, M., & Popp, J. (2003). *Raman Spectroscopy – A Prospective Tool in the Life Sciences*. 14–30.

Photon Engineering. (n.d.). *FRED Optical Engineering Software*. https://photonengr.com/fred-software/

Pico Technology. (2022). *Pico Technology*. https://www.picotech.com/

Raman, C. V. (1928). *A new class of spectra due to secondary radiation Part I*. *419*.

Roithner Lasertechnik GmbH. (n.d.). https://www.roithner-laser.com/

Texas Instruments. (2007). Precision High-Speed Transimpedance Amplifier. *Time*, *September*.

Thorlabs. (n.d.). Thorlabs. In *www.thorlabs.com*.

Thorlabs. (2015). *PDA100A Si Switchable Gain Detector User Guide*. 1–16.

VTB Process. (2000). *Blue Enhanced Ultra High Dark Resistance Photodiode*.

Wedl G., Jordan C., Haddadi B., Harasek M., (TU Wien). (2021). *Verfahren zur Bestimmung zumindest einer Geschwindigkeitskomponente einer Fluidströmung*. Patent Application A 50019/2021. http://seeip.patentamt.at/NPatentSuche/Details/ee519afb-9bd2-4fdc-ba31-d2b89aefe275

List of Figures

Page

List of Tables

Page